“Subsidence evolution of the conjugate passive continental margins of southwestern Africa and eastern Argentina”

Von der Fakultät für Georessourcen und Materialtechnik der

Rheinisch-Westfälischen Technischen Hochschule Aachen

zur Erlangung des akademischen Grades eines

Doktors der Naturwissenschaften

genehmigte Dissertation

vorgelegt von **M.Sc.**

Kai Ingo Dressel

aus Peine

Berichter: Univ.-Prof. Dr. rer. nat. Magdalena Scheck-Wenderoth

Univ.-Prof. Peter Kukla, Ph.D.

Tag der mündlichen Prüfung: 04. Juli 2016

Table of contents

List of Figures

List of Tables

1 Introduction

1.1 Preface

Sedimentary basins along passive continental margins are of general interest because they act as an archive for past processes and therefore provide an excellent starting point for the reconstruction of the evolution of passive margins. In addition, sedimentary basins are of economic interests as they often contain vast amounts of natural resources.

In the case of the South Atlantic passive continental margins, these natural resources are hydrocarbons (Kuhlmann et al., 2011; Marcano et al., 2013; Anka et al., 2014). Due to the fact that deep water drilling in distal margin areas becomes more feasible, knowledge about these areas is of particular interest. Regarding past processes of the South Atlantic, these are related to the breakup of Gondwana during Late Jurassic-Early Cretaceous times (Nürnberg and Müller, 1991; Broad et al., 2006), the successive opening of the South Atlantic and the evolution of the subsequent post-rift phase.

For these reasons, a reconstruction of the past aiming at the restoration of paleobathymetries during the post-rift phase helps to understand the evolution of the South Atlantic passive continental margins. However, to realistically restore paleobathymetries, detailed information about the present-day structural configuration of the subsurface and about lithology dependent physical rock properties is essential.

Several studies have focused on the present-day configuration of the SW African and SE South American margins (e.g., Gladczenko et al., 1997, 1998; Hinz et al., 1999; Bauer et al., 2000; Holtar and Forsberg, 2000; Stewart et al., 2000; Franke et al., 2006, 2007; Autin et al., 2013; Loegering et al., 2013; Maystrenko et al., 2013). The investigation shown in this study focuses on the 3D structural models by Autin et al. (2013) and Maystrenko et al. (2013). Even though the research areas, according to these studies, are different in scale and resolution, they provide an excellent starting point for the margin reconstruction as their databases are constrained by information from seismics, wells, gravity and seismology. By using this information, complex geological processes affecting the margin evolution during the post-rift phase, such as isostasy (Watts, 2009) and thermal cooling of the lithosphere (Stein and Stein, 1992), are investigated to reconstruct paleobathymetries.

Accordingly, in this study individual subsidence components such as load induced subsidence and thermal subsidence are calculated by applying a multi 1D approach to derive the spatio-temporal variations of subsidence on both the SE South American and the SW African margins. The results illustrate areas that are strongly affected by these subsidence

components. Finally, using the information from the backward modelling enables the restoration of paleobathymetries, which are then used to infer the magnitude of past vertical movements. The results of the static 1D backward modelling deliver geologically and physically consistent first-order information on the margin evolution and already allow to propose a hypothesis concerning the reasons behind vertical movements during the post-rift phase. However, this approach cannot ultimately clarify whether the reconstructed paleobathymetries obtained at the SW African and SE South American margins evolve as a consequence of the interaction between thermal and mechanical processes. Furthermore, 1D calculations can rather been seen as an approximation because tectonic and physical processes in general take place in 3D.

For this reason and for the reason that computational power has increased significantly over the past years, 3D numerical modelling is a useful tool to simulate geological and geodynamical processes in more detail (e.g., Burov and Gerya, 2014; Braun et al., 2013). The particular advantage of 3D modelling is the consideration of processes, such as heat transport (conductive cooling of the lithosphere), which act in three dimensions and affect the lithospheric strength among other properties. In turn, the lithospheric strength controls the mode of flexure of the lithosphere, and therefore the amount of subsidence induced by the sedimentary load. Considering three dimensions is worthwhile in detailed margin reconstruction but the advantage to use as much present-day information as possible, similar to a multi 1D approach, should be retained. Consequently, a 3D forward modelling approach (Cacace and Scheck-Wenderoth, 2014) is applied that couples the thermal and mechanical processes during the margin evolution and considering available information on the present-day configuration of the margin.

Combining both approaches and comparing the results finally helps to limit possible uncertainties in modelling, evaluate the restored paleobathymetries in terms of subsidence evolution of the South Atlantic passive margins and to suggest possible causative processes responsible for the differential margin evolution.

1.2 State of the art

The South Atlantic Ocean was formed as a result of the breakup of Gondwana during Late Jurassic-Early Cretaceous times with successive opening in northward direction (Nürnberg and Müller, 1991; Broad et al., 2006). Presently, the South Atlantic Ocean can be divided into

four major segments (Fig. 1.1). From north to south these are the Equatorial Segment, Central Segment, Southern Segment and Falkland Segment, limited by major fracture zones (Moulin et al., 2005; Torsvik et al., 2009). The research areas focused on in this study are located within the Southern Segment.

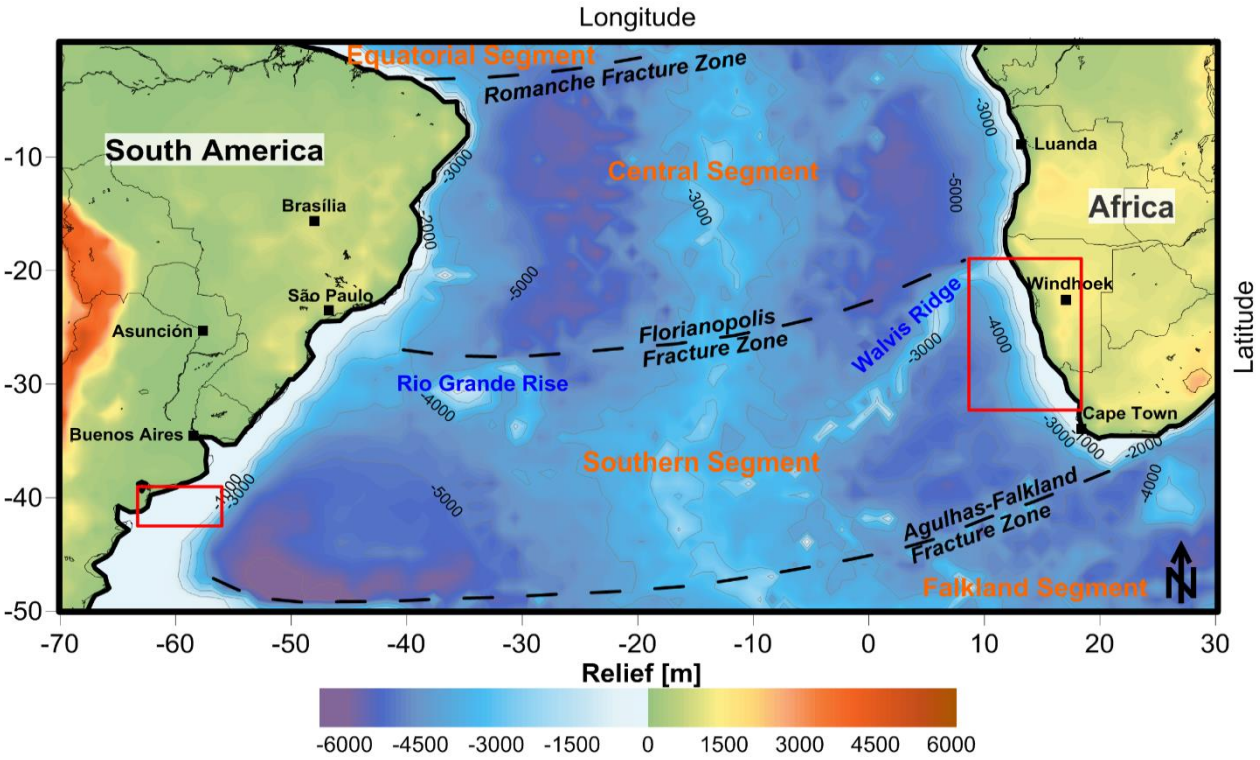

Figure 1.1: Overview of the South Atlantic Ocean indicating its four major segments (from north to south: Equatorial Segment, Central Segment, Southern Segment and Falkland Segment) that are separated by major fracture zones (Romanche Fracture Zone, Florianopolis Fracture Zone, Agulhas-Falkland Fracture Zone; Mounlin et al., 2005, Torsvik et al., 2009). The research areas along the African passive continental margin and along the South American passive continental margin are marked by red rectangles.

These segments have different characteristics concerning their evolution and structural configuration. Particularly, the Central Segment and the Southern Segment can be differentiated as follows: On the one hand, the stratigraphic record varies between both segments because there are evaporite deposits along the margins of the Central Segment, while there are no indications for salt within the basins of the Southern Segment (Karner and Gambôa, 2007; Mohriak et al., 2008; von Nicolai et al., 2013). On the other hand, the

segments can be differentiated according to their crustal architecture into magma poor and magma dominated margins. The magma poor margins, such as in the Central Segment, are characterised by extreme crustal thinning and mantle exhumation (Reston and Pérez-Gussinyé, 2007; Reston, 2009), and there is evidence of a polyphase rifting evolution (Lavier and Manatschal, 2006; Péron-Pinvidic et al., 2007; Blaich et al., 2011).

By contrast, the margins of the Southern Segment can be defined as magma dominated margins. Typical for magma dominated margins are high seismic velocities in the lower crust interpreted as being caused by the presence of igneous rocks (Eldholm et al., 2000; White et al. 2008; Blaich et al., 2011). Enhanced decompression melting by mantle upwelling and accretion of magmatic material during breakup are proposed to be the origin of these igneous rocks (White and McKenzie, 1989; Mjelde et al., 2009). According to investigations by e.g., Maystrenko et al. (2013) for SW Africa, and Autin et al. (2015) for Argentina, such lower crustal bodies (LCBs) occur along both margins that are investigated in this study. Apart from the processes in the lower crust, magma dominated margins also have a volcanic character onshore. Along the continental margins of the southern South Atlantic area, large igneous provinces were emplaced in Africa and South America; the so-called Paraná-Etendeka continental flood basalts (Peate, 1997). Offshore, extrusive manifestations of this magmatic event are observed as seaward dipping reflectors (SDRs). These occur offshore Argentina (Hinz et al., 1999, Franke et al., 2006), Namibia (Bauer et al., 2000; Koopmann et al., 2013, Talwani and Abreu, 2000) and South Africa (Blaich et al., 2009; Hirsch et al., 2009).

Additionally, the strongly thinned crust is typical for the volcanic margins offshore SE South America and SW Africa (e.g., Gladczenko et al., 2008; Franke et al., 2006; Autin et al., 2013; Maystrenko et al., 2013). Due to extensional forces during the breakup of Gondwana, the continental crust was stretched to about $^1/_2$ in average, and locally to less than $^1/_3$ compared to the crust which has not been affected by stretching. This information leads to the assumption that these margins underwent a complex subsidence history as the lithosphere successively cooled creating basins which were then filled by sediments that in turn also affected the subsidence history.

The quantification of the subsidence history certainly also depends on the assumed duration of the post-rift phase. Several kinematic studies address the opening of the South Atlantic Ocean (Rabinowitz and LaBrecque, 1979; Moulin et al. 2010; Heine et al., 2013) using information about ocean spreading and magnetic anomalies, and therefore delivering new insights on the opening procedure of the South Atlantic Ocean in a large scale frame. Combining this

knowledge with a most recent timescale (Cohen et al., 2013) the time-component in subsidence reconstruction is constrained.

Due to complex physical processes along passive continental margins, modelling the subsidence evolution is not simple. On the one hand this complexity is related to the thermal cooling of the lithosphere (McKenzie, 1978; Stein and Stein, 1992); and on the other hand, it is related to isostasy due to deposition of sediments (Watts and Ryan, 1976).

While thermal cooling and isostatic readjustment can be solved analytically for a 1D case that already yields plausible results, it becomes more difficult for 2D and 3D cases. More sophisticated modelling approaches therefore attempt to find numerical solutions for geodynamic questions for 2D, and even 3D cases.

Huismans and Beaumont (2011) modeled the evolution of passive margins and distinguish between narrow and ultra-wide passive continental margins, such as in the North- and South Atlantic, respectively, by means of 2D finite-element numerical solutions. By contrast, Burov and Gerya (2014) found a 3D numerical solution that considers the mantle lithosphere interaction in order to simulate the topographic evolution affected by a mantle plume. For the African continent, a scenario of convective circulation in the deep mantle beneath the African plate is proposed using a different approach of modelling the mantle flow driven by thermochemical density variations, that are inferred from seismic and geodynamic data, to explain the change in the dynamic topography of Africa (Moucha and Forte, 2011). Besides, this study is in agreement with investigations by e.g., Roberts and White, (2010) or Paul et al. (2014) explaining the dynamic topography of Africa by analysing river profiles.

The self-consistent thermo-mechanical models integrate processes and mechanisms in 2D and 3D. These approaches give also suggestions for the processes deep in the mantle, affecting the subsidence evolution of the passive margins. However, they do not consider the structural configuration observable at the present-day. This limitation ignores that the uppermost part of the lithosphere is affected by the additional loading of sediments in a specific and not only generic way.

Using geological knowledge of the South Atlantic margins (such as present-day information about the sedimentary configuration, crustal and lithospheric mantle configuration and their corresponding physical properties) and physical principles (in 1D and 3D) describing margin evolution related processes, this study aims at the understanding of the subsidence evolution of the South Atlantic passive continental margins. So far, such a comprehensive study has not

been conducted. In order to provide a structural overview of this thesis, a major question with further sub-questions will be addressed within the next chapter.

1.3 Objective of the thesis

The main goal of this thesis is to understand the subsidence evolution of the South Atlantic passive continental margins by using present-day information about the margins structural configuration and to derive conclusions on vertical movements (subsidence and uplift), inferred from restored paleobathymetries, during the post-rift phase. Accordingly, the main question at the base of this study is the following:

"What is the (post-rift) subsidence evolution of the South Atlantic margins inferred from information about the present-day structural configuration?"

To find an answer to this general question, three further questions are addressed dividing the main questions into three parts that are discussed in the Chapter 2, 3 and 4. Each of these sub-questions is necessary to achieve the main goal of this thesis:

- Part I: *"How did the paleobathymetry of the SW African margin evolve during the post-rift phase?"*
- Part II: *"What is the paleobathymetric evolution of the Colorado Basin, offshore Argentina, during the post-rift phase and is it comparable to the evolution of the Orange Basin, offshore SW Africa?"*
- Part III: *"What would a dynamic thermo-mechanical forward modelling approach considering the syn-rift phase predict for the margin evolution of SW Africa since the breakup of Gondwana?"*

For a better specification of each of the three parts, the following questions are addressed according to the individual issues that were treated by the questions of part I, II and III:

Part I:

- *How can the present-day structural configuration of the sedimentary succession and the crust be used to reconstruct paleobathymetries?*
- *What is the effect of the load induced by the sediments on the subsidence history?*
- *What is the effect of the thermal relaxation of the lithosphere on the margin evolution?*
- *Is it possible to quantify past vertical movements along the SW African margin using paleobathymetries?*
- *Is it possible to derive conclusions on processes inducing uplift/subsidence of the SW African margin and the African continent?*

Once the SW African margin has been investigated with a multi 1D backward modelling approach in part I, this method is also used to reconstruct paleobathymetries and to infer the subsidence evolution along the SE South American margin. Furthermore, the subsidence evolution of SW Africa is compared to the evolution along the SE South American margin. Accordingly, the second part of this work is based on the following questions:

Part II:

- *How do the paleobathymetries of the Colorado Basin evolve regarding their subsidence history?*
- *Are there similarities/differences between the subsidence histories of the conjugate margins (using information about the Colorado Basin and Orange Basin)?*
- *If there are differences, are they related to the sediment supply or to the thermal relaxation of the lithosphere?*
- *Are there possible explanations for the similarities/differences between both margins in terms of causative processes responsible for their characteristic evolution?*

Part I and part II provide first new insights about the margin evolution of the post-rift phase and lead to assume that the SW African margin was affected by a mechanism causing uplift.

The work of part I and part II is the result of a multi 1D analytical solution focusing on the post-rift phase and so far does not yet consider the syn-rift phase. Consequently, these results might depend on the syn-rift phase and/or on the 1D analytical approach. To validate the results of the 1D analytical approach, a 3D forward modelling technique is used. This technique couples thermo-mechanical processes and considers the syn-rift phase. Correspondingly, the following questions can be formulated:

Part III:

- *What is the thermal evolution of the SW African margin?*
- *How does the thermal evolution affect the rigidity/strength of the lithosphere and therefore its flexural behavior in response to sediment deposition?*
- *What is the amount of vertical movements along the SW African margin assuming 3D thermo-mechanical forward modelling?*

1.4 Overview of the thesis

Chapter 2 has been published in the journal "Marine and Petroleum Geology" while Chapter 3 is submitted to the journal "Tectonophysics – Passive margins Special Issue". Chapter 4 has been accepted for publication in the journal "Arabian Journal of Geosciences – ILP Special Issue".

Within this chapter, the work done is explained briefly and linked to the questions raised in the preceding chapter. In addition, this chapter details my own contribution and the contribution of my co-authors.

Chapter 2 – Reconstruction of the southwestern African continental margin by backward modelling

This paper provides an answer to the question on the paleobathymetric evolution of the SW African margin during the post-rift phase. It therefore presents a detailed description on how present-day information about the structural configuration of the margin can be used to reconstruct paleobathymetries. Accordingly, individual subsidence components are calculated

and subsequently interpreted to understand the effects of the thermal- and load induced subsidence on the margin in the first instance and to restore paleobathymetries in a second step. The paleobathymetries are then used to quantify a minimum estimate of vertical uplift. Finally, these results lead to a discussion in terms of seafloor uplift and probable causative processes.

As the first author, I conducted the modelling to calculate both the amount of load induced subsidence and the amount of thermal subsidence. I also restored the paleobathymetries and finally, wrote the text and prepared the figures. This work is based on discussions with my co-authors M. Scheck-Wenderoth, M. Cacae, B. Lewerenz, H.-J. Götze and C. Reichert. M. Scheck-Wenderoth and M. Cacace supported me with advice during the modelling and in setting up my first publication.

After a peer-review process by "Marine and Petroleum Geology", this manuscript was published as:

> Dressel, I., Scheck-Wenderoth, M., Cacace, M., Lewerenz, B., Götze, H.-J., Reichert, C. (2015) Reconstruction of the southwestern African continental margin by backward modelling. Marine and Petroleum Geology 67, 544-555.
> doi:10.1016/j.marpetgeo.2015.06.006

Chapter 3 – Backward modelling of the subsidence evolution of the Colorado Basin, offshore Argentina and its relation to the evolution of the conjugate Orange Basin, offshore SW Africa

The second paper summarises the investigations on the western passive continental margin of the South Atlantic Ocean. To infer the paleobathymetric evolution from the present-day, the same method as in Chapter 2 is applied to keep a comparability between the conjugate passive continental margins. After calculating the load induced subsidence and the thermal subsidence, the paleobathymetries of the Colorado Basin are restored. According to the new

insights on this paleobathymetric evolution, the results are then compared to the subsidence evolution of the Orange Basin, offshore SW Africa, to detect similarities and/or differences. As differences in the evolution between both margins are found, they are discussed with respect to individual subsidence components. Finally, a hypothesis is proposed that explains these differences which occur even though the research areas are located in a conjugate margin setting. This hypothesis is based on a discussion focusing on probable geodynamic processes affecting both margins.

The modelling part of the individual subsidence components was done by myself. Additionally, I interpreted the results and drew the conclusions, with minor contributions by M. Scheck-Wenderoth and M. Cacace. The text was written by myself with minor advices by my co-authors.

The corresponding manuscript is submitted to "Tectonophysics – Passive margins Special Issue" as:

> Dressel, I., Scheck-Wenderoth M., Cacace, M. (submitted) Backward modelling of the subsidence evolution of the Colorado Basin, offshore Argentina and its relation to the evolution of the conjugate Orange Basin, offshore SW Africa.

Elsevier is kindly acknowledged since this submitted manuscript is used in this dissertation for non-commercial purposes.

Chapter 4 – Coupled thermo-mechanical 3D subsidence analysis along the SW African passive continental margin

Since the preceding chapters indicate seafloor uplift along the SW African margin but not offshore Argentina, the SW African margin is further investigated using a 3D dynamic thermo-mechanical forward modelling approach. This approach and the resulting prediction for the margin evolution offshore SW Africa is described in Chapter 4. Similar to the work

before, the modelling is based on present-day information about the structural configuration of the SW African margin.
In accordance with the approach used, this chapter focuses on the syn-rift and post-rift phases. As a result, the evolution of the thermal field and the subsidence evolution of the margin are presented. Particularly the results on the thermal evolution are worthwhile because the thermal field affects the rigidity/strength of the lithosphere, and therefore the loading stage of the margin in terms of isostasy. Finally, by considering the coupling between thermal evolution and the isostatic readjustment, paleobathymetries are reconstructed and consequently, new insights on the amount of vertical movements are derived.
This work also presents the consequence the reconstructed thermal evolution has on the maturation of organic matter in relevant source rocks by tracing the oil window through time.

The modelling is done by myself using an existing code for numerical modelling by M. Cacace, and the results have been discussed with my co-authors. I prepared the figures and the text with minor contributions by my co-authors M. Cacace and M. Scheck-Wenderoth.

After a peer-review process by ”Arabian Journal of Geosciences”, this manuscript was published in the ILP Special Issue as:

> Dressel, I., Cacace, M., Scheck-Wenderoth, M. (accepted) Coupled thermo-mechanical 3D subsidence analysis along the SW African passive continental margin. Arabian Journal of Geosciences.
> doi:10.1007/s12517-016-2407-9

Springer is kindly acknowledged since the accepted article is used in this dissertation for non-commercial purposes.

Chapter 5 – Final discussion
This chapter presents a cumulative discussion in the context of the evolution of the South Atlantic passive margins in order to interrelate the individual results of the preceding

chapters. Additionally, the possible limitations of the approaches used are discussed with suggestions for future work in the South Atlantic and modelling passive margins in general.

Chapter 6 – Conclusions

This chapter summarises the major outcome of this thesis and provides an answer to the main question of the thesis.

Chapter 7 – References

All references used in each of the individual chapters of this thesis are consolidated in this chapter.

Chapter 8 – Acknowledgements

I am grateful to many people for their support during the last three years whom I would like to thank within this chapter.

Chapter 9 – Appendix

The appendix contains a list of publications and conference contributions related to this work.

2 Reconstruction of the southwestern African continental margin by backward modelling

Abstract

As the evolution of the SW African passive continental margin and in particular, the vertical movements in this area are still a matter of debate, this study aims to quantify the past vertical movements by reconstructing the paleobathymetric evolution of the SW African margin during the post-rift phase. To quantify the vertical movements, inferred from paleobathymetries, different subsidence components that have affected the passive continental margin are calculated and interpreted with respect to the generating processes.

Our investigation takes advantage of information on the present-day sedimentary thicknesses and the crustal configuration along the SW African margin. By using this detailed information and modelling backward in time we attempt to separate different subsidence components such as the load induced subsidence and the thermal subsidence for different time intervals during the post-rift phase. Calculating the amounts of each subsidence component and subtracting them from the present-day configuration yields paleobathymetries which are interpreted with respect to the evolution of the SW African passive margin.

These restored paleobathymetries for different time steps during the post-rift phase indicate spatial and temporal variations of vertical movements including phases of seafloor uplift. As a result, our investigation allows to give minimum estimates of the vertical movements that have occurred during the post-rift phase. In addition to predominant subsidence, about 1000 m of seafloor uplift are deduced for the northern and southern parts of the SW African margin. Quantifying the amounts of vertical movements cannot finally clarify the generating processes behind these movements but the timing and magnitude of seafloor uplift indicates a deep mantle mechanism.

2.1 Introduction

The SW African continental margin, located in the South Atlantic Ocean, includes three major basins: the Walvis Basin, Lüderitz Basin and Orange Basin (Figure 2.1). It extends from north to south for about 1650 km, being limited by the Walvis Ridge in the north and the Agulhas Falkland Fracture Zone further south. The formation and evolution of the margin is

structurally related to the opening of the Atlantic ocean, which can be traced back to the continental separation of the Gondwana supercontinent during Late Jurassic-Early Cretaceous times (e.g., Nürnberg and Müller, 1991; Broad et al., 2006). During the last decade, an increasing number of studies have focused on the southwestern African continental margin with the aim of improving the current understanding of the processes responsible for its tectonic evolution and their relevance for the formation and maturation of hydrocarbon resources. A non-exhaustive list comprises: (1) seismic investigations (e.g., Gladczenko et al., 1998; Bauer et al., 2000, 2003; Weigelt and Uenzelmann-Neben, 2007; Fernàndez et al., 2010; Kuhlmann et al., 2010; Hartwig et al., 2012; Koopmann et al., 2013), (2) potential field modelling (Stewart et al., 2000; Hirsch et al., 2007; 2009; Maystrenko et al., 2013), (3) dating of vertical movements by sequence stratigraphy and geochemical dating methods (Light et al., 1993; Brown et al., 1995; Holtar and Forsberg, 2000; McMillan, 2003; Broad et al., 2006; Paton et al., 2007; Trumbull et al., 2007; Kuhlmann et al., 2011), (4) kinematic analysis (Will and Frimmel, 2013) or (5) a combination of several techniques (e.g., Paton et al., 2008; Hirsch et al. 2010).

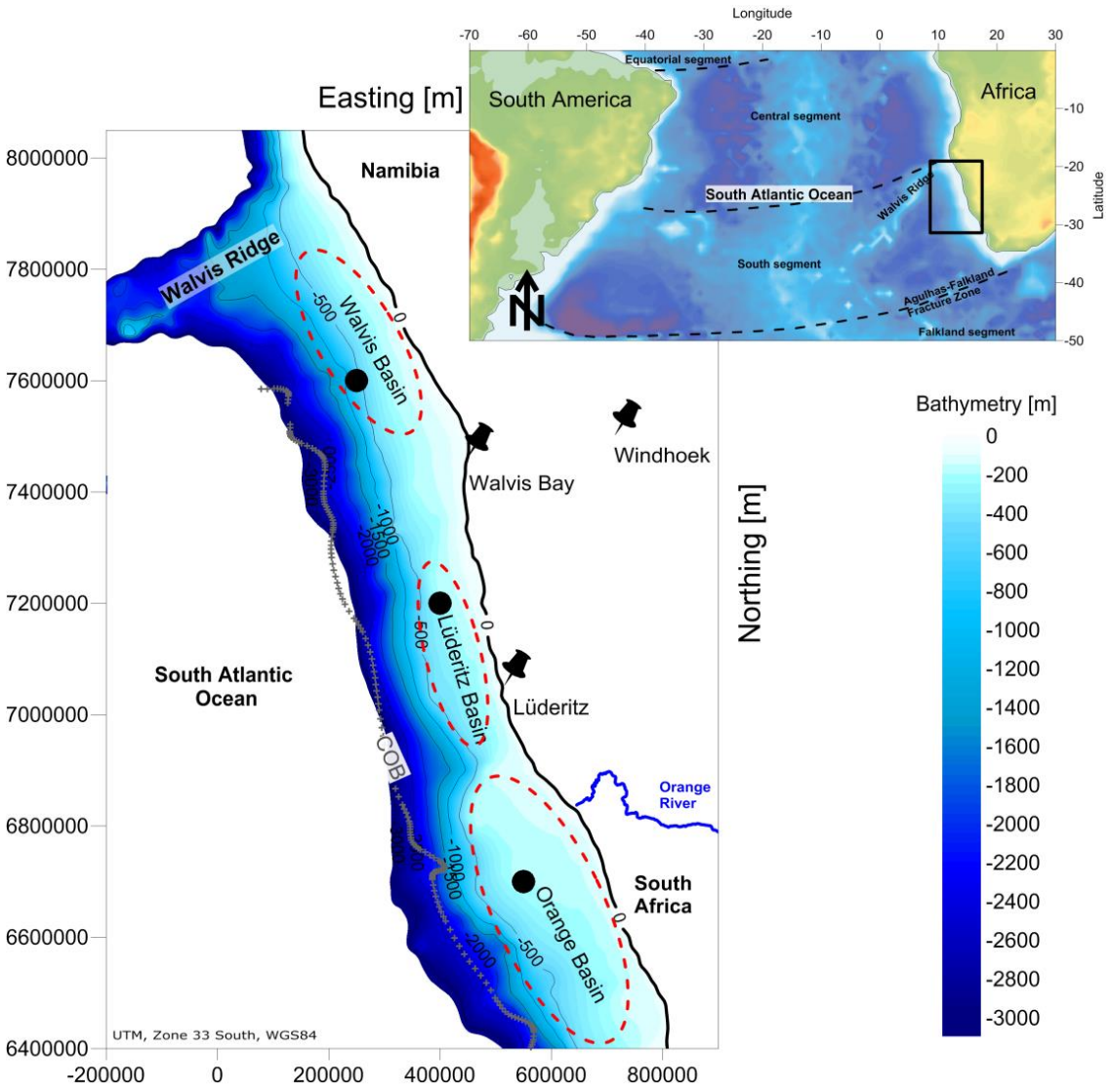

Figure 2.1: Overview of the research area, the continental margin of southwestern Africa (bathymetry after IOC, IHO and BODC, 2003). The red ellipses show the location of the sedimentary basins. The grey dotted line indicates the continent-ocean boundary (COB; after Pawlowski, 2008). The black dots mark the location of synthetic wells used in Figure 2.6. Coordinate system is UTM [m], zone 33 south (WGS 84). Inset: Overview of the South Atlantic Ocean with location of the research area (black box) in geographical coordinates.

The sedimentary basins of the SW African continental margin store the archive of the margin history. The goal of our study is to use this archive as a starting point for investigating the margins evolution during the post-rift phase (the last 125 Ma) by a modelling approach backward through time. Therefore, we use information about the present-day structural

configuration along the SW African margin between the coast and the continent-ocean boundary after Maystrenko et al. (2013).

Our backward modelling approach considers individual subsidence components such as the load induced subsidence and the thermal subsidence. The amount of load induced subsidence is calculated with a multi 1D "backstripping" approach while we calculate the amount of thermal subsidence after the uniform stretching model of McKenzie (1978). These subsidence components are then subtracted from the present-day bathymetry in order to reconstruct paleobathymetries. An in-house software (GeoModellingSystem (GMS), developed at the Helmholtz Centre Potsdam (GFZ); Scheck and Bayer, 1999) is used to assist our modelling of the subsidence evolution of the continental margin.

In particular, our approach differs from the established "backstripping" in that we do not prescribe a certain paleo-water depth but restore the latter.

Worth mentioning is that we do not prescribe any tectonic component in addition to cooling of a stretched lithosphere within the reconstruction, nor uplift events as proposed by e.g., Séranne and Anka (2005) or Colli et al. (2014). Nevertheless, we are able to estimate the magnitude of vertical movements by analysing the reconstructed paleobathymetries. The resulting paleobathymetries help to understand the first-order margin evolution in terms of subsidence and seafloor uplift. We discuss the implications of these results with respect to previously published information on paleobathymetries and derive conclusions for the processes responsible for this evolution.

2.2 Data

The 3D structural model used to carry out our investigation has a horizontal resolution of 5 km and resolves six different geological units. Information about the configuration of the subsurface are mainly taken from Maystrenko et al. (2013), which means that our analysis considers from top to bottom: the water column, four sedimentary sequences and a crystalline crust. The four sedimentary sequences are confined by the horizons representing major unconformities. Post-rift phase III is confined by the base Cenozoic and the seafloor, post-rift phase II by the base Turonian and the base Cenozoic whereas the post-rift phase I is confined by the base Aptian and the base Turonian. The base Aptian represents the unconformity above the syn-rift sediments that extend downward to the top crystalline basement. Lithology-dependent physical rock properties (e.g., density, compaction factors and porosity) are

assigned uniformly to each sedimentary unit to enable the calculation of porosity dependent rock densities throughout the reconstruction process (Table 2.1).

In contrast to Maystrenko et al. (2013), we define the crystalline crust as a single layer between the base of the syn-rift sediments and the Moho. This simplification is made because we focus on the post-rift phase so that the detailed crustal configuration is not crucial as long as the thickness and density distribution is known. To derive the isostatic rebound related to the load of the sediments we first calculate a laterally varying density for the crystalline crust that is in isostatic equilibrium with the sediment load and the Moho (crust-mantle boundary) assuming Pratt isostasy (Pratt, 1855; Figure 2.2). Our reference model for the corresponding calculation uses 2850 kg/m³ for the crustal density, 3300 kg/m³ for the mantle density and a compensation depth of 35 km. The resulting densities (Figure 2.2) are largely consistent with the lateral variations of densities and the distribution of high-density bodies beneath the margin as derived from 3D gravity modelling and deep seismic information (Maystrenko et al., 2013). This implies that the density of the crystalline crust does not change during the post-rift phase, but was established syn-rift.

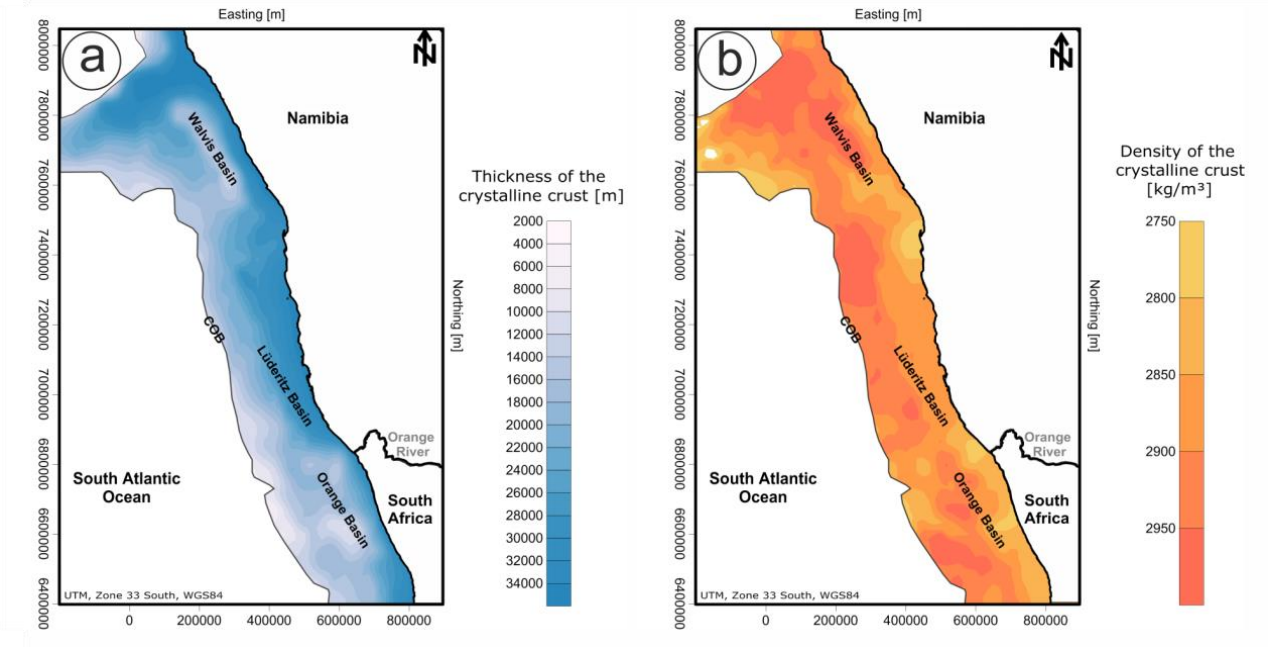

Figure 2.2: (a) Thickness (after Maystrenko et al., 2013) and (b) density distribution of the entire crystalline crust along the SW African margin. See text for detailed description on how the laterally varying density distribution is calculated.

Throughout the sedimentary succession clastic sediments such as sandstone, siltstones and claystones dominate as well as a few shales and subordinate limestones (Table 2.1). The set of properties considered for the different sedimentary units is consistent with previous stratigraphic investigations of Holtar and Forsberg (2000) for the Walvis Basin and with studies by Brown et al. (1995), Hirsch et al. (2007) and Paton et al. (2007) for the southern area, especially the Orange Basin. Complementary, information on lithologies for the entire Namibian margin given by Light et al. (1993) are also considered.

Table 2.1: Names, prevailing lithologies, ages, and assigned physical properties of the individual units used in this study for "backstripping" as well as for the calculation of the thermal subsidence (after Sclater and Christie, 1980; Holtar and Forsberg, 2000; Broad et al., 2006; Paton et al., 2007; Hirsch et al., 2007, 2010; Cohen et al., 2013; Maystrenko et al., 2013).

Name of individual units	Stratigraphic range of individual units	Modified ages of the units [Ma]	Prevailing lithologies used in this study	Matrix Density [kg/m³]	Initial Porosity	Com-paction factor
Seawater				1030		
Post-rift III	Seafloor to base Cenozoic	0-67	Clay; Shale; Sandstone	2720	0.63	0.51
Post-rift II	Top Maastrichtian to base Turonian	67-93	Sandstone; Siltstone	2670	0.56	0.39
Post-rift I	Top Cenomanian to base Albian	93-125	Sandstone (clay rich); Shale	2680	0.51	0.33
Syn-rift	Top Aptian to base sediments		Sandstone; Limestone; Volcanics	2740	0.4	0.2
Crystalline crust				2750-3000		
Lithospheric mantle				3300		

In order to constrain our reconstruction of paleobathymetries to ages, the chronostratigraphic subdivision by Broad et al. (2006; Table 2.1) is used with a modification for the timing of the

breakup (base Aptian) according to the most recent timescale of Cohen et al. (2013). Therefore, we define our post-rift phase I from 125-93 Ma (base Aptian – base Turonian), post-rift phase II from 93-67 Ma (base Turonian – base Cenozoic) and post-rift phase III from 67-0 Ma (base Cenozoic – present-day).

2.3 Method

2.3.1 Load induced subsidence

To calculate the load induced subsidence we apply a "backstripping" procedure during which we remove the sediments successively. Data used for "backstripping" are taken from the 3D structural model of the present-day SW African margin by Maystrenko et al. (2013). Our "backstripping" approach considers isostatic readjustment in response to variations in the sediment configuration by assuming Airy isostasy (Airy, 1855). In addition to the isostatic readjustment we consider decompaction which is implemented in our "backstripping" approach based on a power-law porosity-depth relation (Athy's law; Athy, 1930) which is slightly modified to a porosity-load dependence (Scheck et al., 2003). Additionally, as a simplification, the load of the water column is considered only once in the first "backstripping" step. This simplification is justified as the present-day water depth represents the maximum water depth. Thus, the difference in subsidence due to repeated removing and refilling of water would be small. Moreover, we do not prescribe any paleo-water depth as in the classical "backstripping" but aim to derive the magnitude of subsidence due to loading only.

The result of the successive steps of isostatic readjustment and decompaction is an upward movement of the remaining units and correspondingly yields a respective "backstripped" surface. Calculating the difference between the successive restored surfaces provides the amount of load induced subsidence for the time interval in between the corresponding surfaces (Figure 2.3).

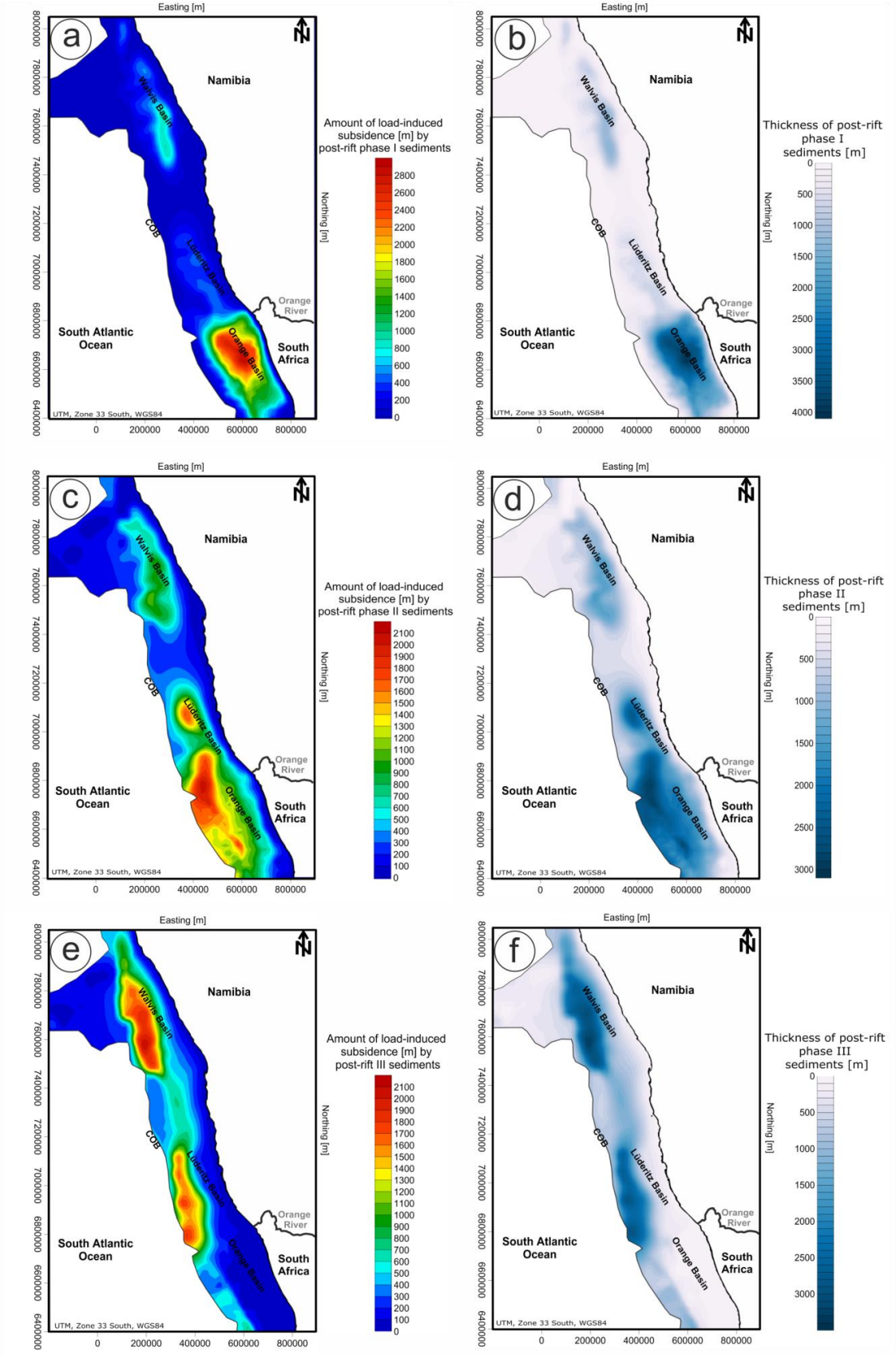

Figure 2.3: Amount of load induced subsidence (a, c, e) in comparison with sediment thickness (b, d, f). a) Amount of load induced subsidence caused by the Turonian-Aptian

sediments. b) Thickness of the Turonian-Aptian sediments (after Maystrenko et al., 2013). c) Amount of load induced subsidence caused by the Cenozoic-Turonian sediments. d) Thickness of the Cenozoic-Turonian sediments (after Maystrenko et al., 2013). e) Amount of load induced subsidence caused by the Cenozoic sediments. f) Thickness of the Cenozoic sediments (after Maystrenko et al., 2013).

2.3.2 Thermal subsidence

The so far described backward in time reconstruction accounts for the vertical movement induced by mechanical loading by sedimentation and rock compaction but it does not incorporate any thermal effects on the resulting subsidence. We integrate the latter component following the uniform stretching model as described by McKenzie (1978). Therefore, the amount of subsidence obtained after each step of our "backstripping" approach is corrected by adding the thermal subsidence component corresponding to the considered time interval. The latter is mainly controlled by the stretching factor β (Figure 2.4). This parameter has been obtained from the ratio between the thickness of the un-stretched crustal domains, i.e., areas not affected by any rifting process, and the present-day crustal thickness derived from our 3D structural model (Figure 2.2). The value chosen for the initial crustal thickness is 35 km as observed in seismic data (e.g., Gladczenko et al., 1998; Bauer et al., 2000) onshore SW Africa along the coast where the crust has not been affected by stretching.

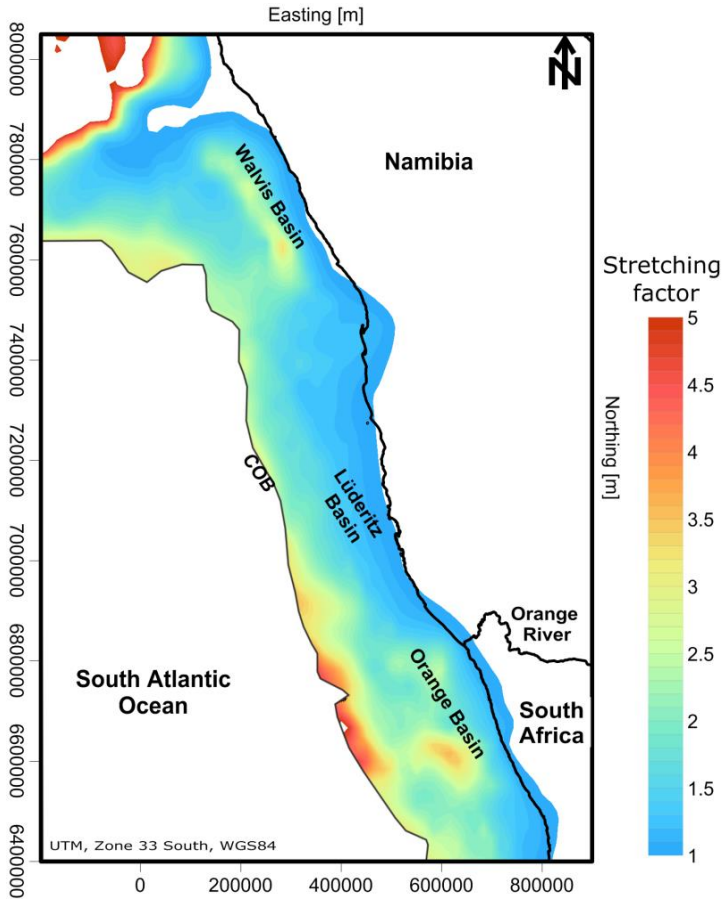

Figure 2.4: Distribution of crustal stretching factor β. The areas of the Walvis and Orange Basin are characterised by large stretching factors (ranging between 1.5 < β > 3.5).

We assume an air-filled basin in the McKenzie equation because we consider the effects of sediment/water loading with the separate "backstripping" approach.

The reason behind our choice of using the model by McKenzie (1978) stems from its simplicity. Indeed, a more detailed investigation would have required a more sophisticated approach to couple in time the thermal and mechanical processes during the evolution of the margin. However, such a detailed analysis is beyond the current scope of our investigation, which aims at a first-order assessment of the vertical movements during the post-rift phase.

Figure 2.4 illustrates the variations of the stretching factor considered in the present study and shows that the stretching factor increases from east to west with a parallel trend to the coast. There are two areas, which show significantly higher stretching factors than their surroundings: The Walvis Basin in the north with stretching factors up to 3.0 and the Orange Basin in the south where stretching factors of up to 3.5 are calculated.

In response to these variations in stretching magnitude, laterally variable amounts of thermal subsidence are calculated (Figure 2.5).

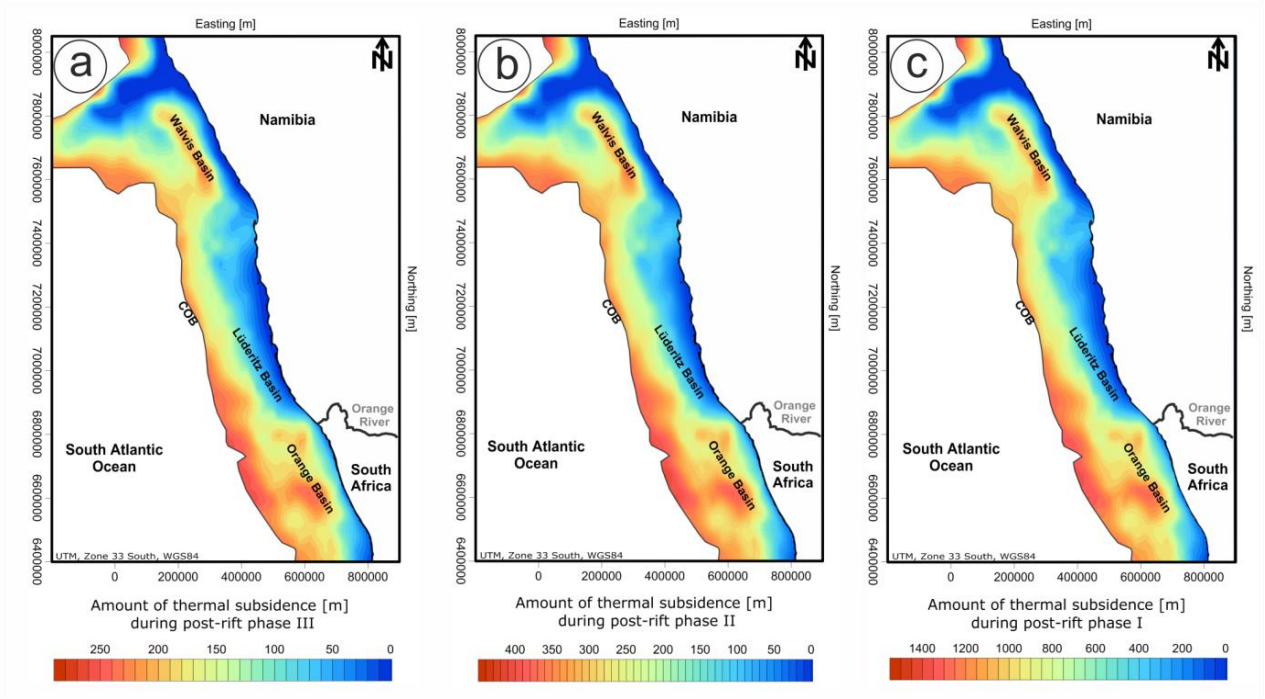

Figure 2.5: Thermal subsidence calculated for three time intervals during the post-rift phase. a) Amount of thermal subsidence during post-rift phase III. b) Amount of thermal subsidence during post-rift phase II. c) Amount of thermal subsidence during post-rift phase I. Although the time intervals vary in duration it is obvious how the margin area is affected by thermal subsidence during the post-rift phase: The largest amount of thermal subsidence took place during the post-rift phase I (c) and subsidence decreases throughout the younger phases (b, a). The areas of the Walvis Basin in the north and the Orange Basin in the south are characterised by larger amounts of thermal subsidence than their surroundings, in response to variations of initial stretching.

2.3.3 Paleobathymetries

In general, the paleobathymetries are derived by "backstripping" a unit of the 3D model, considering decompaction of the underlying units and correcting the resulting top surface by the respective amount of thermal subsidence (Figure 2.5). To derive the paleobathymetry at 67 Ma, we firstly "backstripp" the Cenozoic sediments and the water column. The resulting "backstripped" surface is then corrected for the amount of thermal subsidence calculated for

post-rift phase III (0-67 Ma). The second post-rift paleobathymetry at 93 Ma is calculated by additionally "backstripping" the post-rift phase II sediments and correcting the resulting "backstripped" surface for the amount of thermal subsidence lasting from 67-93 Ma. Finally, the paleobathymetry at 125 Ma is reconstructed by "backstripping" post-rift phase I sediments and correcting the "backstripped" surface by the amount of thermal subsidence of post-rift phase I (93-125 Ma).

2.4 Results

2.4.1 Load induced subsidence

Figure 2.3 shows the amount of the load induced subsidence for the three post-rift phases together with the corresponding maps of preserved sediment thicknesses. Post-rift phase I is marked by significant subsidence localized preferentially in the Orange Basin. The load induced subsidence obtained in this basin amounts up to 2950 m, being significantly larger than the load induced subsidence calculated for the other two sub-basins (550 m in the Lüderitz Basin and 980 m in the Walvis Basin). Post-rift phase II shows a similar trend to the previously described stage. The core of subsidence is still observed in the Orange Basin (up to 2080), while minor amounts of load induced subsidence occurred in the other two depocentres (though showing increased magnitudes with respect to the previous stage; Lüderitz Basin: 1780 m, Walvis Basin: 1140 m). A change in the subsidence pattern is evident for the subsequent post-rift phase III. Within this time window, the subsidence centre shifts to the northern portion of the study area with the maximum load induced subsidence observed in the Walvis Basin (up to 2110 m). Additionally, subsidence is no longer localized beneath the three major basins only, as documented by a new depocentre located westward of the former basin area.

The observed change in the load induced subsidence pattern during the post-rift phase can be reconciled by variations in the style and amount of sedimentation as illustrated by the sediment thickness maps in Figure 2.3. Accordingly, the main depocentre is located in the south during post-rift phase I and near to the coast close to the Orange River while the thickness of post-rift phase II indicates a slightly seaward shifted depocentre as well as increasing subsidence in the northern areas. Since the Cenozoic, the main depocentres are found in the north, which might be related to a decrease in sediment supply by rivers in the southern areas or changes in location of the river mouth (Dingle and Hendey, 1984).

Additionally, the depocentres migrate seaward, both in the north and the south, which could be caused by sea level lowering and therefore reduction of accommodation space. Furthermore, ocean currents may have influenced lateral sediment transport (Schut and Uenzelmann-Neben, 2005).

2.4.2 Thermal subsidence

Figure 2.5 shows the amounts of thermal subsidence calculated for the three different post-rift phases. According to the formulation used, the thermal subsidence decays exponentially with time as the lithosphere cools during its evolution.

Not surprisingly, the overall spatial pattern of the calculated thermal subsidence shows close resemblances to the spatial variations of the stretching factor, with higher amounts of thermal subsidence correlating with domains characterised by stronger lithosphere thinning. Consequently, the Orange Basin and Walvis Basin areas experienced the largest and spatially most extended amount of subsidence, while only minor subsidence is observed beneath the Lüderitz Basin.

The above-described trend in thermal subsidence is evident during all three post-rift phases considered. Post-rift phase I shows significant amounts of thermal subsidence within the Walvis Basin (up to 1200 m) and in the Orange Basin (up to 1300 m), whereas post-rift phase II is characterised by about 350 m of thermal subsidence in the Walvis Basin and 400 m in the Orange Basin, respectively. Finally, we obtain about 200 m of thermal subsidence during the last 67 Ma of the post-rift phase III in the Walvis Basin and about 250 m of thermal subsidence in the Orange Basin with slightly lower amounts of thermal subsidence in the Lüderitz Basin.

2.4.3 1D synthetic subsidence

To better illustrate the interplay between load induced subsidence, thermal subsidence and their individual effects on the total subsidence, Figure 2.6 shows 1D subsidence curves for three synthetic wells located in the major sedimentary basins (Walvis Basin, Lüderitz Basin, Orange Basin). The well locations are chosen such that they intersect the sediments where

they are thickest. Therefore, the change of the sediment depositions through time is considered.

As shown in Figure 2.6 the thermal effects play only a minor role in affecting the overall deformation. On the one hand, this can be related to the assumptions included in our formulation (i.e., 1D McKenzie model does not account for lateral heat dissipation, internal radiogenic heat production within the different layers or for thermal blanketing effects by sediments). On the other hand, the observed subsidence pattern is easily explained in terms of the thickness of the sediments (up to a total of ~8000 m during the entire evolution) which characterise the whole study area.

In addition, the curves clearly show the differences in subsidence between the three major basins, which is related to the different amounts of stretching in the subareas as well as to different amounts of sediments deposited.

The largest amount of total post-rift subsidence is evident in the synthetic well in the Walvis Basin, followed by the Orange Basin and Lüderitz Basin. By contrast, the Orange basin is characterised by the highest amount of thermal subsidence (up to a total of 1440 m) when compared to the other two locations.

Although the final amount of thermal subsidence varies only by a few meters (87 m) within the Walvis and the Orange Basin, these basins are characterised by a total post-rift subsidence, which varies strongly (a difference of up to 484 m). This observation can be explained in terms of differences in sediment deposition and therefore load induced subsidence, experienced by the two basins (6064 m in the Orange Basin; 6635 m in the Walvis Basin). Furthermore, the curves of these basins also illustrate the northward shift in sediment deposition. From the beginning of the post-rift phase I to 67 Ma before present, the Orange Basin subsides more than the Walvis Basin, this trend is a direct consequence of more sedimentation in the former area as indicated by the respective subsidence curves. At 67 Ma, the curves cross, thus indicating a change in the subsidence pattern.

In contrast to the Walvis and Orange Basin the amount of total post-rift subsidence is significantly lower (~5000 m) in the Lüderitz Basin, being the net result of less sedimentation and less lithosphere stretching.

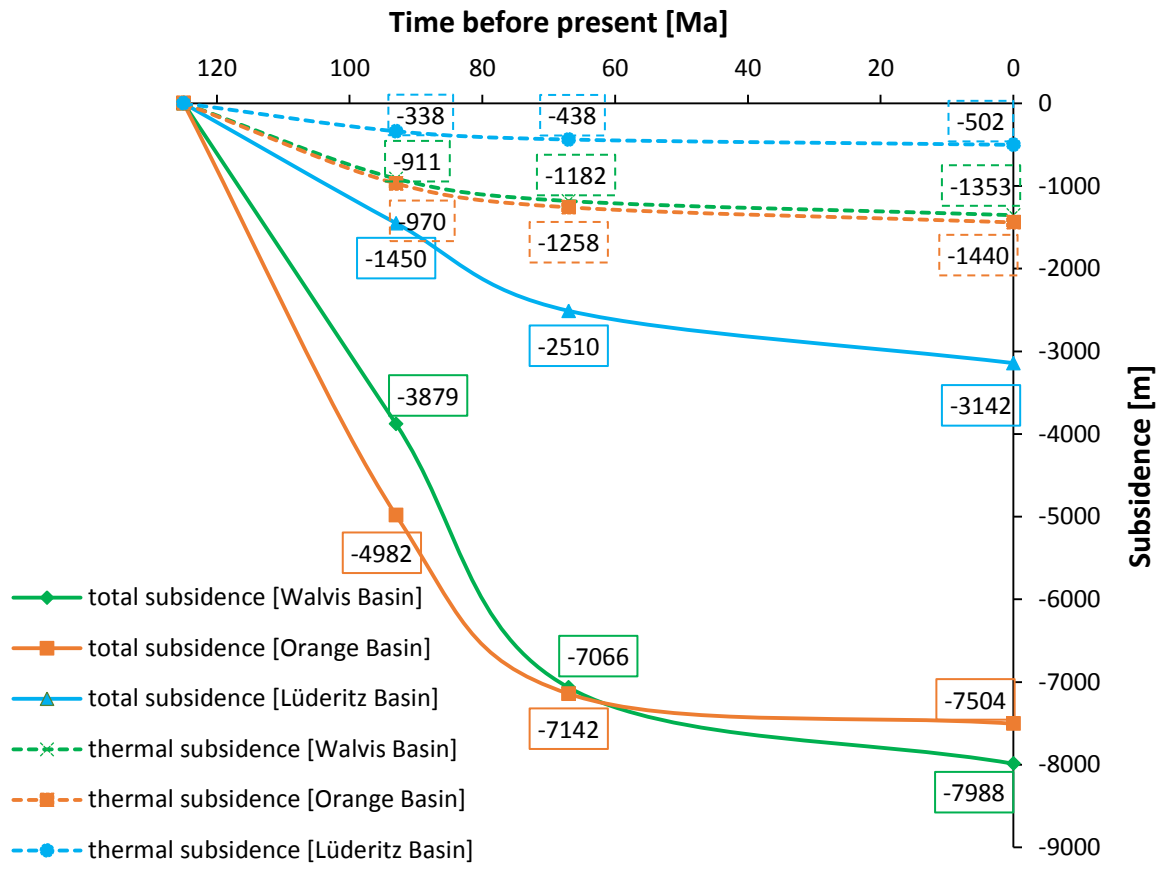

Figure 2.6: Total amount of post-rift subsidence for three synthetic wells, separated into individual subsidence components (see Figure 2.1 for location). The solid curves indicate the total amount of subsidence; the dashed curves show the thermal subsidence. The space in between the dashed and solid curves of the respective colour code marks the amount of load induced subsidence.

2.4.4 Paleobathymetries

Figure 2.7 illustrates the three paleobathymetries which have been restored for the beginning of the post-rift phase III (67 Ma), post-rift phase II (93 Ma) and post-rift phase I (125 Ma). A general decrease of the water depth from post-rift phase III (up to 2000 m) to post-rift phase I (up to 500 m) and from west to east is obtained.

In the restored paleobathymetries at 67 Ma the larger part of the margin is below sea level with a paleo-water depth ranging between a few hundred meters on the margin and up to 2000 m at the continent-ocean boundary. Locally, domains in the north and south are evident, where an elevation above sea level has been calculated. We refer to this as positive

paleotopography in the following. The second restored paleobathymetry at 93 Ma has also a few hundred meters water depth on the margin and up to 1500 m at the continent-ocean boundary. Additionally, a positive paleotopography is observed in the north as well as in the south but with higher elevation than the positive paleotopography of 67 Ma. Finally, the third paleobathymetric map at 125 Ma is characterised by less than 1000 m water depth all over the margin and strongly increased positive paleotopography, both in elevation and spatial distribution, in comparison to younger restored paleobathymetries.

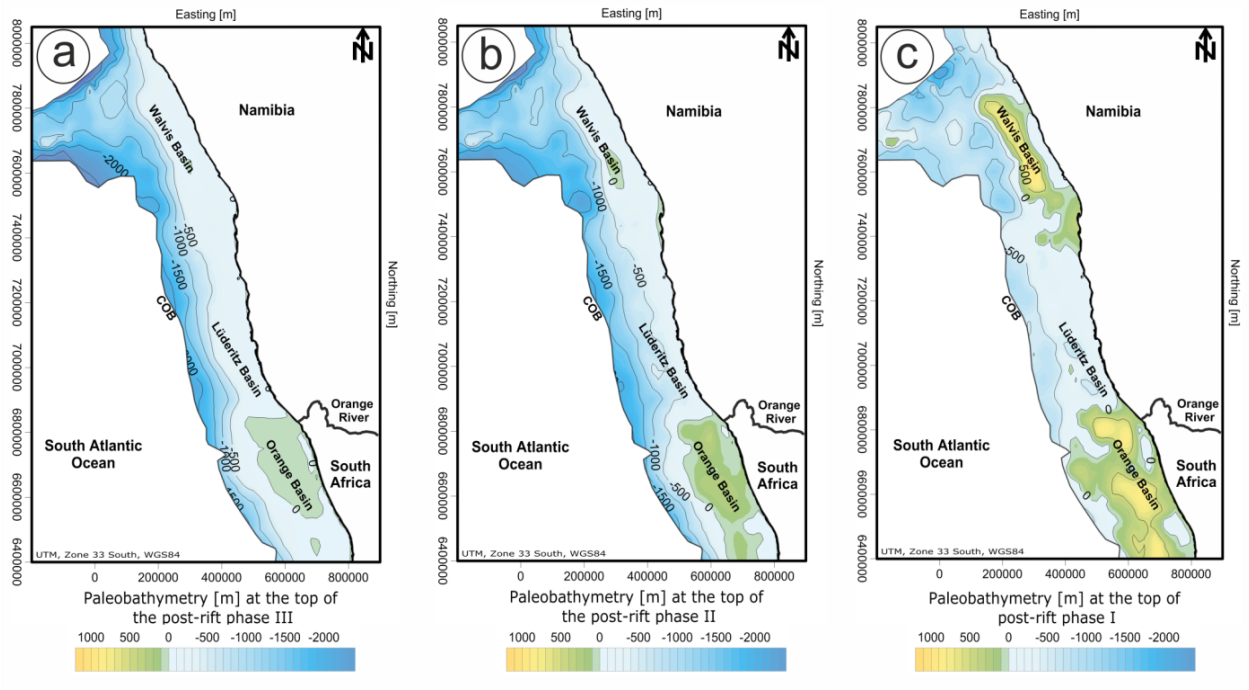

Figure 2.7: Reconstructed paleobathymetries of the southwestern continental margin for three time steps: a) post-rift phase III (67 Ma), b) post-rift phase II (93 Ma), c) post-rift phase I (125 Ma).

The restored paleobathymetries agree with the results given by the information about the individual subsidence components. Indeed, a direct correlation between the resulting paleobathymetries and the obtained amount of subsidence can be traced, with largest positive paleotopographies for periods with largest amounts of load induced subsidence. Comparing the paleobathymetries (Figure 2.7) of the Walvis Basin and the Orange Basin it is apparent that the Walvis Basin has less positive paleotopography during post-rift phase III because of a larger load induced subsidence component during the Cenozoic (Figure 2.6). Post-rift phase II

shows a positive paleotopography that is higher in the south than in the north which is consistent with the amount of load induced subsidence in the southern part at that time. By contrast, the paleobathymetry of post-rift phase I indicates a larger positive paleotopography in the Walvis Basin than in the Orange Basin.

2.5 Discussion

2.5.1 Minimum estimate of seafloor uplift

As we aim to achieve a temporal reconstruction of the vertical movements along the southwestern African continental margin, the subsidence components are used to restore paleobathymetries. This has the advantage to get insights on the margin wide evolution. The derived paleobathymetric maps allow to estimate the amount and spatial distribution of subsidence/seafloor uplift. In addition, the knowledge about the spatio-temporal change in bathymetry can be interpreted as a result of causative processes behind the vertical movements.

As our approach uses present-day data in order to have insights to the past by applying a backward modelling method, we start the discussion of seafloor uplift from the youngest time interval (post-rift phase III) to the oldest interval (post-rift phase I).

Post-rift phase III:

The restored paleobathymetry at the beginning of the Cenozoic (67 Ma; Figure 2.7a) indicates cumulative positive paleotopographic elevations of up to 115 meters above sea level (m.a.s.l.) in the Orange Basin and only 40 m.a.s.l. in the southern part of the Walvis Basin. For the Lüderitz Basin in between, a bathymetry of about -220 m.a.s.l. has been reconstructed. As the areas for which an elevation above sea level has been reconstructed were subsiding again during the Cenozoic (indicated by the preserved sediment thicknesses), the reconstructed positive paleotopography corresponds to an estimate of seafloor uplift prior to Cenozoic times. However, it is a "minimum" estimate of seafloor uplift because in our approach, we only consider the preserved sediments and do not restore any potentially eroded sediments or other tectonic processes.

Our findings, indicating seafloor uplift, confirm the investigation by Burke (1996) who suggested that the Great Escarpment surrounding Africa is a young feature due to uplift of Africa since 30 Ma. Additionally, we confirm the findings by Séranne and Anka (2005) who

propose a younger uplift event during the Cenozoic. In their study this event is interpreted to correspond to the younger so-called African Superswell during the Cenozoic (began in the Oligocene). Similar results are also shown by Colli et al. (2014), from analysing the upper mantle flow. Their proposed Oligocene-Miocene uplift is also coincident with the timing of magmatic activity onshore Africa and the emplacement of kimberlites (Jelsma et al., 2009). Finally, Stollhofen et al. (2014) suggested further uplift during younger times (Pliocene-Pleistocene) with uplift rates of about ~12 m/Ma yielding about 60 m of uplift. Although these studies focused on the onshore part of Africa while we focus on the SW African continental margin it is most probable that onshore uplift did not stop at the coastline and therefore has affected the margin as well.

Our results also confirm the findings of detailed but more local studies about Cenozoic erosion assumed to be related to uplift within the Orange Basin. From seismic stratigraphy the amount of eroded sediments has been estimated as reaching up to 750 m at the inner margin within the Orange Basin (Paton et al., 2008) and about 400 m in average for both, the inner and outer margin (Kuhlmann et al., 2011). Simulations of erosion events within the exploration Block 2 in the Orange Basin indicate about 500 m of erosion (Boyd, 2010). After Hirsch et al. (2010) and their modelling, the amount of eroded material across their working area of the Orange basin is up to 500 m at the inner margin during the Late Cenozoic. Consequently, our minimum estimate of Cenozoic seafloor uplift in the Orange Basin of 115 m is about 400 m lower than in previous studies, but of a comparable magnitude as estimates derived from earlier studies.

Post-rift phase II:

The second restored paleobathymetry is for the beginning of the Turonian (93 Ma; Figure 2.7b). The map shows a cumulative positive paleotopography of up to 365 m.a.s.l. in the Orange Basin. In post-rift phase III, we already have derived a positive paleotopography of 115 m which needs to be subtracted from the 365 m of post-rift phase II in order to provide a minimum estimate of seafloor uplift for the time period between 93 Ma and 67 Ma. Accordingly, the corrected minimum estimate of seafloor uplift for post-rift phase II is 250 m in the Orange Basin. Similarly, the Walvis Basin in the north is characterised by a seafloor uplift of about 170 m after removing the 40 m of positive paleotopography of the Cenozoic time interval. The Lüderitz Basin is marked by an average paleobathymetry of about 450 meters below sea level (m.b.s.l.).

An erosion map for the Orange Basin, derived from seismic isopach maps assuming a constant thickness for the eroded layer (Kuhlmann et al., 2011), indicates up to 930 m of erosion during the phase between 75 Ma and 67 Ma. By contrast, Hirsch et al. (2010) calculated a maximum uplift of 340 m across the southern margin. While the latter is in the same range as our minimum estimate of seafloor uplift of 250 m, the study by Kuhlmann et al. (2011) documented a larger amount of uplift.

After Scharf et al. (2013), the onshore denudation rate along the western margin is about 30 m/Ma during the Late Cretaceous yielding approximately 500 m of denudation for the entire Late Cretaceous. If this onshore denudation is an effect of uplift processes, our minimum estimate of seafloor uplift of 250 m can be related to the investigation of Scharf et al. (2013).

The seafloor uplift event derived for post-rift phase II correlates temporally well with results by Séranne and Anka (2005) who proposed an uplift event corresponding to the Senonian-phase during the Late Cretaceous (starting in the Turonian). Furthermore, this result is also supported by thermochronology studies in southwestern Africa (e.g., Gallagher and Brown, 1999; Raab et al., 2002; Kounov et al., 2009, 2013; Stanley et al., 2013). Moreover, a study of macroforms onshore Africa by Guillocheau et al. (2013) also pointed to a Late Cretaceous uplift (around 75 Ma). In addition, Rouby et al. (2009) suggested a rapid phase of erosion on the African plateau during the Late Cretaceous which they interpret as related to uplift. Furthermore, a recent analysis on sedimentary flux data indicates a major phase of rapid denudation during the Late Cretaceous that is related to uplift induced by the tilting of the African continent in response to its migration over a fixed source of mantle upwelling (Braun et al., 2014).

Post-rift phase I:

Finally, the third restored paleobathymetry at the beginning of the post-rift interval (125 Ma; Figure 2.7c) indicates a cumulative positive paleotopography of about 995 m.a.s.l. within the Orange Basin area. Subtracting the effects of the younger post-rift phases yields a relative positive paleotopography of 630 m pointing to seafloor uplift for the time interval between the beginning of the post-rift phase to the end of Cenomanian (125-93 Ma). The estimated seafloor uplift in the northern part of the research area is 940 m for the corresponding time interval after the cumulative amount of positive paleotopography of younger time intervals is taken into account. The Lüderitz Basin has also a small amount of seafloor uplift at its

southern boundary; however, the mean paleobathymetry is about -100 m.a.sl. By contrast to the seafloor uplift events during post-rift phase II and III, these findings cannot be directly related to other studies because there are no detailed investigations on the Lower Cretaceous. From sequence stratigraphy within the Orange Basin by Brown et al. (1995) we only know two major unconformities (13 At1 and 14 At1, after Brown et al., 1995) between the breakup unconformity (6 At1, after Brown et al., 1995) and the base Turonian unconformity (15 At1, after Brown et al., 1995). These unconformities could indicate that uplift occurred during post-rift phase I causing these unconformities.

2.5.2 Causative processes for seafloor uplift

Our results indicate simultaneous seafloor uplift in the northern and southern areas of the margin, thus raising the question whether a structural and possibly geodynamic relationship exists between these two features. As already discussed by several authors before, different processes may be responsible for post-rift margin seafloor uplift. Two processes are discussed in the following: (1) deep mantle processes and (2) compressional forces due to ridge-push of the South Atlantic mid-ocean ridge.

(1) Deep mantle dynamics as proposed by the "African superswell" advocates (e.g., Nyblade and Robinson, 1994; Lithgow-Bertelloni and Silver, 1998; Moucha and Forte, 2011) would explain the large area affected by the uplift and would be consistent with the observed low shear wave velocity anomaly of the mantle beneath Africa (Ritsema et al., 1999; Al-Hajri et al., 2009). The studies investigating deep mantle flow on the one hand (Forte et al., 2010; Colli et al., 2013, 2014) and the paleo-plate movement in relation to hot spot tracks and large igneous provinces (Thorne et al., 2004; Torsvik et al., 2009, 2010; Conrad et al., 2013) on the other hand support the hypothesis that buoyant (hotter) mantle may be responsible for the uplift events deduced. Apart from these general findings, the study by Gurnis et al. (2000), discussing the hypothesis of a large-scale buoyant structure (4000 km x 2000 km in the lowermost mantle), provided some constraints on magnitudes and rates of uplift for the southern African plateau which can be compared to our results. According to Gurnis et al. (2000), the African plateau appears to have moved upward with a rate of 5 to 30 m/Ma, the latter being a value averaged for the entire Cenozoic period. These results imply a total amount of

uplift ranging between a minimum of approximately 300 m to a maximum of more than 2 km for southern Africa if we assume 67 Ma for the duration of the Cenozoic. In contrast, the minimum estimate derived from our study is 115 m for the southern domain of the margin and thus less than indicated by the results of Gurnis et al. (2000). However, the rates of uplift derived by Gurnis and co-workers (2000) concern only the onshore part of southern Africa rather than the continental margin as addressed in our study. Therefore, assuming the uplift to be related to mantle processes localized below the central domain of the continent, would likely result in less seafloor uplift along the margin, thus explaining the differences between our results and those of Gurnis et al. (2000).

The observed small wavelength of vertical movements and their spatial distribution within the margin area are difficult to reconcile in terms of deep mantle dynamics only. Indeed, the surface manifestation of the latter processes would likely result in supra-regional features (e.g., 10^7 km², after Gurnis et al., 2000) with a wavelength far larger than the one derived from our study. Nevertheless, the rather local observations pointing to deep mantle sources inducing uplift within our study cannot be ruled out. It is most probable that a large area was affected by a deep mantle source which cannot be reconstructed by our approach due to a lack of data.

(2) Another mechanism which may have caused seafloor uplift of the margin is compression due to mid-ocean ridge-push as discussed by several authors (e.g., Cloetingh et al., 2008; Pedoja et al., 2011; Japsen et al., 2012). Japsen et al. (2012) suggested that repeated episodes of compression-induced uplift can contribute to the elevated passive continental margins. Linking this theory to our results, showing only local seafloor uplift features, it remains enigmatic why the different domains have responded with different amounts of seafloor uplift. On the one hand, this can be referred to differences in the mechanical weakness of the crust along the margin. On the other hand, if compressional forces would have caused the vertical movements only in the northern and southern part of the research area, both regions have to be separated by a fracture zone located in between both areas. Jungslager (1999) presented a map with major tectonic elements at the SW African margin where a probable fracture zone is located at the northern boundary of the Orange Basin. However, there are rather

indications for extensional stresses on the SW African continent next to the margin (Kipata et al., 2013; Will and Frimmel, 2013; Salomon et al., 2014).

2.5.3 Limitations of the method

Although our investigation confirms observations from several studies e.g., the analysis of the sediment budget by Tinker et al. (2008a, 2008b) or Guillocheau et al. (2012), in some respects, the approach makes strongly simplified assumptions concerning the thermal and mechanical behavior of the system that bring along sources of error. In this context, there are two major limiting factors: (1) the independent treatment of the loading and cooling history and (2) the multi 1D approach.

In particular, the rheological consequences of the feedback between delayed cooling in response to thermal blanketing by sediments may be such, that the McKenzie-type post-rift thermal subsidence may be delayed. Thus our estimate of the amount of subsidence for the individual time steps may correspondingly vary in our approach.

However, our findings on seafloor uplift, derived by using a uniform stretching scenario to calculate the amount of thermal subsidence and a "backstripping" approach to determine the amount of load induced subsidence, are in agreement with those by Gurnis et al. (2000) pointing towards a deep mantle source as discussed above. At the same time our results would also be consistent with a depth-dependent lithospheric thinning scenario with stronger thinning of the sub-crustal mantle to explain the subsidence history (Hirsch et al., 2010; Huismans and Beaumont, 2014). This also points to mantle processes in the area of the southern SW African margin.

In addition, the thermal structure controls the finite strength of the lithosphere (i.e., thermal rigidity) and thus the flexural response of the latter to sediment loading (e.g., Watts and Ryan, 1976; Watts and Burov, 2003). Assuming local Airy isostatic compensation is equivalent to a very weak lithosphere and therefore predicts a larger depression caused by the load of the sediments than a flexural isostatic approach would entail in general. In contrast, an increase in rigidity would decrease the amplitude of the deflection of the basin while loading it by sediments. For this reason, our observed amount of seafloor uplift is again a minimum estimate because flexural isostatic models would result in a less deep basin and therefore a higher amount of cumulative positive paleotopography.

Stewart et al. (2000) compared the results from local isostasy "backstripping" with those from flexural "backstripping". They obtain uplift by using the Airy isostatic model and interpret it as a consequence of the local compensation and therefore suggest flexural "backstripping" as the appropriate method in subsidence analysis. However, as the composition and thickness of the crust varies considerably across the margin, according to Maystrenko et al. (2013), this assumption might be questionable. Stewart et al. (2000) assumed a laterally constant and only time varying effective elastic thickness which is geologically rather improbable.

To quantify the related errors, a 3D analysis considering dynamic coupling between cooling and loading would be required. Accordingly, future studies should consider this feedback between loading and cooling history. Although recently published thermodynamic models (e.g., Huismans and Beaumont, 2011; Brune et al., 2014) already consider the complex processes behind margin subsidence/uplift, they do not consider the preserved sediment record and the present-day geophysical configuration of the system as a modelling input. Though we utilize this information in our study, we admit that a more detailed reconstruction than with a multi 1D approach is possible by considering mechanical and thermal processes and their interaction.

Once the thermal evolution is described in more detail this will allow also a better prediction of the isostatic behavior of the margin, e.g., regarding flexural isostasy and the variation of the effective elastic thickness.

Apart from the major thermo-mechanical issues and the multi 1D approach a minor limitation of the method is the sea level variation. Although it is speculative if global sea level drops may have caused an observed erosional unconformity (e.g., Brown et al., 1995; Paton et al., 2008) that does not require uplift at all, the effect of sea level fluctuations might be discussed: The magnitude of cumulative seafloor uplift derived with our subsidence analysis is still too large to be explained by a sea level variation alone. If sea level would be higher than today (e.g., Late Cretaceous, Haq et al., 1987), the additional load would not prevent our observed positive paleotopography which correlates to the suggested uplift events as discussed above. After Haq et al. (1987), the sea level fluctuations are in the order of +/- 200 m in maximum which would yield about 60 m of isostatic rebound that introduces an error of +/- 6% to our minimum estimate of cumulative uplift (~1000 m).

Finally, it is helpful to investigate not only the subsidence history of the eastern part of the South Atlantic passive margin but also the conjugate western part of the South Atlantic

Ocean, the passive margin offshore Argentina and Brazil, in order to compare the amounts of seafloor uplift, if there is any seafloor uplift on the South American site. In particular, it would be helpful to know if the paleobathymetric evolution of both margins correlates with comparable amounts and timing of vertical movements and therefore may be caused by similar generating processes. If the amount and temporal evolution of seafloor uplift at the South American passive continental margin is comparable, it would support the theory of ridge-push as there are no indications of mantle upwelling beneath South America. By contrast, if the restored paleobathymetries offshore South America do not give evidence for a post-rift seafloor uplift, the ridge-push theory can be ruled out as both margins should be more or less affected by the same compression.

2.6 Conclusions

We quantify the load induced subsidence and thermal subsidence based on the preserved present-day configuration of the sediments and the crystalline crust at the SW African continental margin. The reconstructed paleobathymetries of the SW African margin show the post-rift evolution for three time steps and support the conclusion that in addition to dominant subsidence also upward vertical movements occurred. Furthermore, based on a subsidence analysis using a margin configuration constrained by geological and geophysical data, minimum estimates of vertical movements are derived.

Summarizing the paleobathymetric evolution of the SW African margin from the beginning of the post-rift to the present-day shows a long-lasting but exponentially decreasing subsidence interrupted by phases of seafloor uplift. A general decrease in the amount of seafloor uplift for successively younger post-rift phases in the Walvis Basin area and the Orange Basin area is derived. By contrast, in the Lüderitz Basin area between the Walvis Basin and Orange Basin no distinct seafloor uplift event is found during the post-rift phase, but continuous subsidence. Summarizing all amounts of seafloor uplift during the entire post-rift phase, results in a total amount of seafloor uplift of about 1200 m in the Walvis Basin area and about 1000 m in the Orange Basin area.

From the amounts of seafloor uplift no final conclusion concerning the processes generating the upward vertical movements can be drawn, whether seafloor uplift is the result of mantle upwelling/hotspot or of compressional forces as a consequence of seafloor spreading. Of

course, there is the possibility of a combination of both but the magnitudes of the minimum estimate of seafloor uplift rather indicate a deep mantle source.

Acknowledgements

Funding by the German Research Foundation (DFG; grant no. SCHE 674/5-2) within the priority program SAMPLE (South Atlantic Margin Processes and Links with Onshore Evolution; SPP 1375) is greatly acknowledged. We are grateful to Yuriy P. Maystrenko for providing the thickness maps used in this study.

Furthermore, we want to thank two anonymous reviewers for their constructive comments which helped to improve the manuscript.

3 Backward modelling of the subsidence evolution of the Colorado Basin, offshore Argentina and its relation to the evolution of the conjugate Orange Basin, offshore SW Africa

Abstract

In this study we focus on reconstructing the post-rift subsidence evolution of the Colorado Basin, offshore Argentina. We make use of detailed information about its present-day configuration of the sedimentary infill and the crystalline crust. This information is used as input in a backward modelling approach which relies on the assumption of local isostasy to reconstruct the amount of subsidence as induced by the sedimentary load through different time stages. We also attempt a quantification of the thermal effects on the subsidence as induced by the rifting; here included by following the uniform stretching model of lithosphere thinning and exponentially cooling through time. Based on the available information about the present-day geological state of the system, our modelling results indicate a rather continuous post-rift subsidence for the Colorado Basin, and give no significant evidence of any noticeable uplift phase.

In a second stage, we compare the post-rift evolution of the Colorado Basin with the subsidence evolution as constrained for its conjugate SW African passive margin, the Orange Basin. Despite these two basins formed almost coevally and therefore in a similar large scale geodynamic context, their post-rift subsidence histories differ. Based on this result, we discuss causative tectonic processes likely to provide an explanation to the observed differences. We therefore conclude that ridge-push by spreading of the South Atlantic Ocean cannot be considered as the only force acting on these settings, but that it is likely that additional tectonic components are required to explain the differences in the subsidence of the two basins along the conjugate passive margins. Such additional tectonic components might be related to a dynamic mantle component in the form of either plume activity (Africa) or a subducting slab and the presence of an ongoing compressional stress system as revealed for different areas in South America.

3.1 Introduction

In the last decades, the passive continental margins of the South Atlantic have been the subject of a still increasing number of studies (e.g., Jungslager, 1999; Katz and Mello, 2000; Séranne and Anka, 2005; Hirsch et al., 2007, 2009; Dupré et al., 2011; Maystrenko et al., 2013). Efforts focused on detailed analysis of their sedimentary cover, their present-day architecture and configuration and tectonic history as based on geophysical (Gladczenko et al., 1997; Hinz et al., 1999; Stewart et al., 2000; Franke et al., 2006; Kuhlmann et al., 2010, 2011; Loegering et al., 2013; Autin et al., 2013, 2015), geochemical (Trumbull et al., 2007; Hartwig et al., 2012), sedimentological (Brown et al., 1995) or geodynamical (Torsvik et al., 2009; Flament et al., 2013; Braun et al., 2014; Colli et al., 2014) evidence. The results from these studies have inspired more recent efforts aiming at investigating the details of the subsidence history of these settings, mainly published for the margins offshore SW Africa (Hirsch et al., 2010; Rouby et al., 2013; Dressel et al., 2015) and are rarely made at the conjugate margin of SE South America (Sachse et al., 2015). So far, attempts to compare the evolution of the two South Atlantic margins (in terms of major controlling factors on hydrocarbon generation) have only been made by Marcano et al. (2013).

In addition, previous studies relied on two-dimensional forward numerical models of the large-scale rift dynamics (Burov et al., 2007; Burov and Cloetingh, 2010; Huismans and Beaumont, 2011, 2014; Brune et al., 2014) and even three-dimensional approaches (Allken et al., 2012; Le Pourhiet et al., 2012; Brune et al., 2013 Brune, 2014; Koopmann et al. 2014; Liao and Gerya, 2015). These studies have provided a significant advance in the current understanding of continental rifting dynamics, and have been beneficial to explain first-order differences in the basic configuration of the margins. The main limitation of these approaches is that they are based on a highly simplified geometry of the lithosphere, where sediments are either not considered or integrated as a passive load on the plate. These aspects hinder the use of these models to reconcile the details of the sedimentary infill as constrained in such basins.

In this study, we focus on reconstructing the post-rift subsidence of the Colorado Basin, offshore Argentina (Figure 3.1). We rely on a detailed 3D geological model of the present-day crustal configuration as well as sedimentary succession of the Colorado Basin offshore Argentina according to Autin et al. (2013; 2015). The preserved sediment thicknesses are used in a backward modelling approach to derive the subsidence history and past vertical movements along the passive continental margin of Argentina since its beginning after the breakup of the southern segment of the South Atlantic Ocean. In our study, we do not attempt

any modelling reconstruction of the rifting stage initiating the basin, but we rather focus on the post-rift subsidence evolution. Therefore, we base our approach on the simple assumption of one dimensional uniform stretching (McKenzie, 1978) to parameterise the amount of additional thermal subsidence throughout the post-rift evolution and are aware of the limitations inherent in the uniform stretching model (e.g., ignoring radiogenic heat production and thermal blanketing by the sediments; assuming a fixed temperature at the depth of the lithosphere). The main reason on adopting a simple, one dimensional analytical solution is that it does not require a wide spectrum of parameters, which are usually difficult to constrain, if not disputable, as more sophisticated solutions to the thermal problem do. In addition, our study does not attempt any modelling of the complex and non-linear physics initiating the subsidence. It rather makes a systematic use of available geological data to derive information about the complex history of the Argentine margin, in a way that might help identifying most likely causative tectonic processes. These geological data constrain the preserved thickness of sediments and thus the amount of subsidence induced by sedimentary loading. In addition, we consider it justifiable to use a simplified kinematic representation of the thermal evolution of the system, by taking at the same time all limitations behind our choice into account while discussing the results obtained from the investigation. To quantify the thermal subsidence we consider another source of geological data, namely the preserved thickness of the crystalline crust to determine crustal stretching factors.

In a second stage, the results obtained for the Colorado Basin are compared to a published subsidence reconstruction using the same method at the conjugate Orange Basin, offshore SW Africa (Dressel et al., 2015). Although these margins evolve simultaneously after the breakup of the South Atlantic Ocean (~125 Ma) our investigation indicates a different subsidence evolution of the Colorado Basin (offshore SE South America) and the Orange Basin (offshore SW Africa). The results from this comparison therefore opens a discussion about possible causative tectonic processes responsible for the evolution of these two settings as detailed in the last part of this manuscript by also taking their geological context into account.

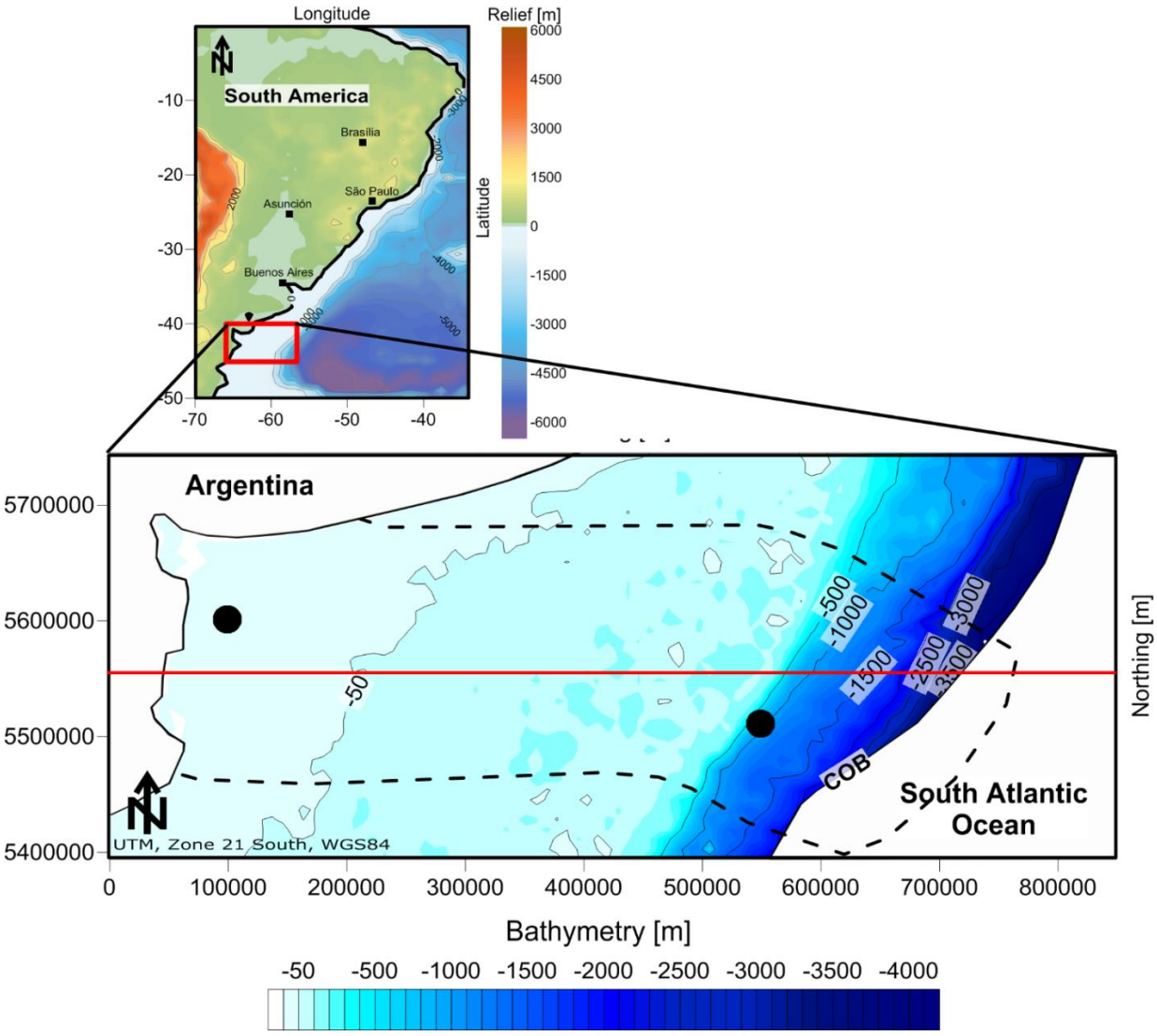

Figure 3.1: Map of the research area with overview of the location in the eastern South America (bathymetry after IOC, IHO and BODC, 2003). The contour of the Colorado Basin is marked by the black dashed line. The black dots mark the location of synthetic boreholes used for Figure 3.4 and Figure 3.10 as these locations represent the areas of the thickest sediment deposition whereas the red solid line shows the location of the cross-section shown in Figure 3.5. Coordinate system is UTM [m], zone 21 south (WGS 84).

3.2 Geological Setting and dataset

It has been long recognized that the origin of the volcanic passive margins of SE America and SW Africa was coeval and resulted from the breakup of Gondwana during the Early Cretaceous (Rabinowitz and Labrecque, 1979; Austin and Uchupi, 1982; Sibuet et al., 1984). Supercontinental breakup was followed by the opening of the South Atlantic Ocean showing

a preferential northward propagation which was accompanied by extensive volcanism and the emplacement of lower crustal bodies and seaward dipping reflectors within the Southern Segment of the South Atlantic Ocean (Hinz et al., 1999; Franke et al., 2007, 2010; Schnabel et al., 2008).

After breakup had ceased (around approximately 125 Ma), the Argentine margin underwent a phase of long post-rift subsidence marked by lithospheric cooling of the rift-related thermal anomaly and consequent sediment accumulation. At present, the Colorado Basin shows two major domains in style of deformation (Autin et al., 2013, 2015). While the western part of the basin is underlain by a NW-SE striking depocentre, its distal segment has a NE-SW orientated axis (Figure 3.2). According to previous studies (Franke et al., 2006; Dominguez et al., 2011; Autin et al., 2015) four segments (western-, central-, eastern- and distal segment; Figure 3.2) can be further distinguished as associated to major transfer zones proposed to represent strike-slip-like structures.

The post-rift subsidence created accommodation space for a total sediment fill of up to ~8500 m in the main depocentres, with a sediment supply mainly consisting of siliciclastic rocks as well as subordinate gypsum, limestones and marine shales.

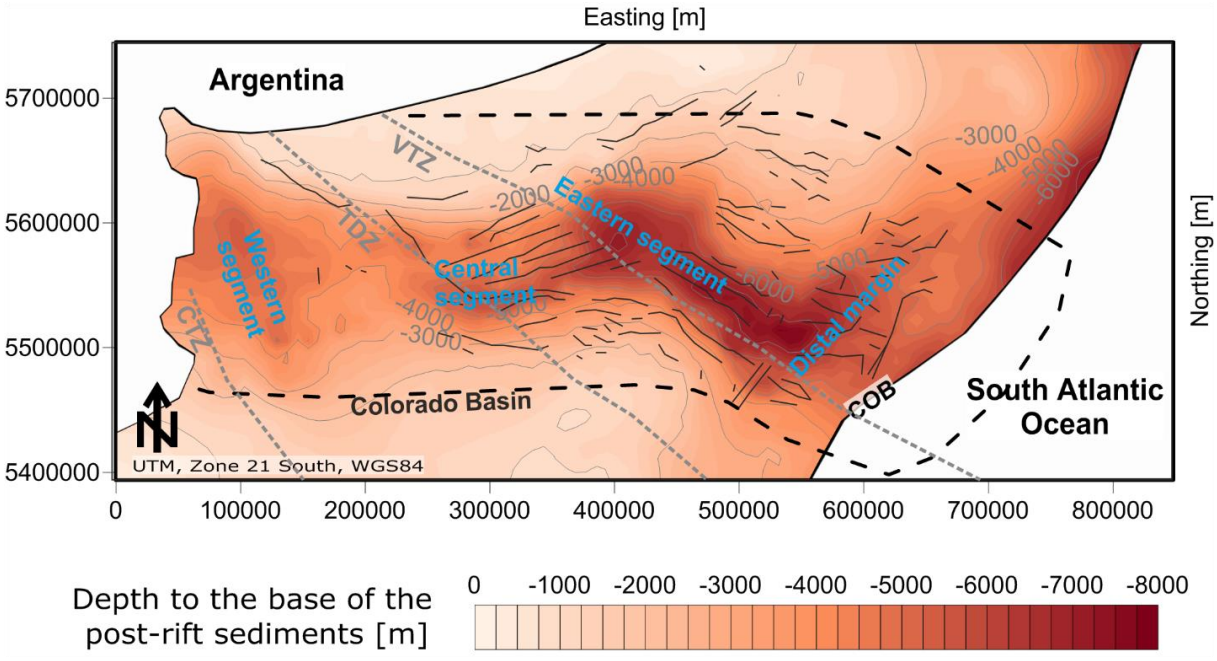

Figure 3.2: Depth to the base of the post-rift sediments (Autin et al., 2013) indicating a NW-SE oriented depocentre in the western segment and a rather NE-SW oriented depocentre in the distal margin. The contour of the Colorado Basin is marked by the black dashed line and segmented into four major segments according to Autin et al. (2015). Major faults of the pre-

rift basement are highlighted by the solid black lines (Autin et al., 2015) and transfer zones by grey dashed lines (CTZ: Colorado Transfer Zone; TDZ: Tona Deformation Zone; VTZ: Ventana Transfer Zone; Franke et al., 2006; Dominguez et al., 2011).

For our investigation, we make use of an existing 3D structural crustal-scale model of the Colorado Basin (Autin et al., 2013; 2015). The model has an extension of 350 x 850 km in N-S and W-E direction, respectively. It distinguishes a water column unit according to the present-day bathymetry, and seven post-rift units, which from top to bottom are listed as followed: Shallow, 0-27 Ma; Caotico, 27-35 Ma; Elvira, 35-55 Ma; Pedro Ludro, 55-70 Ma; Colorado III, 70-85 Ma; Colorado II, 85-100 Ma; Colorado I, 100-125 Ma. In Figure 3.3, we illustrate the thickness maps for the seven post-rift units according to the 3D geological model by Autin et al. (2013; 2015). These thickness maps can be interpreted in terms of areas of deposition and illustrate the lateral variations. In general, the isopach maps indicate a major depocentre in the west, close to the Argentine coast, as well as in the east, along the distal margin. Older units (125-70 Ma), such as Colorado I, Colorado II and Colorado III are marked by larger thicknesses while younger sedimentary units (70-25 Ma) become thinner (Pedro Luro, Elvira and Caotico) with a final thickening of the Shallow unit (25-0 Ma).

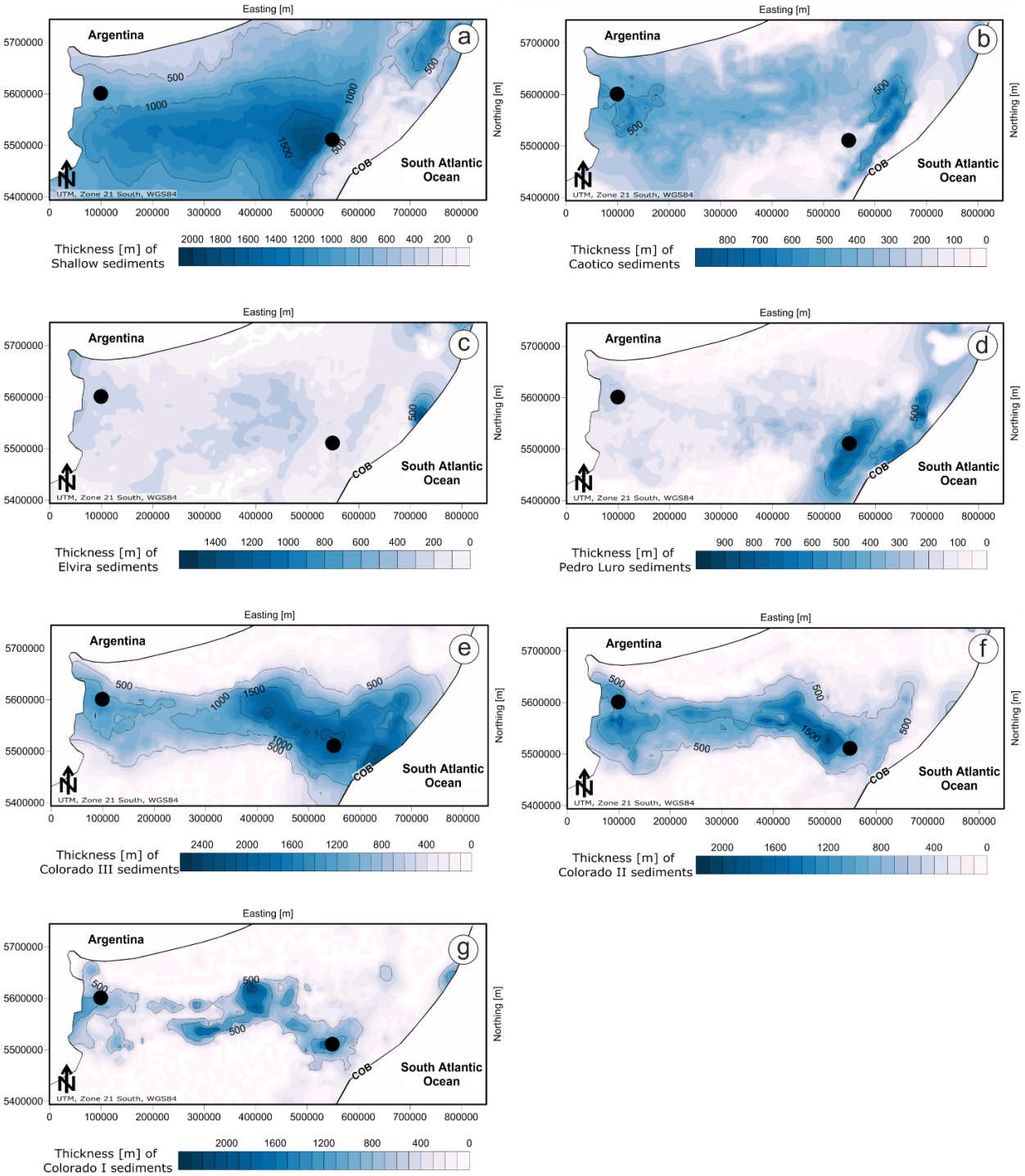

Figure 3.3: Thickness maps (after Autin et al., 2013, 2015) indicating the two major orientations of deposition. (a) Shallow unit (0-25 Ma). (b) Caotico unit (25-40 Ma). (c) Elvira unit (40-55 Ma). (d) Pedro Luro unit (55-70 Ma). (e) Colorado III unit (70-90 Ma). (f) Colorado II unit (90-98 Ma). (g) Colorado I unit (98-125 Ma). The black dots mark the area of synthetic wells shown in Figure 3.4 and Figure 3.6.

As mentioned above, two major depocentres are characteristic for the Colorado Basin. However, they vary in accommodation space. Figure 3.4 illustrates the stratigraphy of two synthetic wells with thicknesses according to the published structural model by Autin et al. (2013, 2015). The location of the synthetic wells is chosen such that they represent the major depocentres. Apart from the Elvira unit and Colorado II unit that are thicker in the western segment, larger sediment thicknesses are obtained in the distal segment.

According to the original model, these seven post-rift units overlay a syn-rift sedimentary unit resting upon a crystalline crustal basement. Autin et al. (2015) differentiated the crystalline crust into different domains in terms of bulk density including seaward-dipping reflectors (SDRs), a crystalline crust and lower crustal bodies (LCBs). These are schematically depicted in Figure 3.5, which shows a profile across the Colorado Basin highlighting the distribution of the sediments, the location of the different crustal bodies in the crystalline crust as well as the depth to the Moho.

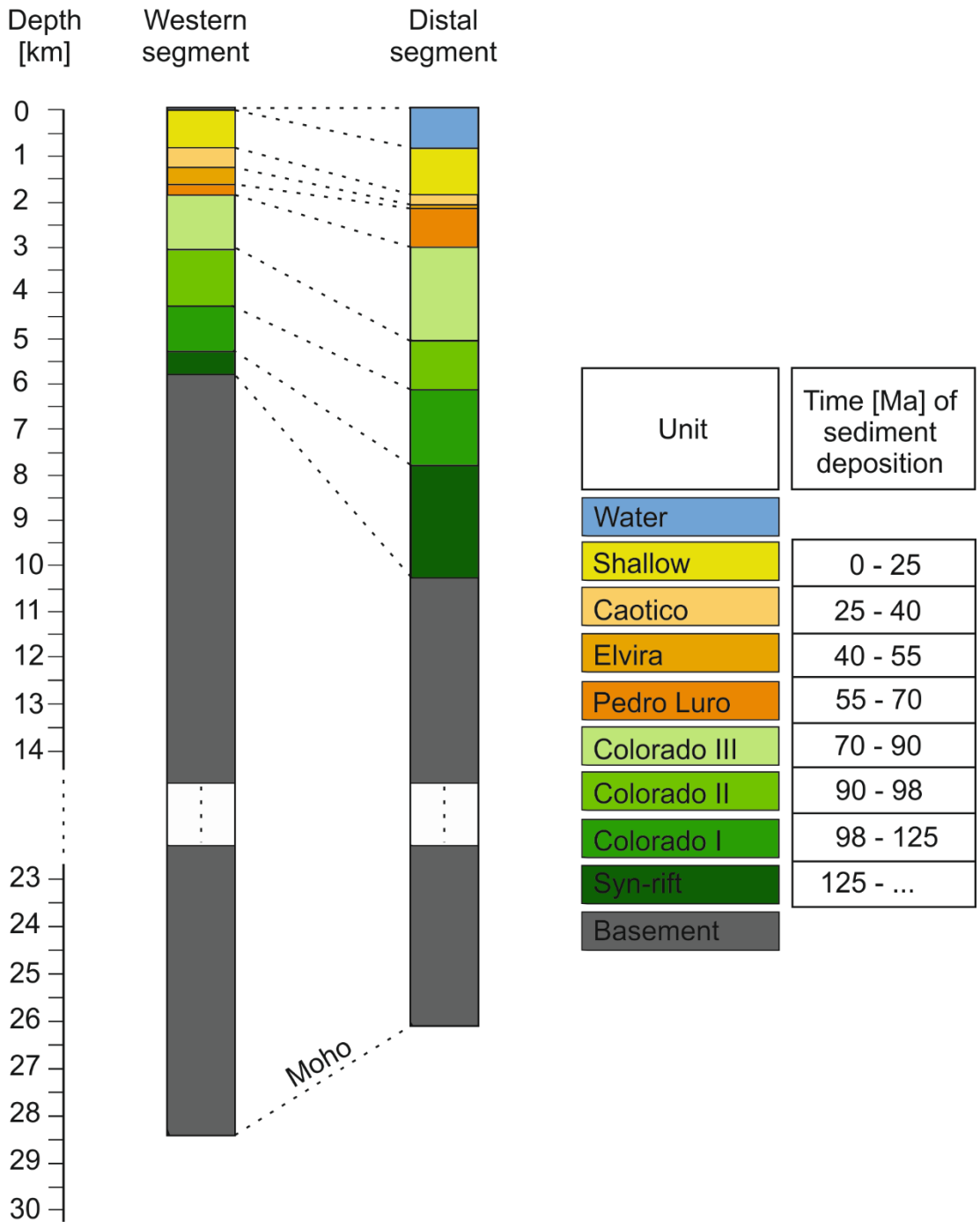

Figure 3.4: Stratigraphy of two synthetic wells in each of the major depocentres. See Figure 3.1 or Figure 3.3 for the location. Information about thicknesses is taken from Autin et al. (2013, 2015).

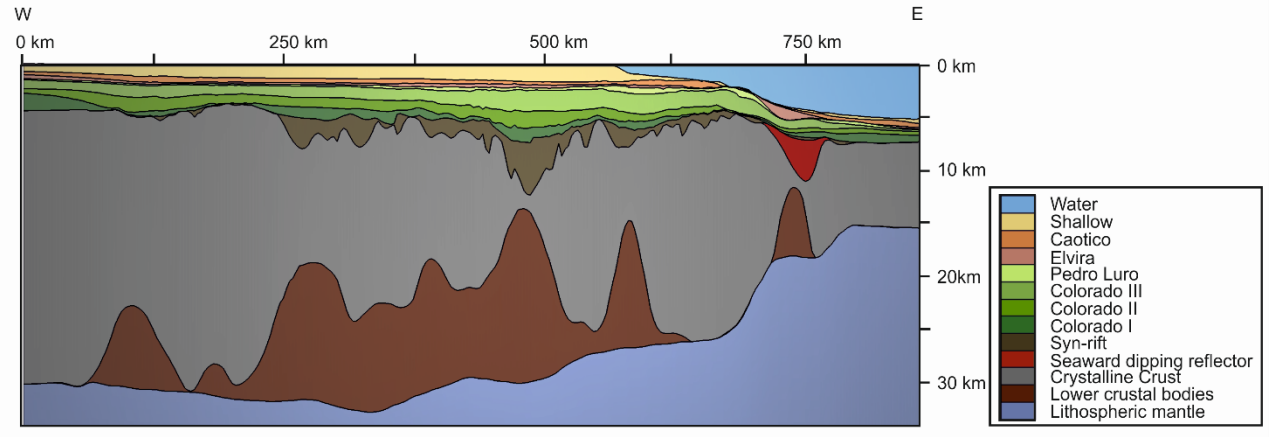

Figure 3.5: West-East profile across the centre of the Colorado Basin indicating a heterogeneous crustal configuration as well as the syn-rift and post-rift units. See Figure 3.1 for profile location. Information about thicknesses is taken from Autin et al. (2013, 2015).

For the aim of this study to investigate the post-rift phase, we assume the SDRs and LCBs to have been emplaced before or coeval to rifting. This assumption has been suggested by Autin et al. (2015) for the Colorado Basin and by Scheck-Wenderoth et al. (2007) or Thybo and Artemieva (2013) for other passive margin settings. Therefore, we integrate in our calculations a single crustal domain extending beneath the base of the syn-rift sediments down to the Moho boundary (Figure 3.5). The isostatic feedback from the previous emplacement of these crustal bodies onto the post-rift subsidence evolution of the basin is implicitly considered in that we calculate a laterally varying density for the crystalline crust. This was done by assuming local isostatic equilibrium at the Moho and by applying Pratt isostasy (Pratt, 1855) against a reference crustal density model for which we took 35 km as isostatic compensation depth, 2850 kg/m³ and 3300 kg/m³ for the average crustal and mantle density, respectively.

Figure 3.6 shows the thickness of the present-day crystalline crust including the SDRs and LCBs as well as the corresponding laterally varying density. Figure 3.6a illustrates how the crust is thinned in eastern direction. Accordingly, the thinnest crust is obtained along the continent-ocean boundary (COB; less than 15 km), whereas the thickest crust is obtained in the north and the south of the research area (35 km).

The calculated laterally varying density distribution (Pratt isostasy) is shown in Figure 3.6b. There is a strong spatial correlation between the areas of higher densities and the occurrence of SDRs and LCBs according to Autin et al. (2015). Higher densities are obtained within the

central segment of the basin as well as along the distal margin. Autin et al. (2015) differentiate between areas of LCB emplacement as depocentre-related LCBs, distal margin-related LCBs and SDR-related LCBs. Comparing their map of LCB thickness with the density distribution illustrated in the present study (Figure 3.6b) shows a strong spatial correlation in location of LCBs and areas with higher density. Furthermore, the same is valid for the map of SDR thickness (Autin et al., 2015), showing a NE-SW striking trend of SDRs which is in agreement to the higher densities along the COB presented in Figure 3.6b.

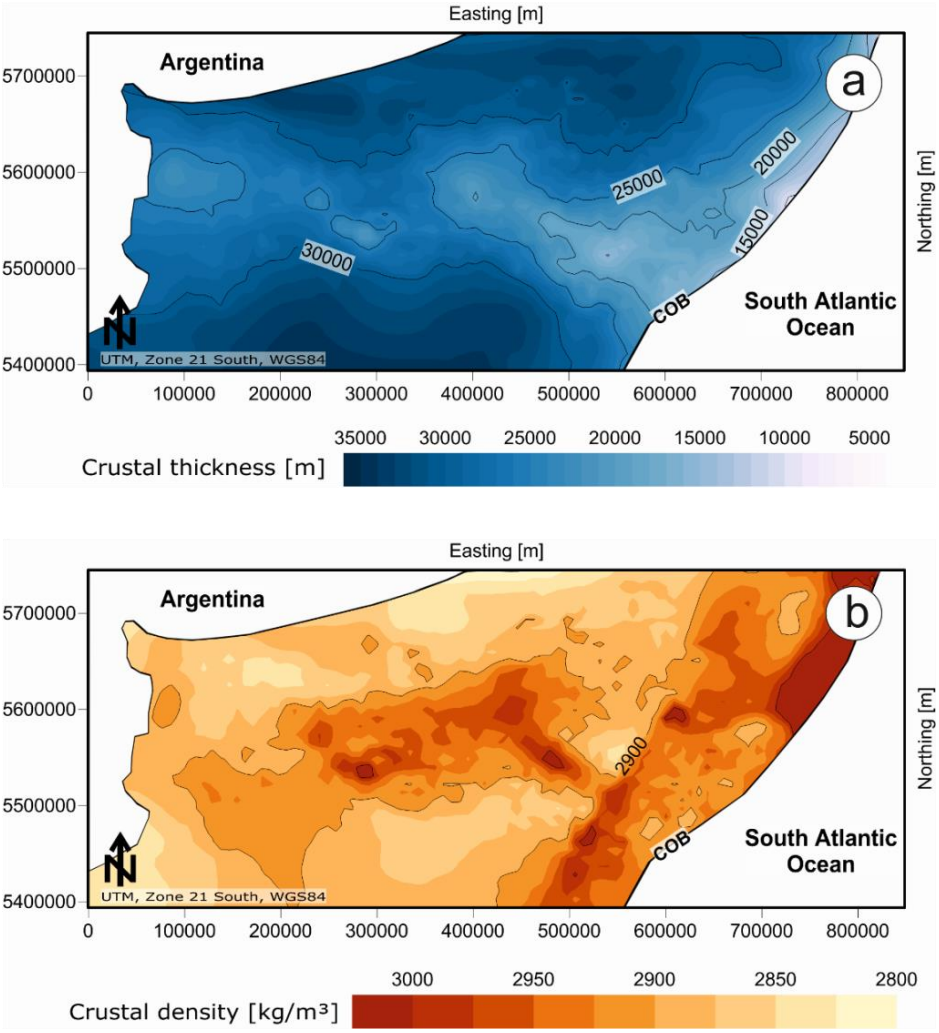

Figure 3.6: (a) Thickness of the present-day crust including SDRs, crystalline crustal domain and LCBs. (b) Laterally varying density of the crust (LCBs + crystalline crustal domain + SDRs) calculated assuming Pratt isostasy. Accordingly, areas of SDRs and LCBs are characterised by higher densities. See text for detailed description on how the laterally varying density distribution is calculated.

3.3 Method

We use a multi 1D backward modelling approach to quantify the subsidence evolution during the entire post-rift stage (from 125 Ma until the present-day) of the Colorado Basin. Following this approach, the amount of load induced subsidence due to sedimentation is determined. Accordingly, after removal of each unit we back-calculate the amount of isostatic readjustment of the column following the concept of local Airy isostasy (Airy, 1855). Our calculation takes decompaction of the remaining sediments according to unloading into account and is parameterised following Athy's exponential porosity-depth relation (Athy, 1930) by considering an additional porosity-load dependence (Scheck et al., 2003). Table 3.1 lists all properties adopted for each individual sedimentary unit (Autin et al., 2015) as well as the age subdivision after Autin et al. (2013) with modifications on the most recent timescale by Cohen et al. (2013).

Moreover, we do integrate the additional load from the water column only at the beginning of our calculation. There are two main reasons behind our assumption: First, the water depth was shallower during the past because load (due to sediments) and thermal subsidence (due to relaxation of the lithosphere) affected the margin during the post-rift phase. For this reason, the water depth at the present-day represents the maximum water depth during the entire post-rift phase. Second, in our study area the average water depth at the present-day is only about 300 m beneath the areas of the major deposition. From this it follows that the water column would only yield about 100 m of isostatic rebound, which is negligible when compared to the isostatic rebound induced by the sedimentary load with a thickness of up to about 7000 m.

Successive removal of the water column and the sedimentary units yields the amount of subsidence as induced by the deposition of each sedimentary unit (considered here as instantaneous) and a final "backstripped" surface as a result.

As common to all backstripping approaches, it is not possible to take into account the additional effects of lithosphere cooling during the sediment deposition and resulting thermal subsidence. A study by Loegering et al. (2013) emphasized the role of this additional subsidence component related to conductive cooling of the lithosphere to explain the post-rift thermal subsidence within the Colorado Basin. In an attempt to correct the "backstripped" surface for lithospheric cooling, we calculate the amount of thermal subsidence separately by following the uniform stretching model (McKenzie, 1978). As discussed in the introduction, our workflow comes with some limitations mainly related to the validity of the uniform stretching model for the Colorado Basin. Indeed, it might be likely that rifting was not

instantaneous but rather consisting of multiple rifting stages of finite duration, and that the sediments accommodated on a relaxing lithosphere of finite strength. However, insufficient information about input parameters to constrain the details of the rifting dynamics as well as the internal rheological configuration of the entire plate hindered any detailed quantification of such processes. Therefore, we decide to use a simple, analytical approach, without attempting any detailed reconstruction of the rifting phase. Furthermore, the reason for relying on a uniform stretching model to initialize and parameterise thermal cooling of the lithosphere stems from its simplicity to describe the model configuration by means of a dimensionless parameter, which is the β-factor. We have inferred the β-factor from the ratio between the thickness of the initial (i.e., un-stretched) and present-day crust affected by stretching (illustrated in Figure 3.8h). The reference value for the un-stretched crust has been derived from the crustal thickness onshore Argentina as published by Autin et al. (2013). Accordingly, the crustal thickness ranges between a minimum of 30 km up to a maximum of 36 km. Therefore, a reference value of 35 km has been adopted for our study. This value also well compares to the average crustal thickness computed for the conjugate margin of SW Africa (Maystrenko et al., 2013).

Finally, the obtained thermal subsidence is used to correct the "backstripped" surfaces determined from the "backstripping" methods for each time interval considered, as listed in Table 3.1, and to restore paleobathymetries. Exemplarily, the paleobathymetry at 25 Ma is reconstructed by "backstripping" the water column and the Shallow unit with the result of a "backstripped" surface at 25 Ma, the top of the Caotico unit. This surface is then corrected for the amount of thermal subsidence calculated for the time interval between 0 Ma and 25 Ma. Following this procedure, the remaining seven paleobathymetries are obtained, always considering the thermal subsidence between 0 Ma and the respective stratigraphic unit.

Table 3.1: Names, prevailing lithologies, ages, and assigned physical properties used in this study for "backstripping" as well as for the calculation of the thermal subsidence (after Autin et al., 2013, 2015; Cohen et al. 2013).

Name of individual units	Prevailing lithologies used in this study	Modified ages of the unit [Ma]	Maxtrix Density [kg/m³]	Initial porosity	Compac-tion factor
Seawater			1030		
Shallow	Siltsones; Sandstones; gravels; gypsum; marls; loes; pyroclastics	0-25	2720	0.63	0.77
Caotico	Gypsum; shales; sandstones; glauconitic sandstones; basalt;tuffs	25-40	2640	0.56	0.4
Elvira		40-55	2640	0.52	0.4
Pedro Luro	Shales; limestones; conglo-merates; tuffs; basalts	55-70	2680	0.5	0.35
Colorado III	Continental clastics with marine shales	70-90	2600	0.5	0.35
Colorado II		90-98	2550	0.48	0.3
Colorado I	Continental to marine sandstones and conglomerates	98-125	2550	0.45	0.3
Synrift	Shales; sandstone; andesite and pyroclastic extrusion		2670	0.4	0.2
Crust (including SDR and LCB)			2700-3000		
Lithospehric mantle			3300		

3.4 Results

3.4.1 Results – Load induced subsidence

According to the "backstripping" procedure, we can estimate the amount of load induced subsidence within the Colorado Basin. Figure 3.7 shows the amount of load induced subsidence for the seven post-rift units. The largest amounts of subsidence occur during the early stages in the post-rift evolution (125-70 Ma). Subsidence during the last 70 Ma of the evolution of the basin is considerably less due to the deposition of smaller amounts of

sediments during this time window. A detailed analysis of the subsidence, induced by each sedimentary unit, reads as follows:

The deposition of the Colorado I unit induces about 1300 m of subsidence in the distal part, and about 1700 m in the central part and only a minor subsidence in the western part (about 700 m). Although deposition of the Colorado II unit lasts only for 8 Ma, the load induced subsidence is comparable with the one determined for the Colorado I unit with about 1500 m of load induced subsidence in the distal to central part and about 1100 m in the western part. Similar to the Colorado II unit, the Colorado III unit induces up to 1700 m of load in the central to distal area and about 1000 m in the western part. By contrast, the Pedro Luro unit contributes significantly less to the load induced subsidence with 580 m in the distal part, 240 m in the central part and 160 m in the western area of the Colorado Basin. The Elvira unit has its largest sediment thickness close to the COB. Accordingly, an amount of about 1000 m of load induced subsidence is obtained in this local area while the central and western areas of the Colorado Basin are characterised by about 200 m and 100 m of load induced subsidence, respectively. Although the Caotico unit deposited almost uniformly beneath the entire Colorado Basin it is also characterised by a relative small thickness when compared to the other sedimentary units. Therefore, we also obtain a minor amount of load induced subsidence of about 480 m in the distal part that decreases in westward direction to about 240 m in the central part and increases again up to 360 m in the western segment. Finally, the Shallow unit thickens again. For this reason, the amount of load induced subsidence is about 1300 m in the central part and about 700 m in the western part.

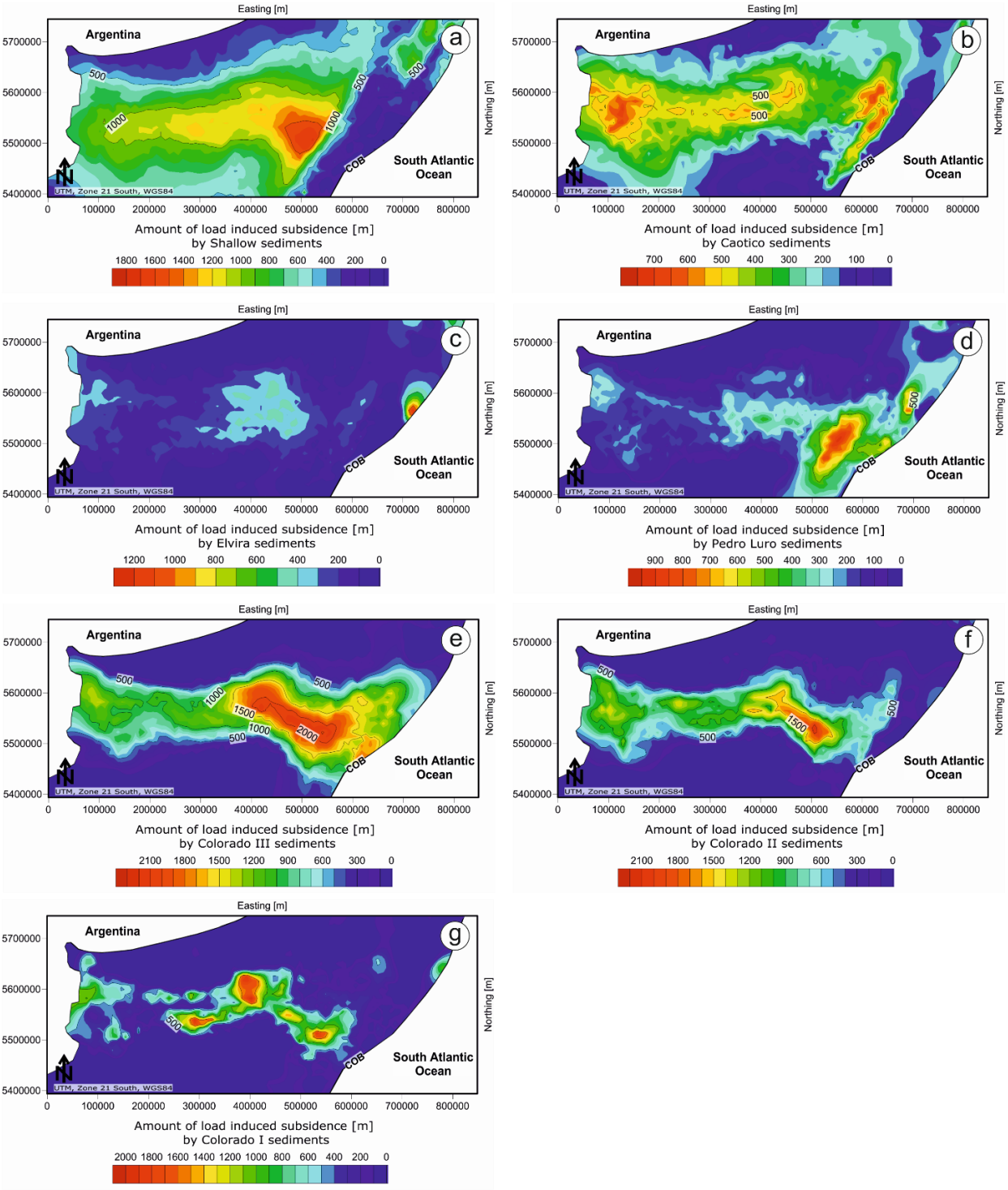

Figure 3.7: Amount of load induced subsidence for each of the post-rift phases. Colourbar is changing through time. (a) Amount of load induced subsidence from 25-0 Ma. (b) Amount of load induced subsidence from 40-25 Ma. (c) Amount of load induced subsidence from 55-40 Ma. (d) Amount of load induced subsidence from 70-55 Ma. (e) Amount of load induced subsidence from 90-70 Ma. (f) Amount of load induced subsidence from 98-90 Ma. (g) Amount of load induced subsidence from 125-98 Ma.

3.4.2 Results – Thermal subsidence

Figure 3.8 illustrates the amount of thermal subsidence as determined at the end of each of the seven post-rift phases. Following the uniform stretching model (McKenzie, 1978), the amount of thermal subsidence exponentially decays with time. This trend is generally also observed in our subsidence maps. Indeed, the amount of thermal subsidence is the largest during the early stages, that is, between 125 Ma and 70 Ma and significantly drops during the last 70 Ma. Not surprisingly, spatial variations in thermal subsidence strongly reflect variations in the β-factor considered (Figure 3.8h). Therefore, we obtain the largest amount in thermal subsidence along the COB where stretching is highest as well as in the distal to central area where the stretching factor ranges between 1.5 and 3. In westward direction the amount of stretching and therefore the amount of thermal subsidence decreases.

Furthermore, magnitudes of thermal subsidence also linearly depend on the time interval considered to calculate them. Shorter time-periods have a relatively smaller net amount of thermal subsidence when compared to larger time windows. According to the temporal resolution of our model and the respective duration of the deposition of the individual sedimentary units, the individual amounts of thermal subsidence can be described as follows:

After the first 27 Ma of the post-rift phase (deposition of Colorado I unit; 125-98 Ma), higher amounts of thermal subsidence (~1050 m) are found across the COB and up to 950 m in the distal area. Subsidence decreases while moving inward the basin to values of approximately 780 m in the central and 680 m in the western area. During the second post-rift interval (Colorado II unit; 98-90 Ma), the amount of thermal subsidence is relatively small (compared to the previous stage) with only 175 m at the COB decreasing to 150 m in the distal part and 125 m in the central part. These lower values are related to the short duration of this stage lasting approximately 8 Ma. During the deposition of the Colorado III unit (90-70 Ma), the amount of calculated thermal subsidence increases with respect to the previous stage, from about 280 m at the COB to about 220 m in the western area with 210 m in between. The time interval between 70-55 Ma (Pedro Luro unit) is characterised by about 120 m of thermal subsidence along the COB as well as in the distal area. A relative drop in thermal subsidence (to about 90 m) is obtained for the central part while for the western part only 72 m of thermal subsidence are predicted. From 55 Ma onward, the lithosphere is almost re-equilibrated as shown by only minor amounts of thermal subsidence. During 55-40 Ma (Elvira unit) the amount of thermal subsidence ranges between 75 m in the distal part and 50 m in the western part. Likewise, the next younger time interval encompassing the deposition of the Caotico

unit (40-25 Ma) is characterised by an amount of thermal subsidence less than 45 m along the COB and about 30 m in the western part with 38 m in between. Finally, the last 25 Ma (Shallow unit; 25-0 Ma) show almost no variations compared to the time interval before. Accordingly, we obtain 40 m of thermal subsidence along the COB, 36 m in the distal part, 31 m in the central part and only 27 m in the western part.

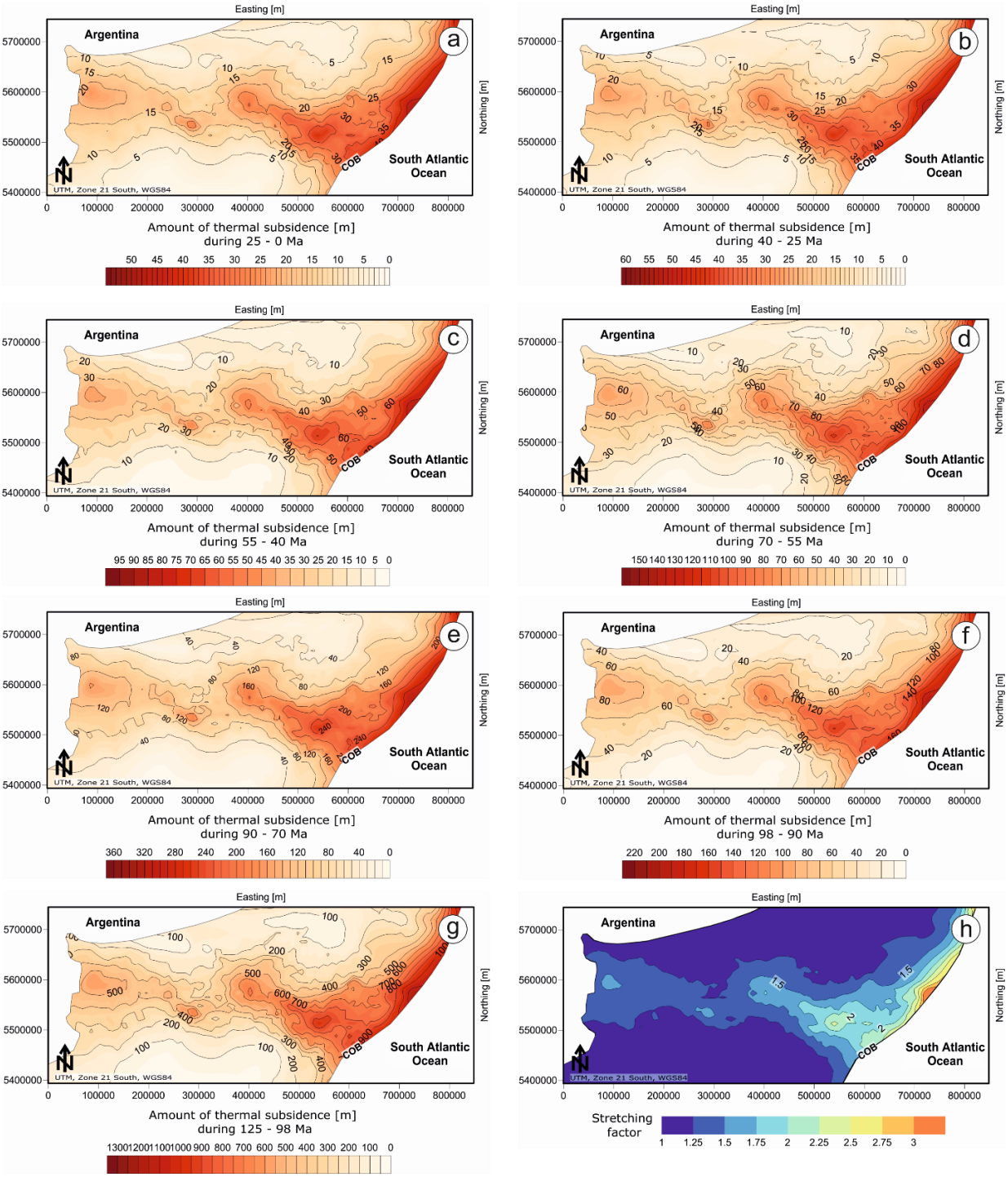

Figure 3.8: Amount of thermal subsidence for each of the post-rift phases. Colourbar is changing through time. (a) Amount of thermal subsidence from 0-25 Ma. (b) Amount of

thermal subsidence from 25-40 Ma. (c) Amount of thermal subsidence from 40-55 Ma. (d) Amount of thermal subsidence from 55-70 Ma. (e) Amount of thermal subsidence from 70-90 Ma. (f) Amount of thermal subsidence from 90-98 Ma. (g) Amount of thermal subsidence from 98-125 Ma. (h) The map illustrates the distribution of the stretching factor β. β is the result of the ratio between initial crustal thickness of 35 km and the present-day crustal thickness (including LCBs and SDRs).

3.4.3 Results – Paleobathymetries

In an attempt to discuss the net effect of thermal subsidence by lithospheric cooling and load induced subsidence from sedimentation, we discuss in the following the obtained paleobathymetries for each of the seven post-rift stages (Figure 3.9).

By inspecting these figures, it is evident that the Colorado Basin has been affected by continuous subsidence from breakup to the present-day as the water depth shallows after correcting for the load induced subsidence and thermal subsidence.

Going backward in time, the restored paleobathymetry at the start of deposition of the Shallow unit (top of the Caotico unit; 25 Ma) displays water depths less than 200 meter below sea level (m.b.s.l.) in the western and central part of the Colorado Basin that deepens to about 280 m.b.s.l. in the north and 480 m.b.s.l. in the south. A rapid deepening to about 700 m.b.s.l. occurs at about 100 km westward of the COB (to which we refer as distal margin in the following). The area along the COB is characterised by about 2800 m.b.s.l. At 40 Ma (top of the Elvira unit), the paleobathymetry is less than 300 m.b.s.l. in the western and central segment with larger depths of up to 550 m.b.s.l. in the south and 400 m.b.s.l. in the north. Towards the Atlantic Ocean, we obtain a paleobathymetry ranging from 800 m.b.s.l. along the distal margin up to a maximum of 2800 m.b.s.l. at the COB. The paleobathymetry at the top of the Pedro Luro unit (55 Ma) does not show any sensible changes with respect to the one discussed previously, mainly because of the presence of thin sediments which have deposited during this time window. The restored paleobathymetry at the start of the deposition of the Pedro Luro unit (top of the Colorado III unit; 70 Ma) shows values as low as 150 m.b.s.l. in the central- and western part, increasing gradually to 400 m.b.s.l. in the north, 580 m.b.s.l. in the south and up to a maximum of 2800 m.b.s.l. at the COB. Removing the Colorado III unit and correcting for the respective thermal subsidence yields the paleobathymetry at the top of the Colorado II unit (90 Ma). We obtain about 500 m.b.s.l. of paleobathymetry in some

central areas with larger values of 700 m.b.s.l. in the southwest. A depth-range between 1000 m.b.s.l. and 2800 m.b.s.l. is obtained at the distal margin. At the top of the Colorado I unit (98 Ma) the paleobathymetry shows values of 900 m.b.s.l. in the central and western part with an exception of 300 m.b.s.l. in between the western and central segment. By contrast, the north and the south is marked by about 500 m.b.s.l. of depth. The distal part has a paleobathymetry of about 1100 m.b.s.l. and up to 2600 m.b.s.l. at the COB. Finally, we obtain the last paleobathymetry at 125 Ma which is the top of the syn-rift unit. The resulting paleobathymetric map has an overall paleobathymetry of 750 m.b.s.l. in the western and central part and down to 1700 m.b.s.l. at the COB. In addition, the north area is locally (close to the present-day coast line) characterised by elevations above sea level up to 100 m.

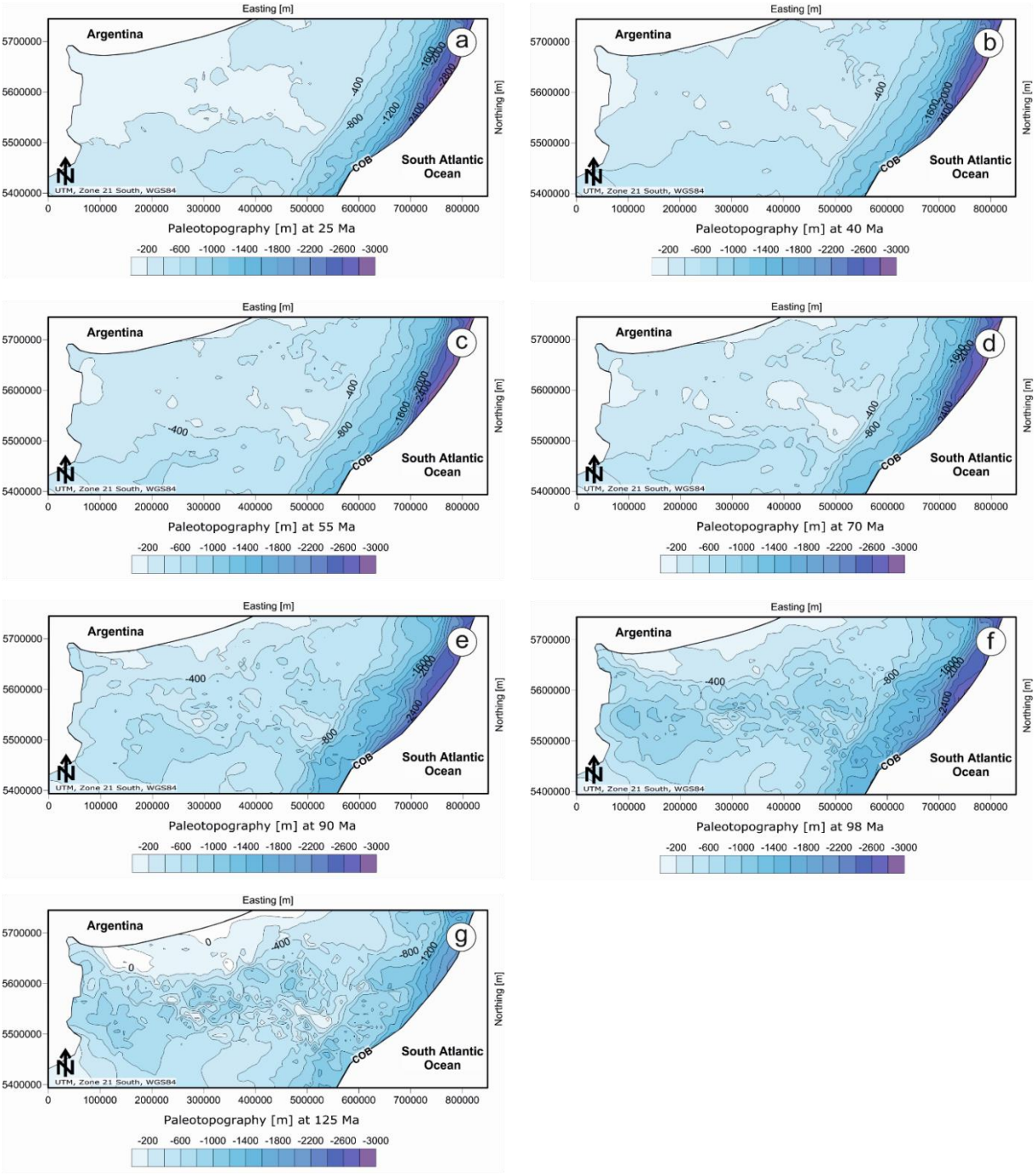

Figure 3.9: Paleobathymetries for seven times during the post-rift phase according to the model resolution. The maps are the result of the backward modelling approach assuming Airy isostasy and decompaction as well as thermal subsidence. (a) Paleobathymetry at the end of the Caotico unit (25 Ma). (b) Paleobathymetry at the end of the Elvira unit (40 Ma). (c) Paleobathymetry at the end of the Pedro Luro unit (55 Ma). (d) Paleobathymetry at the end of the Colorado III unit (70 Ma). (e) Paleobathymetry at the end of the Colorado II unit (90 Ma). (f) Paleobathymetry at the end of the Colorado I unit (98 Ma). (g) Paleobathymetry at the end of the syn-rift unit (125 Ma).

3.5 Discussion

As discussed above, major changes in the depth of the paleobathymetries occur during the early times after the breakup (from 125-70 Ma) while only minor ones are depicted for the remaining 70 Ma up to present-day. This latter time period is also characterised by deposition of smaller amounts of sedimentary units (Shallow, Caotico, Elvira, Pedro Luro; Figure 3.7) than those during the early post-rift stage (Colorado III, Colorado II, Colorado I; Figure 3.7). Besides, the oldest units (125-70 Ma) were mainly deposited beneath the central and eastern part, whereas the younger units (70-0 Ma) were deposited more towards the eastern part, thus marking the major depocentres as presently observed within the basin area (Figure 3.2).
Additionally, because the lithosphere is almost equilibrated, these latest stages have also the smallest amounts of thermal subsidence (Figure 3.8). Therefore, we can identify a two stage subsidence evolution for the Colorado Basin on first-order effects, characterised by higher vertical movement during the first 55 Ma after breakup and only relatively minor ones occurring during the remaining 70 Ma, during which time period also the paleo-water depths did not change significantly.

To discuss the evolution of the subsidence constrained for the Colorado Basin and to carry out a comparison with the reconstructed subsidence at the conjugate margin offshore SW Africa, we plot one dimensional subsidence profiles as extracted from two synthetic wells beneath the Colorado Basin: one chosen as representative for the western and one for the eastern segment (Figure 3.10). In addition, the subsidence curves derived from a previous study, focused on the Orange Basin (Dressel et al., 2015), are also plotted to facilitate our discussion.
The 1D profiles are representative of a trend considered typical of a passive margin setting not disturbed by external forcing (Bott, 1992). According to Figure 3.10, the western and eastern areas of the Colorado Basin vary in the amount of total subsidence in that the eastern segment experienced more subsidence than the western segment, giving a final difference of approximately 2500 m of subsidence at present-day. The difference can be interpreted as being partially the result of larger amounts of stretching in the eastern segment ($\beta = 2.52$) than in the western segment ($\beta = 1.73$). However, the magnitudes of variations in the stretching factors alone are insufficient to explain the amount of difference in the calculated total subsidence. Most likely, variation in the sedimentation (rates and supply, i.e., load induced subsidence) are to be called for in order to reconcile these observations. The amount of load induced subsidence can be calculated from Figure 3.10 as the area between the thermal and

total subsidence curves. By calculating the individual amounts of load induced subsidence at each time interval, no general relationship between the two segments can be discriminated. Accordingly, we obtain a larger load induced subsidence in the western segment for the time interval between 40 Ma to 25 Ma (deposition of the Caotico unit) and between 55 Ma to 40 Ma (deposition of the Elvira unit) of 475 m and 331 m, respectively. During the time interval of 98 Ma to 90 Ma (deposition of Colorado II unit), the amount of load induced subsidence is almost the same in the western and eastern segment. For the other time intervals, the eastern segment has larger amounts of load induced subsidence. These aspects suggest that although the Colorado Basin has been characterised by continuous subsidence since breakup, its post-rift history is likely the result of several components (e.g., change in depositional environment) which acted at different temporal and spatial scales.

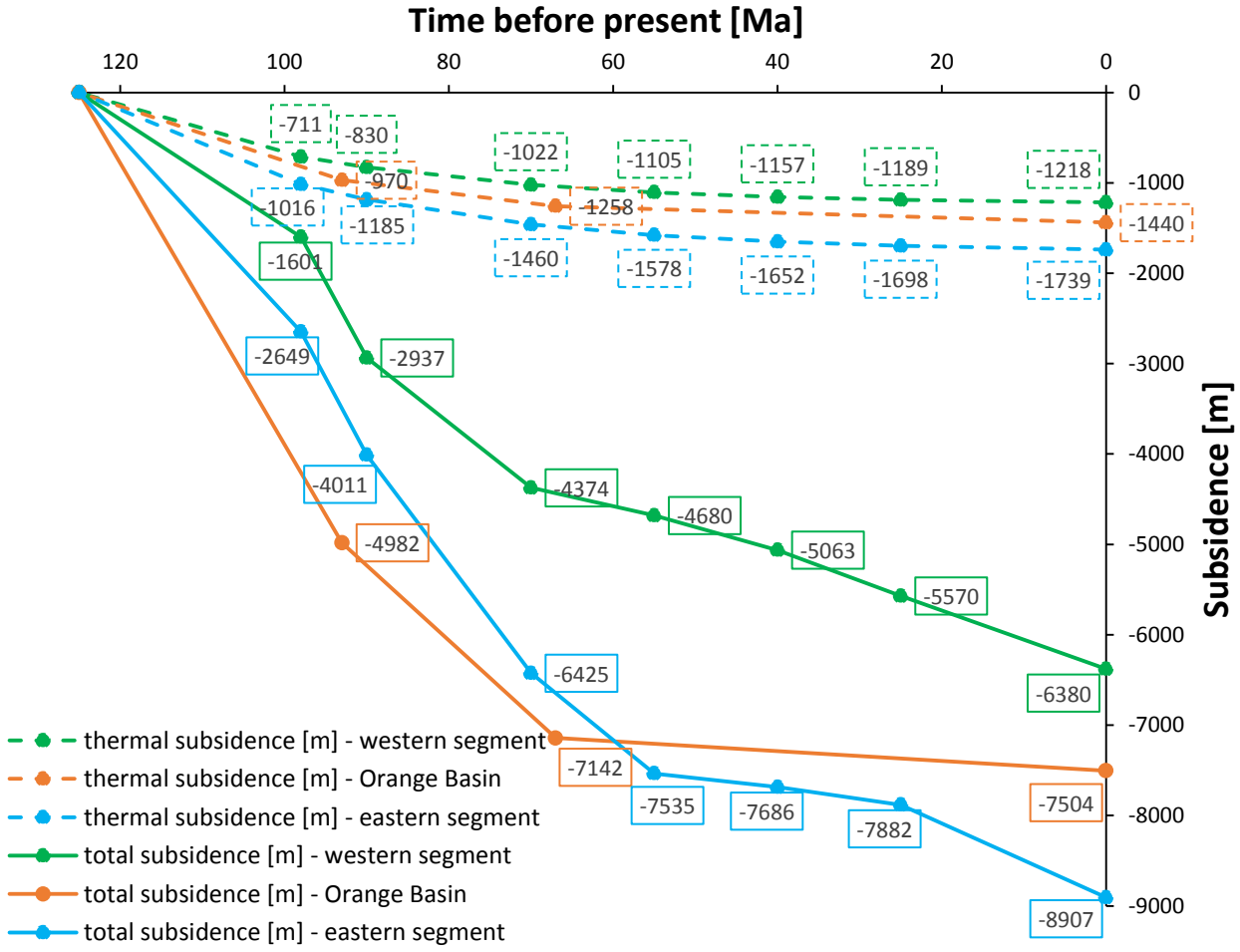

Figure 3.10: Post-rift subsidence curves for two synthetic wells in the eastern and western segment of the Colorado Basin, respectively (green and blue curve) as well as the subsidence curves for a synthetic well in the Orange Basin (orange curve, after Dressel et al., 2015). See Figure 3.1 for location. Solid curves show the thermal subsidence (β = 1.73 for western

segment; β = 2.0 for Orange Basin; β = 2.52 for eastern segment) while the dashed curves indicated the total subsidence; i.e., the sum of the thermal subsidence and the load induced subsidence. The amount of the latter is characterised by the space between the respective solid and the dashed curves.

Comparing the subsidence curves as described before with a one dimensional profile extracted for the conjugate Orange Basin, offshore SW Africa (Dressel et al., 2015) reveals differences between the two margins. The amount of thermal subsidence, determined for the Orange Basin, is comparable with the Argentine margin, which is plausible given the fact that similar stretching conditions during breakup occurred at both settings. While the stretching factor for the Colorado Basin is 1.73 (western segment) and 2.52 (eastern segment), respectively, the Orange Basin thermal subsidence curve is calculated using a β of 2.0 (Figure 3.10). Therefore, it represents an average between the thermal subsidence curves of the Colorado Basin. By contrast, the amount of total subsidence significantly varies between the Orange and the Colorado Basin. The Orange Basin experienced its largest total subsidence during the Cretaceous, while the eastern segment of the Colorado Basin experienced also a larger total subsidence during Cenozoic times. At about 67 Ma the total subsidence curves of the Orange Basin and the eastern Colorado Basin cross each other with the result of more total subsidence within the western Colorado Basin than in the Orange Basin (a difference of up to 1115 m at the present-day). As the amount of thermal subsidence is within the same order of magnitude, the reason for the varying total subsidence relates to different amounts of sediment supply in the two basins, higher for the Colorado Basin than for the Orange Basin. This is in agreement with the sedimentation rates suggested by Loegering et al. (2013). However, while a change in sediment supply could have surely played a role in shaping the overall subsidence history of the two basins, it is also possible that other processes might have come into play as well. In this regard, seismic profiles across the Orange Basin showed several unconformities that are partially interpreted as erosional truncation horizons (Brown et al., 1995; Paton et al., 2007; Hirsch et al., 2010; Kuhlmann, et al. 2010). In addition, Hirsch et al. (2010) evaluated that the best fit between modeled and observed vitrinite reflectance data can be achieved only by considering an erosion of about 1000 m. Furthermore, erosional events are also in agreement with investigations onshore South Africa by Braun et al. (2014). These authors relate the erosion of the South African plateau to a major uplift episode during

the Late Cretaceous. Consequently, it is most probable that differences between the subsidence curves for the Colorado Basin and the Orange Basin can, at least partly, result from extensive post-depositional erosion of the sediments in the Orange Basin. These erosional processes may have been related to tectonic uplift along the SW African margin that did not affect the SE South American margin.

If this was the case, the question that remains is which mechanisms could have caused such asymmetric uplift. Furthermore, it remains open which tectonic force has been the cause of the SW African seafloor uplift and during which time in the evolution of the two settings it was acting. In this sense, a possibility would be the ridge-push due to the spreading of the South Atlantic Ocean (Japsen et al., 2012). Alternatively, the detected uplift could be the surface expression of a deep mantle mechanism (Nyblade and Robinson, 1994), an aspect to which there is still an open debate. Some studies identified plume activity beneath the African continent as a possible force triggering the uplift and leading to erosion of the younger strata (Moucha and Forte, 2011; Colli et al., 2014). Regarding the African continent, results from of Dressel et al. (2015) also indicated post-rift seafloor uplift along the SW African margin interpreted as the result of either a deep mantle mechanism or of another a tectonic force, possibly related to compressional forces as a consequence of seafloor spreading.

Regional uplift in the Colorado Basin area during the Upper Cretaceous and Paleocene/Eocene has also been discussed by Autin et al. (2013). However, this study offers no explanation for these events. The results from the study by Cobbold et al. (2007) indicated a regional compressional stress state within South America since the Cretaceous (and possibly ongoing) as induced by the subduction of the Nazca Plate beneath the South American plate and ridge-push forces from ongoing opening of the South Atlantic. However, their discussions rather focus on the Santos Basin, north of the Colorado Basin offshore SE Brazil. Therefore, their results cannot be directly transferred to the Colorado Basin. Furthermore, Sachse et al. (2015) reported uplift in the Austral Basin, located on- and offshore South America and the Malvinas Basin, both 1200 km south of the Colorado Basin. Accordingly, it is likewise difficult to compare the evolution of those basins with the Colorado Basin. For the research area of the present study, Demoulin et al. (2005) linked Cretaceous sediments within the Colorado Basin to erosion in the Ventana massif (NW of the Colorado Basin, onshore South America). They concluded from their morphogenetic model that the Ventana massif underwent two uplift phases that are in accordance with the observed increase in sedimentation rates in the Colorado Basin. They interpreted these uplift episodes as caused by

the South Atlantic opening during the Cretaceous and a Neogene reactivation of structures in the foreland of the Andes.

In the light of the results of all the previous studies as described above, obtained differences in the subsidence evolution of the conjugate Argentine and SW African margins give evidence that ridge-push forces related to the dynamics of the South Atlantic are to be considered at most of secondary relevance in affecting the evolution of the South Atlantic margins. Therefore, we agree with other studies in assuming mantle dynamics as a causative mechanism for the recorded uplift across SW Africa (Lithgow-Bertelloni and Silver, 1998; Ritsema et al., 1999; Gurnis et al., 2000; Braun et al., 2014; Colli et al., 2014; Dressel et al., 2015). Uplift along the SW African margin is in agreement with the presence of erosional unconformities within the stratigraphic record of the Orange Basin (Hirsch et al., 2010; Kuhlmann et al., 2010) and with the main conclusions of Loegering et al. (2013) demonstrating no evidence for any significant erosion (even as low as few tens of meters) in the Colorado Basin since the breakup of the South Atlantic.

3.6 Conclusions

The subsidence analysis of the Colorado Basin using present-day information about the configuration of the sediments and the crystalline crust allows quantifying the amount of load induced subsidence as well as the amount of the thermal subsidence for seven time intervals during the post-rift phase. This information is used to reconstruct paleobathymetries of the Colorado Basin indicating rather continuous subsidence through the entire post-rift phase.

Comparing the paleobathymetries restored for the Argentine margin with those of the conjugate margin offshore SW Africa reveals significant differences of the subsidence history on both margins. In contrast to the Argentine margin paleobathymetries, those at the SW African margin indicate intermittent periods of uplift and erosion (as indicated by positive paleotopographies). Compression by ridge-push inducing margin uplift cannot account for positive paleotopographies as its consequence should be evident at the Argentine margin to the same extent as at the conjugate SW African margin. As we do not consider a mantle component in our approach this leads us to conclude that the only force which can cause the reconstructed seafloor uplift, only at the SW Africa but not at the Argentine margin, is related to deep mantle processes beneath SW Africa.

Acknowledgements

This study has been done within the framework of the priority program SAMPLE (South Atlantic Margin Processes and Links with onshore Evolution; SPP 1375), funded by the German Research Foundation (DFG; grant no. SCHE 674/5-3). We are grateful to Julia Autin for providing the thickness maps used in this study.

4 Coupled thermo-mechanical 3D subsidence analysis along the SW African passive continental margin

Abstract

Sedimentary basins along the SW African margin deliver information about processes, which occurred in the past and serve as a good starting point for reconstructing the margin's evolution. By integrating detailed information on the present-day configuration of the SW African margin into a 3D thermo-mechanical forward modelling framework, we attempt a margin-wide reconstruction of its subsidence history since its onset during breakup.

The 3D forward modelling approach as applied on the SW African margin area and makes use of the coupling between thermal relaxation of the lithosphere and flexural isostatic balance in response to sediment deposition and build-up of thermal stresses during lithosphere cooling.

On the one hand, our results provide useful information about the behavior of the lithosphere during breakup and the subsequent post-rift phase. On the other hand, restored paleobathymetries for specific time intervals during the post-rift evolution give evidence for possible uplift events superposed on the long-term subsidence history of the margin. Restored paleobathymetries are in agreement with conclusions derived from former studies and provided strong indications for the presence of a rather heterogeneous crustal configuration of the margin marked by a mechanical decoupling of the upper and lower crustal domains during most of the rifting phase.

4.1 Introduction

Several tectonic processes (i.e., ridge-push from the spreading of the South Atlantic Ocean and deep mantle convective instabilities) have affected the thermal and mechanical configuration of the SW African continental margin since the breakup of Gondwana (~125 Ma). As a result, the margin underwent a rather complex subsidence evolution characterised by a general deepening of the seafloor superimposed by local phases of upward vertical movements of the basement (e.g., Nyblade and Robinson, 1994; Burke, 1996; Gurnis et al., 2000; Jackson et al., 2005; Guillocheau et al., 2013). Understanding the dynamics of interaction among these processes and their effects on the thermo-mechanical configuration of the margin is therefore crucial to deepen our current knowledge of the geodynamic history of

the sedimentary basins and its relation to the formation and maturation of their georesources. Previous studies mainly focused on characterising the margin's configuration (e.g., Gladczenko et al., 1998; Bauer et al., 2000; Paton et al., 2008; Maystrenko et al., 2013), post-breakup vertical movements (Japsen et al., 2012; Dressel et al., 2015), sedimentation history and tectonic evolution for specific areas (e.g., Brown et al., 1995; Stewart et al., 2000; Broad et al., 2006; Uenzelmann-Neben et al., 2007; Hirsch et al., 2007, 2009, 2010). However, apart from some recent efforts (Braun et al., 2013; Rouby et al., 2013), these studies usually neglected to consider thermo-mechanical feedback effects on the subsidence and uplift processes along the continental margin. Additional work has been focused towards a quantification of the surface expression of mantle dynamics (e.g., Burov and Guillou-Frottier, 2005; Burov et al., 2007; Burov and Cloetingh, 2010; Faccena and Becker, 2010; Moucha and Forte, 2011; Flament et al., 2013; Burov and Gerya, 2014). Although these investigations provided useful insights into the dynamics of the deep mantle and its interactions with surface deformation processes, they usually relied on first-order geodynamic principles thus hampering to link modelling results to available observations on the present-day margin configuration.

In the present study, we carry out a 3D thermo-mechanical subsidence analysis of the SW African margin (Figure 4.1) by taking into account the coupling between thermal cooling of the lithosphere, incremental and time varying loading by active sedimentation and their effects on the flexural behavior of the lithospheric plate. Similar to the work on 2D flexural modelling by Millán et al. (1995), we based our 3D forward modelling on detailed information available on the present-day configuration of the major basins along the SW African margin as summarised in a comprehensive 3D geological model by Maystrenko et al. (2013). In the final stage of the study, the results of the forward modelling are "validated" against available observations on the present-day bathymetry. At this stage, the aim is not to minimise the misfit between observations and model results by "ad hoc" tuning of the model parameters. Differences between model results and observation rather serve to lead a final discussion centred on additional processes that likely affected the margin evolution and the influence of which is neither directly stored in the sedimentary archive nor included in the modelling approach. Therefore, the advantage of the work stems not only from describing a 3D margin-wide thermo-mechanical model of its subsidence evolution, but by integrating detailed information about the sedimentary configuration as constrained at present, it also

provides a data-driven approach to assist any reconstruction of the geodynamics of the margin since its formation.

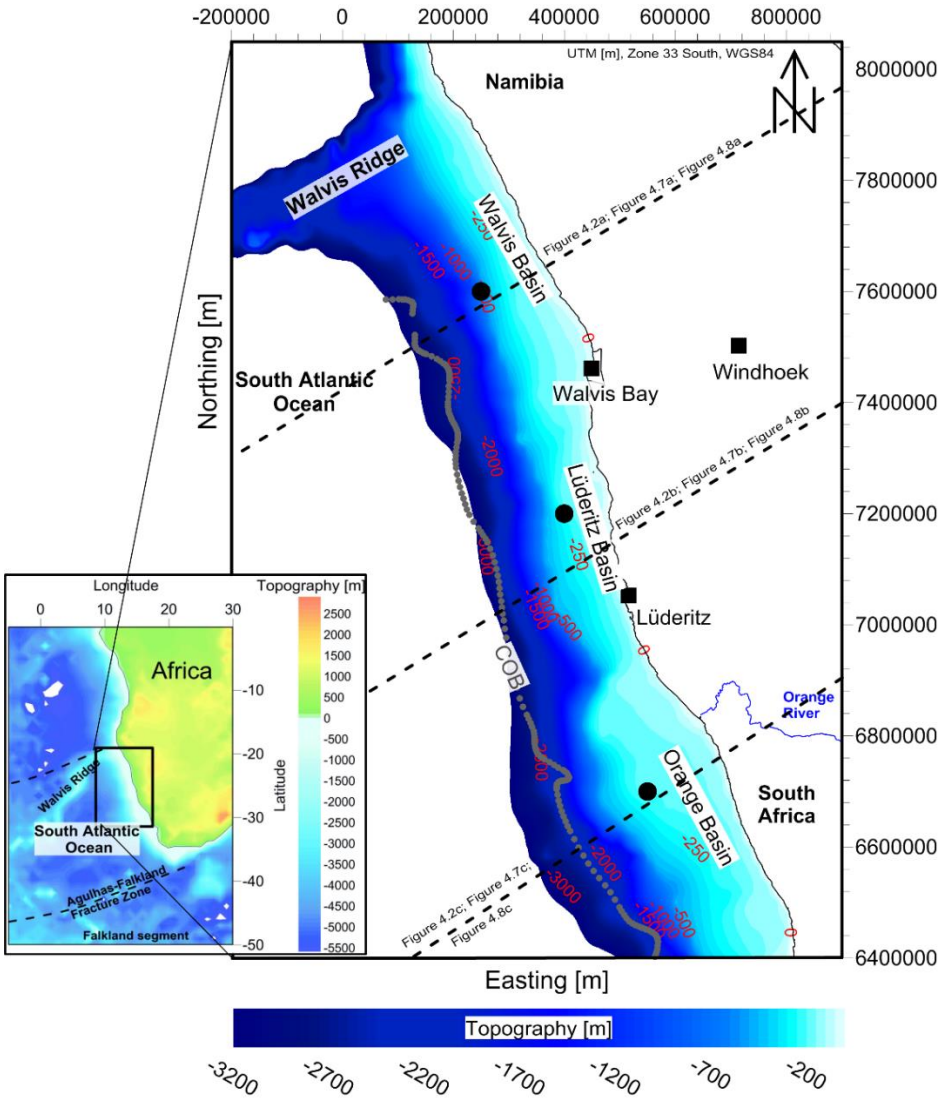

Figure 4.1: Map showing the research area, the SW African continental margin (bathymetry after IOC, IHO and BODC, 2003) with continent-ocean boundary (COB; grey dotted line, after Pawlowski, 2008). Black dashed lines mark the profile locations used to illustrate the modelling results in Figure 4.2, Figure 4.7 and Figure 4.8. The black dots mark the locations of the synthetic boreholes used in Figure 4.3 and Figure 4.10. Coordinate system is UTM [m], zone 33 south (WGS 84). Inset: Overview of the southern African continent and the South Atlantic Ocean with location of research area (black box) in geographical coordinates.

4.2 Model parameterisation and input data

Information about the sedimentary sequences as well as the deeper crustal and lithospheric mantle configurations have been summarised in a 3D structural model by Maystrenko et al. (2013). The model is based on different types of available data comprising seismics and seismological data, wells and it was finally constrained by 3D gravity modelling. We make use of grid-files as derived from this model to carry out our 3D forward modelling study. The rather complex sedimentary and crustal architecture of the SW African margin is exemplarily illustrated in Figure 4.2 along cross-sections running along each of the three main sedimentary basins.

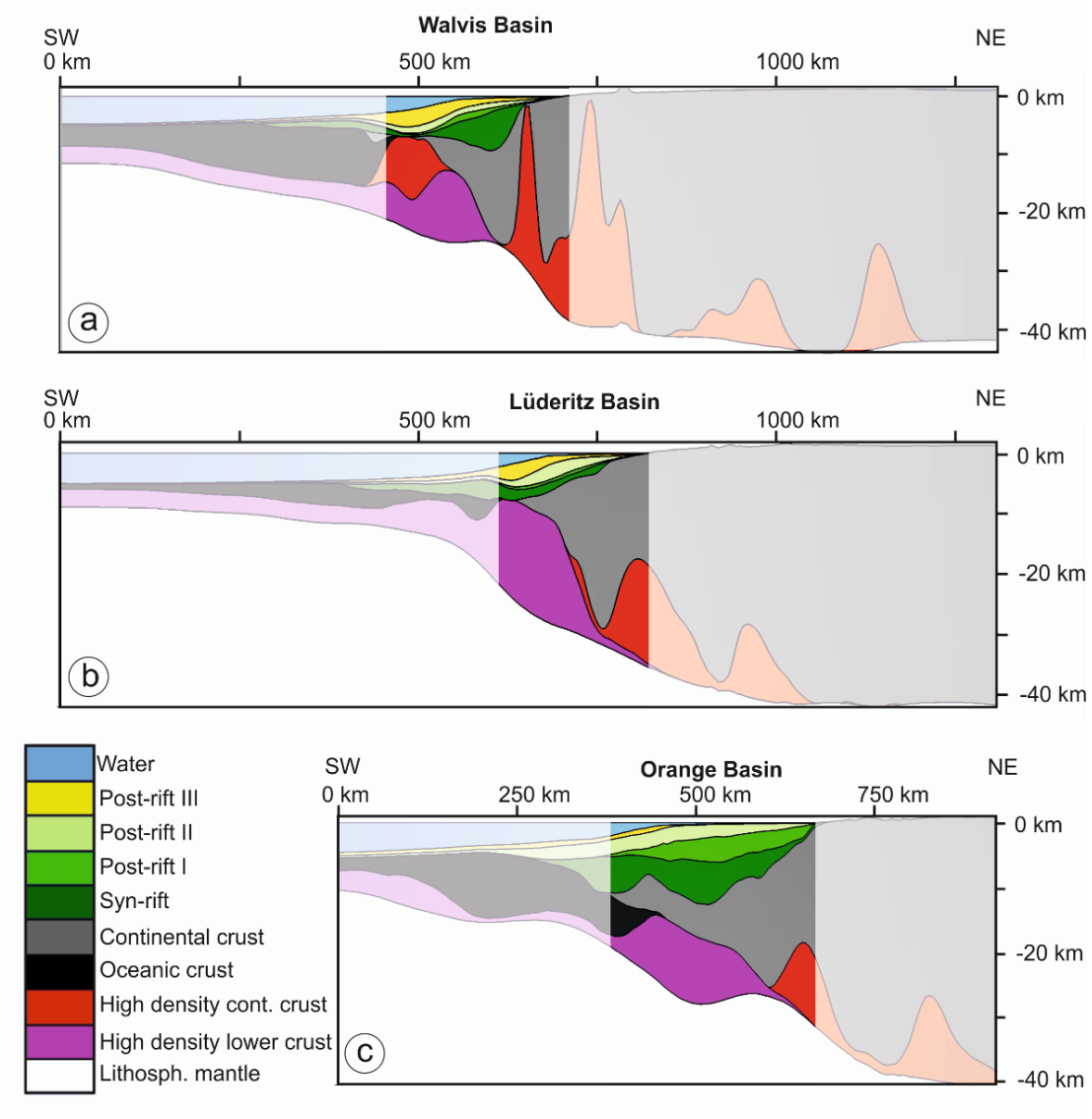

Figure 4.2: Profiles across the three major sedimentary basin in the study area: (a) Walvis Basin (b) Lüderitz Basin (c) Orange Basin. The area of the continental margin is highlighted as it is the focus on the study. The cross sections show the distribution of sediments as well as

the crustal architecture and the depth to the Moho (after Maystrenko et al., 2013). See Figure 4.1 for the exact profile locations.

The model differentiates between four major sedimentary units, each confined by horizons representing major unconformities: (1) syn-rift (base Aptian – top basement), (2) post-rift I (base Aptian – base Turonian), (3) post-rift II (base Turonian – base Cenozoic) and (4) post-rift III (base Cenozoic – seafloor). Clastic sediments comprising mainly sandstone and claystone as well as few shales and subordinate limestone dominate the entire sedimentary succession. In contrast to the African margin north of the Walvis Ridge, there is no evidence for salt deposition and halokinetics in the study area (Gladczenko et al., 1998; Karner and Driscoll, 1999; von Nicolai et al., 2013).

Figure 4.3 illustrates isopach maps for all individual units resolved in the present study, showing their spatially varying thickness distribution throughout the area. Additionally, in Figure 4.4 we illustrate exemplarily synthetic wells chosen for three representative locations that will be used to discuss details of the subsidence evolution in the following chapters. This information is here added in order to better understand the distribution of the sediment in each of the major sedimentary basins. According to both figures (Figure 4.3 and Figure 4.4), it becomes obvious that the northern part of the SW African margin (Walvis Basin) and the southern part (Orange Basin) accommodate the thickest syn-rift unit and post-rift units. By contrast, the area in between (Lüderitz Basin) stores the thinnest sedimentary units but the deepest basement.

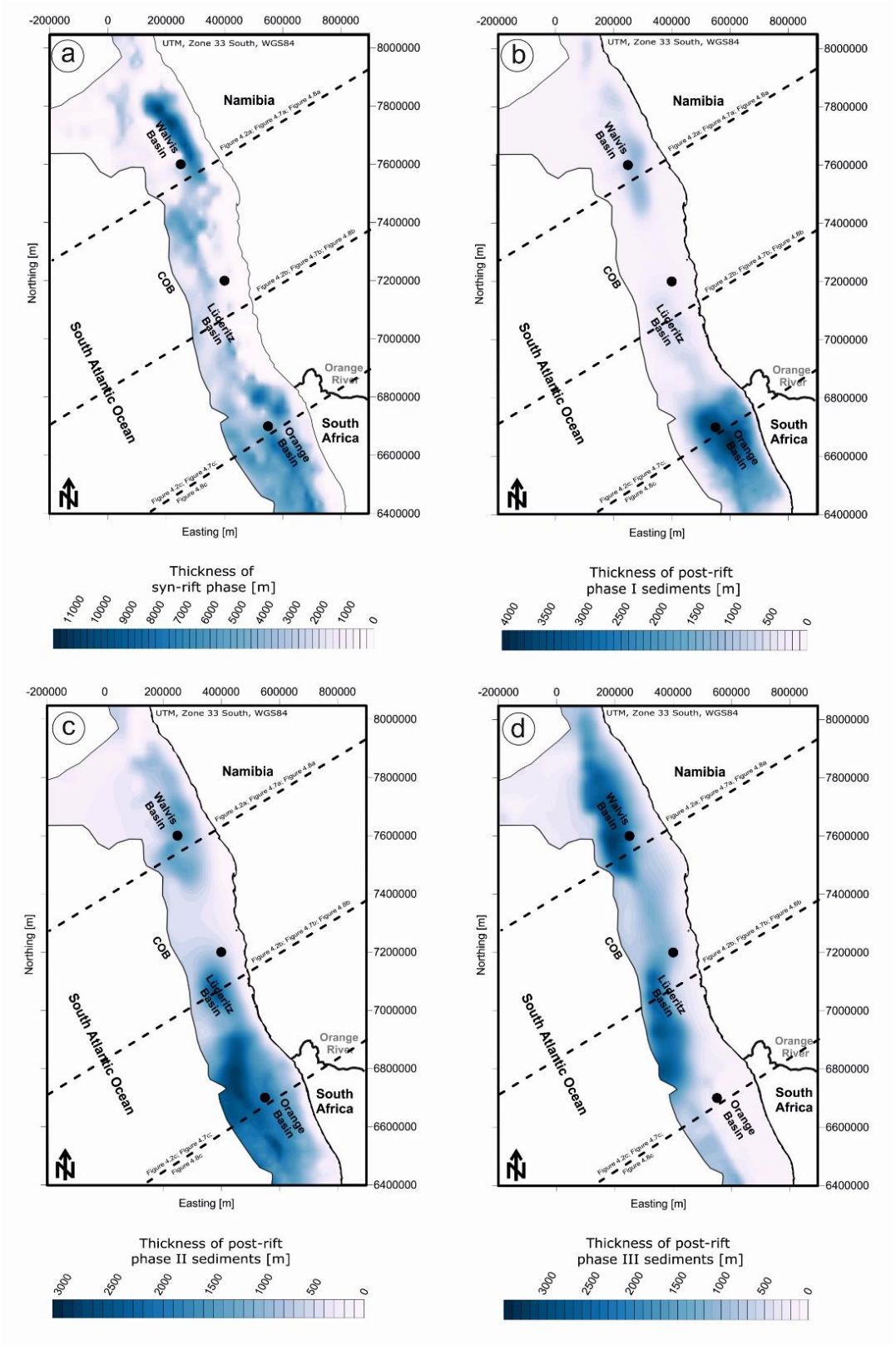

Figure 4.3: Isopach maps of the syn-rift unit (a) and of the three post-rift units (b-c). The dashed lines mark the locations of the cross sections shown in Figure 4.2 as well as Figure 4.7 and Figure 4.8. The black dots mark the area of the synsthetic wells further discussed in Figure 4.4 and Figure 4.10.

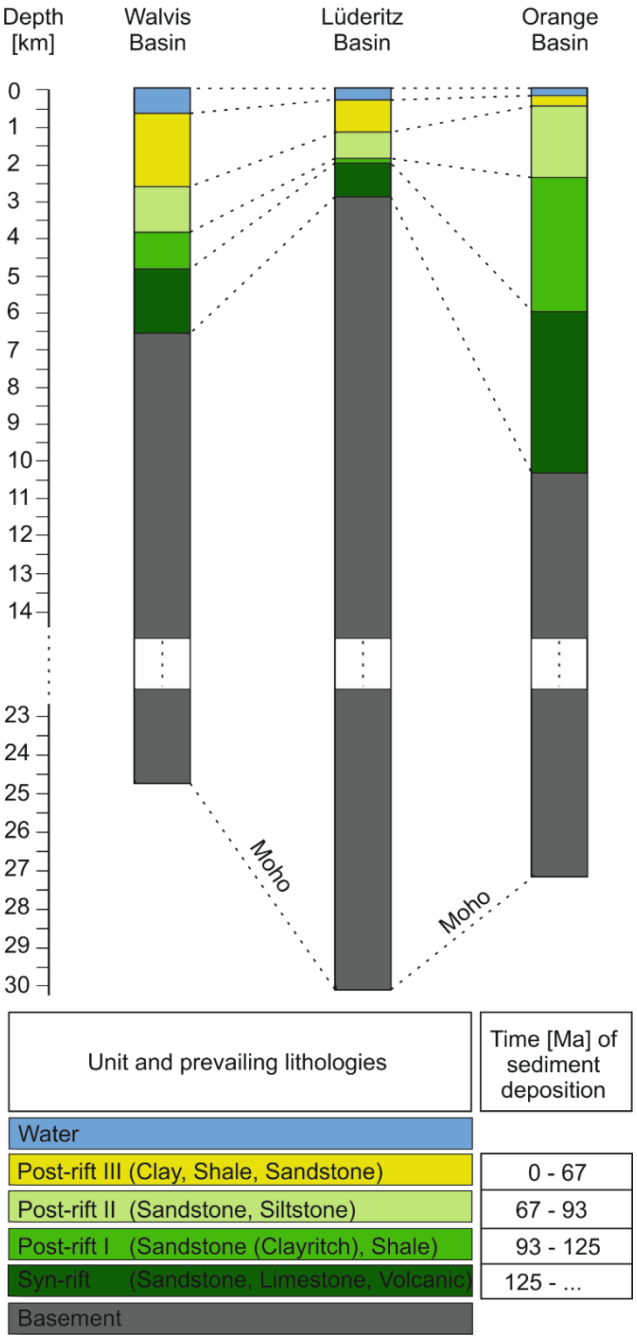

Figure 4.4: Stratigraphy of three synthetic wells in each of the major sedimentary basin. See Figure 4.1 for their locations.

Furthermore, as shown in Figure 4.2 the model by Maystrenko et al. (2013) differentiates the crust between domains of high-density and high-shear wave velocity embedded in a rather homogeneous crystalline crust. Thybo and Artemieva (2013) proposed underplating along volcanic rifted continental margins during late stages of rifting and breakup but not post-breakup. For the reason that our study focuses on the margin evolution during the post-rift

phase considering coupled thermo-mechanical processes, we assume these lower crustal bodies to have been emplaced pre-breakup. This assumption enables us to consider the crustal domain as a homogeneous layer (down to the crust-to-mantle boundary (Moho) of Maystrenko et al., 2013) for which an average density has been imposed (Table 4.1); however, an attempt to quantify the differences in the paleobathymetric evolution has been carried out and is further discussed in the discussion part. The other geological layers included in the study comprise a lithospheric mantle overlying an iso-viscous asthenospheric layer. The latter has been implemented in the modelling for mainly numerical reasons in order to buffer the basal thermal input within the model domain. This was deemed necessary because of the choice of a thermal basal boundary, adopted, which consists of a fixed temperature rather than of a heat influx in the model domain. Therefore, the presence of such an adiabatic layer across the base of the model will guarantee a constant heat input from the bottom into the model thus avoiding possible boundary effects affecting the transient cooling of the system. Table 4.1 summarises the relevant properties adopted for all layers in the forward modelling. As the focus of the present study is to reconstruct the subsidence evolution of the continental margin of SW Africa, the continent-ocean boundary (COB) after Pawlowski (2008) is used to define the extent and boundary of the continental margin.

Table 4.1: Names, lithology, ages, and assigned physical properties of the individual units used for the 3D forward modelling (after Sclater and Christie, 1980; Holtar and Forsberg, 2000; Waples and Waples, 2004; Broad et al., 2006; Hirsch et al., 2007, 2010; Paton et al., 2007; Hartwig et al., 2012; Cohen et al., 2013; Maystrenko et al., 2013).

Name of individual units	Modified ages of the units [Ma]	Prevailing lithologies used in this study	Density [kg/m³]	Conduc-tivity [W/mK]	Heat produc-tion [µW/m³]	Heat capacity [10^{-3}J/kg K]	Thermal expansion coefficient [*10^{-5}/°C]
Post-rift III	0 - 67	Clay; Shale; Sandstone	2150	1.50	1.00	0.92	
Post-rift II	67 - 93	Sandstone; Siltstone	2420	1.90	1.00	0.88	
Post-rift I	93 - 125	Sandstone (Clay rich); Shale	2550	2.00	1.10	0.84	
Syn-rift		Sandstone; Limestone, Volcanics	2570-2700	2.60	1.30	0.95	
Continental crust			2850	2.80	1.30	0.68	2.80
Lithospheric mantle			3330	3.95	0.03	1.05	3.28
Asthenos-phere			3250				

4.3 Method

We follow a 3D thermo-mechanical approach (Cacace and Scheck-Wenderoth, 2014) to model the post-rift evolution of the SW African margin taking into account details of the dynamic coupling between sedimentation, lithospheric flexure, and thermal contraction on the resulting subsidence. Figure 4.5 schematically illustrates the basic workflow. In the present study, we do not attempt any modelling of the rifting stage predating breakup. Instead, we introduce such a rifting event in terms of an initial destabilization of the thermo-mechanical configuration under pure shear and uniform stretching (McKenzie, 1978).

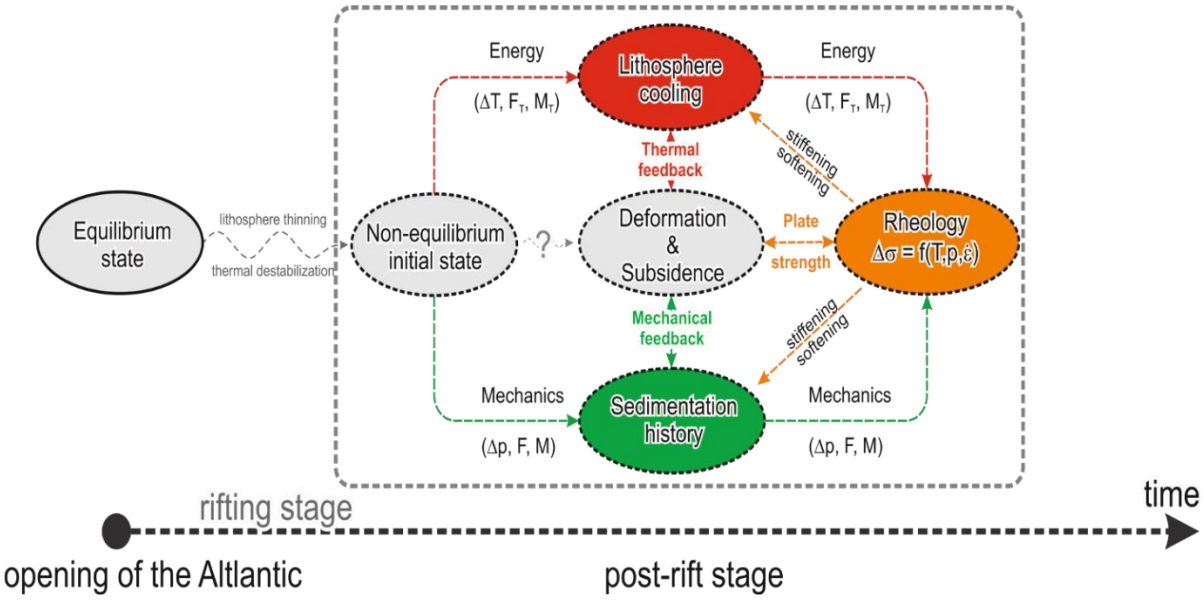

Figure 4.5: Scheme of forward modelling approach after Cacace and Scheck-Wenderoth (2014) and Scheck-Wenderoth et al. (2015). An initial perturbation (i.e., lithosphere thinning and thermal destabilization) moves the system out of thermal and mechanical equilibrium. This leads to the generation of internal stresses resulting from variations in the thermal configurations (ΔT) in the forms of a net shear force (F_T) and a bending moment (M_T) as well as to a change in the rheological configuration of the lithosphere. Those variations will trigger vertical crustal deformation (i.e., subsidence and/or uplift), which will retro-affect the thermal configuration thus promoting new thermal stresses and renewed vertical deformation (i.e., thermal feedback). Sedimentation additionally affects the deformation history through time by imposing a direct load acting on the plate, and by retarding the cooling via thermal blanketing (mechanical feedback). In our approach, we do not consider a rheological model to parameterise the Effective Elastic Thickness (EET), but we constrain its thickness by means of a specified isotherm (T=450°).

The starting model at equilibrium consists of a uniform crust (35 km thick) overlying a uniform lithosphere (125 km thick). These values have been chosen because they represent present-day thicknesses as constrained for the lithosphere near the continental margin, therefore, not affected by any stretching kinematics. Figure 4.6 illustrates a map showing the variations in the stretching factor considered in the modelling to destabilize the input model geometry. The stretching factor is here defined as the ratio between the crustal thickness at equilibrium (35 km) and the thickness observed at present-day, the latter being derived based

on the 3D structural model as described in the previous paragraph. Following McKenzie (1978), instantaneous stretching of the lithosphere results in crustal and mantle thinning thus inducing a first stage of (syn-rift) subsidence and a thermal destabilization of the lithosphere.

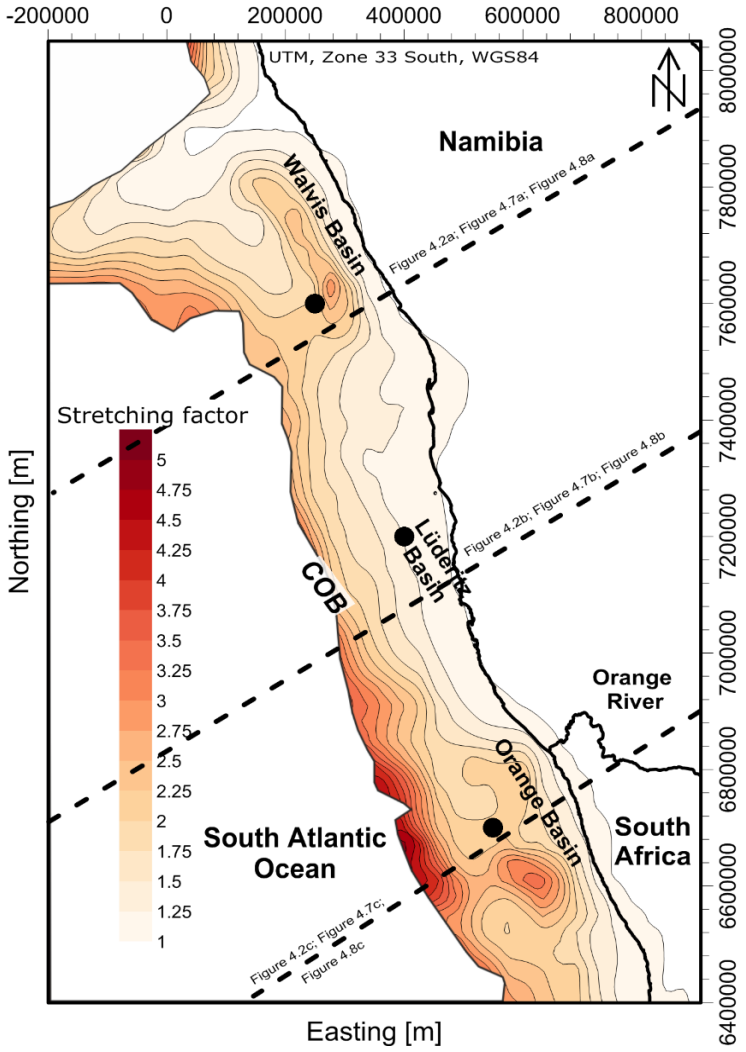

Figure 4.6: Map of stretching factor along the continental margin as used to calculate the syn-rift subsidence and the initial conditions at the start of the post-rift phase. In general, there is a decrease in the amount of stretching from west to east with areas of significantly higher stretching factors (up to 3.5) in the areas of the Walvis Basin in the north and the Orange Basin in the south.

The obtained geometric and thermal configuration is then used as initial conditions for forward modelling the post-rift evolution of the margin. Following our approach, subsidence results from flexural deformation of the lithospheric plate as induced by mechanical stresses

during active sedimentation as well as by thermal stresses during cooling. Worth mentioning is that these two processes are not solved independently, but are considered as dynamically coupled by means of a staggered iterative approach for solving the system of algebraic equations describing 3D conduction and advection and 3D beam flexure. Dynamic coupling is imposed in terms of a time and spatially varying flexural rigidity of the lithosphere taking into account both thermal and mechanical contributions. According to variations in the flexural rigidity of the plate, the deformation and subsidence of the continental margin varies in space and time and has a feedback effect on the thermal and mechanical evolution of the model.
For each time step, first the thermal field is solved by means of a bilinear Finite Element approximation of the following equation:

$$(\rho c_p)\frac{DT}{Dt} = \boldsymbol{\nabla} \cdot (k\nabla T) + H \qquad (1)$$

where ρ is the rock density, c_p is the isobaric heat capacity, T is the temperature, k is the thermal conductivity, and H is the amount of heat produced within the rock by decay of radiogenic elements. $\frac{DT}{Dt} = \frac{\partial}{\partial t} + (\mathbf{v} \cdot \nabla)$ is the total (Lagrangian) derivative, with $\mathbf{v}$ representing the sedimentation rate, here included to take into account advective heat transport component by sedimentation. Two sets of boundary conditions are imposed in order to close the system of equations. Temperature along the topmost surface, representing the seafloor, is kept fixed at T=5°C. Worth to mention is that the geometry of this upper boundary does not remain constant during the simulation but it varies in time according to the sedimentation and subsidence history. The base of the mantle lithosphere is described by a partial melt isotherm for which a value of 1350°C has been chosen. The topology of this isotherm is not maintained fixed, but it varies during the entire simulation depending on the cooling path followed by the lithospheric plate. Within the lowermost asthenosphere an adiabatic thermal gradient of 0.3°C km^{-1} is maintained with a reference potential temperature of 1350°C. The imposed initial thermal configuration is calculated based on the model geometry at the beginning of the post-rift stage, thereby taking into account thermal destabilization as induced by uniform lithospheric stretching. Time discretization is performed via a Crank-Nicholson implicit scheme within a constant time stepping of 1 Ma.
Variations in the thermal field lead to the development of thermal stresses, which are then parameterised in terms of a bending moment and in-plane torque. The latter are added to the

couple of moment-torque determined by sedimentation in order to solve for the 3D flexural equation (e.g., Kooi and Cloetingh, 1989; van Wees and Cloetingh, 1996):

$$\nabla^2 M + \nabla(\mathbf{N} \cdot \nabla\omega) - K\omega = q - \nabla(\mathbf{N} \cdot \nabla\omega_0) \quad (2)$$

where M is the total plate bending moment (taking into account both mechanical and thermal processes), **N** is the net horizontal force component acting on the plate, ω is the deflection, K is the module of a linear elastic Winkler foundation imparting a normal traction to the base of the plate, and ω_0 is an initial vertical displacement for a stress-free preloaded stage.

Although it is possible to parameterise the flexural rigidity via a rheological approach (i.e., based on strain rate independent yield strength envelope concept), in the present study, we opted for a relatively simpler approximation and we parameterised the flexural rigidity by means of a specified isotherm (e.g., Watts, 1992; Burov and Diament, 1995; McKenzie and Fairhead, 1997). For the latter, a value of 450°C has been chosen, as this temperature roughly corresponds to the transition between brittle and ductile behavior at pressure and temperature conditions typically encountered at crustal level. Worth noticing is that this approach fails to account for stress (re)distribution within the plate during subsidence, and therefore, flexural rigidity values calculated should be considered as upper bounds.

Apart from the syn-rift sediments which are deposited instantaneously soon after lithospheric stretching, post-rift sedimentation is introduced in the modelling as a gradual process (in 1 Ma steps). Sediments are deposited during a time window of finite duration. At this purpose, we follow the age subdivision after the chronostratigraphy by Broad et al. (2006) with a modification of the most recent timescale after Cohen et al. (2013). Table 4.1 illustrates the temporal subdivision adopted to include sedimentation in the forward modelling. In the present model, we do not consider any external tectonic forcing, while we do integrate the contribution to the bending as induced by sea level variations following the global dataset provided by Haq et al. (1987).

4.4 Results

4.4.1 Thermal evolution

Since the breakup of Gondwana, the thermal field across the SW African continental margin changed strongly. Initial thermal destabilization during rifting went along with high heat flow related to stretching and breakup manifested in a shallow thermal LAB and elevated isotherms across the margins. At the end of the syn-rift phase (Figure 4.7), the 1350°C isotherm, is as shallow as -35 km at the COB whereas its depth rapidly increases while moving towards the continental domain reaching values up to about -125 km at the coastline. Local positive thermal anomalies occur beneath both the Walvis and Orange Basins, areas that are characterised by relatively thick syn-rift sediments (Walvis Basin ~3 km; Orange Basin ~5 km; Figure 4.3). Here, heat retained within the sedimentary blanket causes higher temperatures resulting in LAB reaching values up to -50 km depths. By contrast, beneath the Lüderitz Basin the presence of a relatively thin sedimentary cover (~1 km; Figure 4.3) affects less significantly the overall thermal gradients as imposed by the thermal boundary conditions. As a result, the temperature field gradually and continuously decreases towards the interior domains of the African continent.

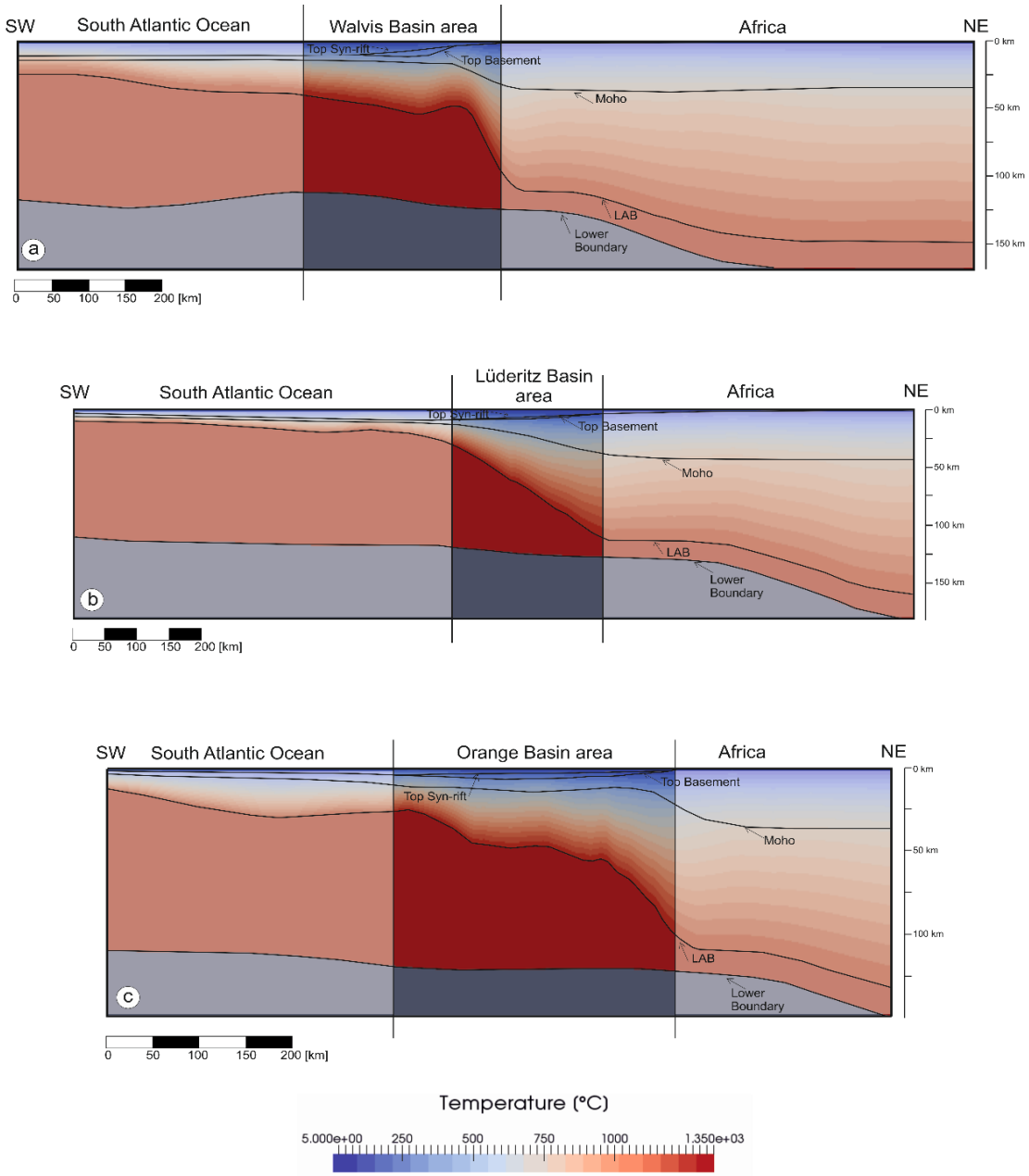

Figure 4.7: Temperature profiles across the 3D model at the end of the syn-rift phase (125 Ma). The locations of the profiles are the same as illustrated in Figure 4.1 and Figure 4.2. (a) Profile across the Walvis Basin. (b) Profile across the Lüderitz Basin. (c) Profile across the Orange Basin. The margin area is strongly affected by stretching and shallow isotherms that deepen towards the continent.

Cooling of the initial thermal anomalies at the onset of rifting continues throughout the entire post-rift evolution of the margin with a thermal configuration reaching approximately steady-state conditions at present-day (Figure 4.8). The retarding effects by sediment thermal

blanketing are also visible in the present-day thermal configuration of the margin, which is characterised by relatively higher temperatures located beneath the three major depocentres of sedimentation. Since the amount of heat retained within the sedimentary cover scales linearly with the amount of sediment deposited, areas that underwent extensive sedimentation during the post-rift evolution are characterised by the highest temperatures. Indeed, this effect is most pronounced beneath the Orange Basin, where the greatest amount of post-rift sediments (around 6 km; Figure 4.3) has been deposited.

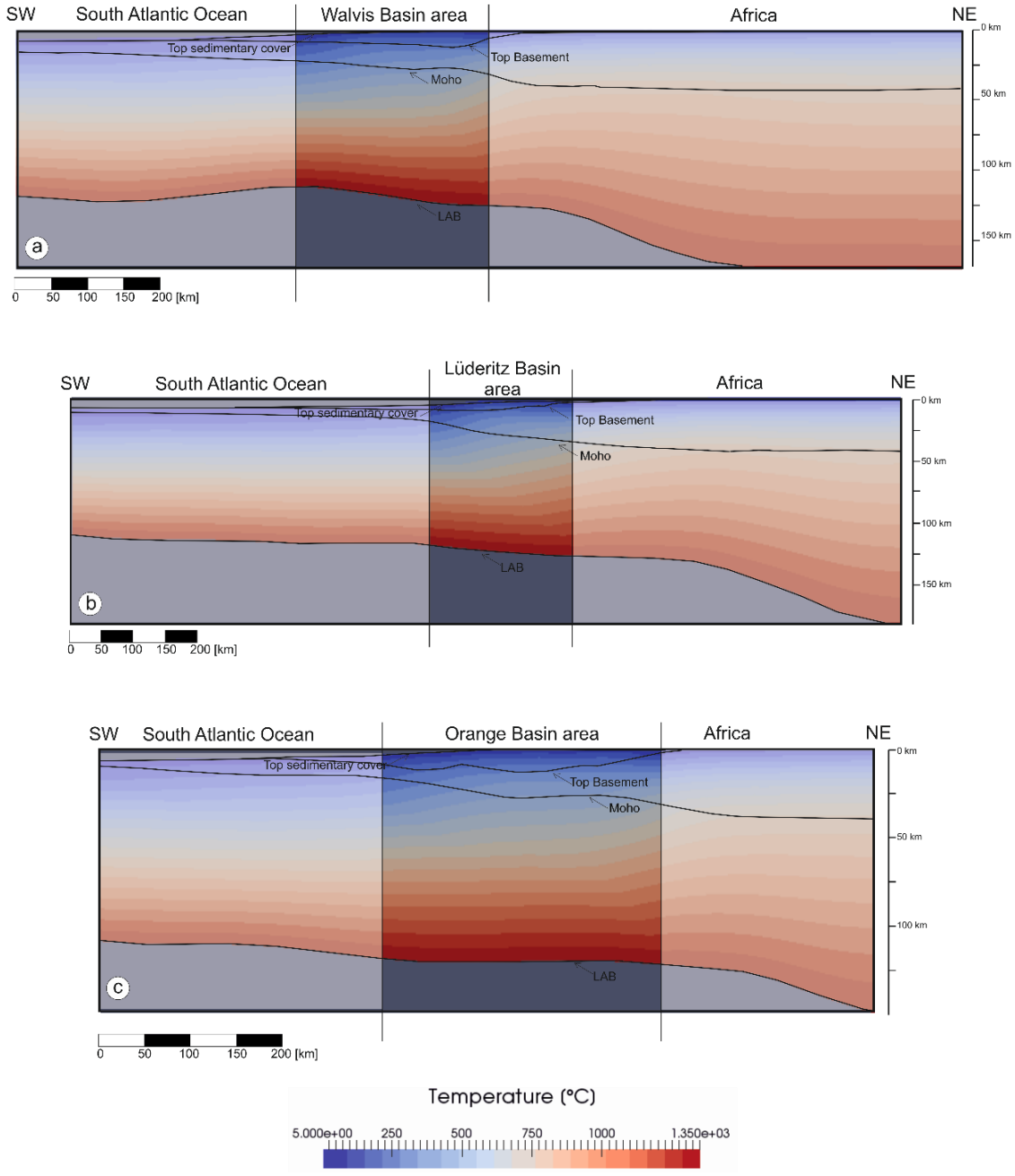

Figure 4.8: Temperature profiles, as in Figure 4.7 but at t = 0 Ma. (see Figure 4.1 for their locations). (a) Profile across the Walvis Basin. (b) Profile across the Lüderitz Basin. (c)

Profile across the Orange Basin. These profiles illustrate the elevated isotherms in the areas of the sedimentary basins.

4.4.2 Evolution of the effective elastic thickness (EET)

By influencing rates of lithospheric cooling, the presence of a sediment cover of varying thickness exerts also a direct control on the mechanical behavior of the lithosphere. Consequently, thermal blanketing, causing higher than normal temperature conditions at the base of the infill, also affects the flexural rigidity of the lithosphere (here parametrized in terms of the 450°C isotherm). These aspects are schematically summarised in Figure 4.9, which shows the evolution of the flexural rigidity of the lithosphere in terms of Effective Elastic Thickness (EET) variations during the different post-rift stages. The EET within the study areas varies significantly during the 125 Ma after breakup. This is particularly the case within the first ~40 Ma of the post-rift evolution, during which time EET variations along the continental margin are the largest.

Given the linear relationship between the lithospheric thermal field and the corresponding flexural state, variations in modelled EET structurally correlate with temporal changes in the thermal configuration across the margin. The initial stages in the post-rift evolution are characterised by the presence of a higher, in magnitude, thermal anomaly as inherited from the rifting and therefore show a highly variable thermal configuration. Conductive cooling within the plate smoothes thermal destabilization with time thus reducing gradients in the flexural rigidity accordingly. At the beginning of post-rift phase I, the calculated EET amounts to 12 km at the COB and 20 km along the coastline (Figure 4.9a). The Walvis and Orange Basin are characterised by an EET of about 12 km while the Lüderitz Basin has a thicker EET of about 18 km. 25 Ma after the breakup the EET has a thickness of 20 km at the African coastline and 20 km in the area of the COB (Figure 4.9b). Calculated EET values show only moderate variations during the remaining phase. This final period is characterised by a thickening trend in the area of the COB (maximum values up to 25 km at 85 Ma, 30 km at 67 Ma, 35 km at 25 Ma, and 37 km at the present-day), whereas the EET remains almost constant (20 km) in the coastal areas (Figure 4.9c-f). The sedimentary basins are also characterised by a general thickening of the EET. Accordingly, the Walvis Basin has an EET of 21 km at 85 Ma, 23 km at 67 Ma, 25 km at 25 Ma, and 27 km at the present-day. More to the south, the Lüderitz Basin is marked by 20 km of EET at 85 Ma, 21 km at 67 Ma, 23 km at

25 km and 26 km at the present-day. The Orange Basin which has initially the thinnest EET reaches an EET of 18 km at 85 Ma, 20 km at 67 Ma, 26 km at 25 Ma, and 29 km at present-day.

The effects of sedimentation on the resulting thermal field and consequently flexural rigidity variations are also captured by the evolution of calculated EET through time during the post-rift evolution of the margin. By inspecting the different maps shown in Figure 4.9, it can be noticed that during early stages (until ~67 Ma) the southern domain of the study area is characterised by smaller EET thickness values than the domains further to the north. This is in agreement with higher volumes of sediments being deposited during this time window especially in the area of the Orange Basin. The gradual northward shift in the main depocentres of sedimentation (Maystrenko et al., 2013) spatially correlates with a change in the EET configuration during the last phases of the post-rift evolution of the margin and a general deepening within the southern domain.

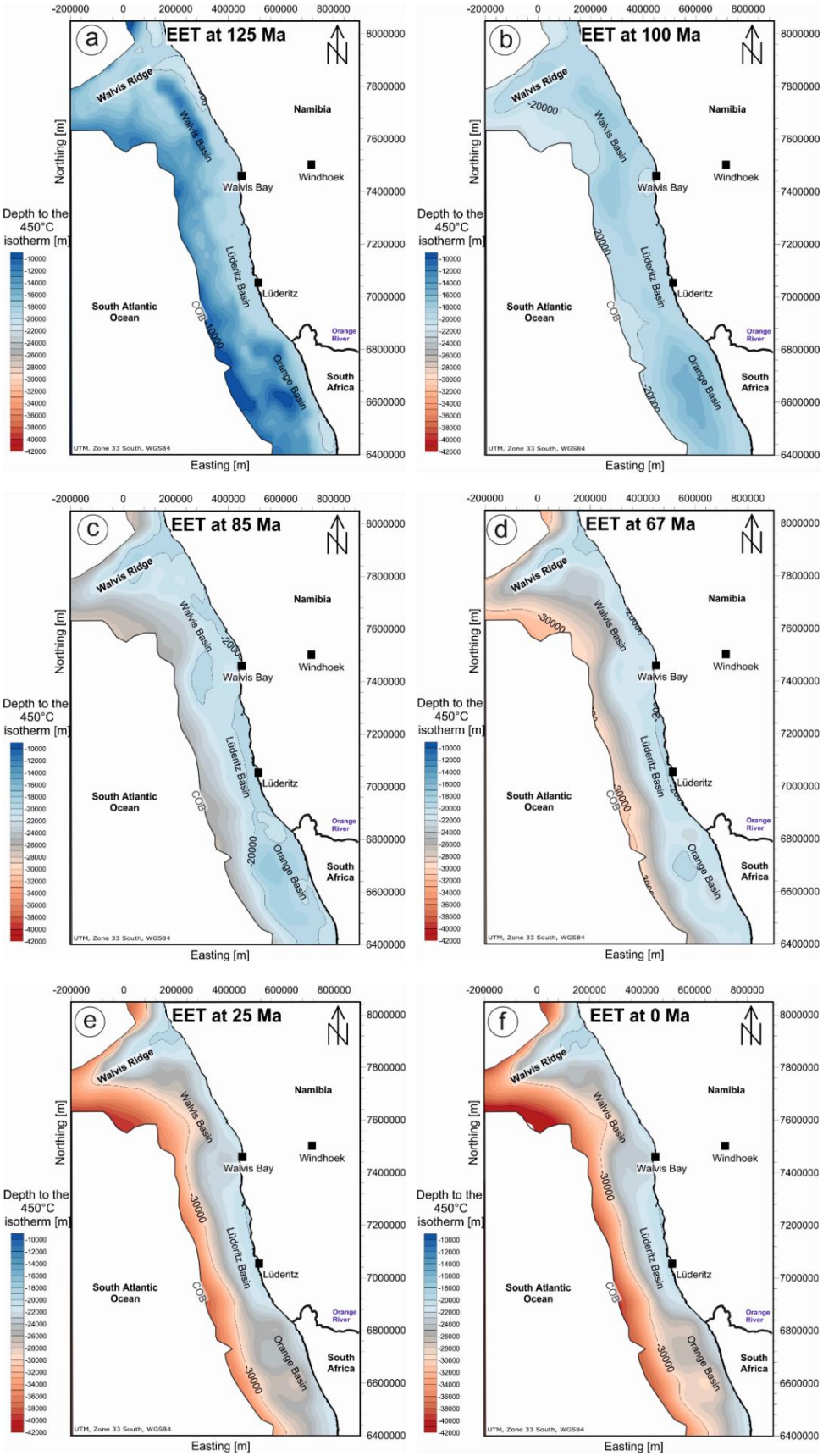

Figure 4.9: Evolution of the EET with time. (a) Depth to the EET at 125 Ma. (b) Depth to the EET at 100 Ma. (c) Depth to the EET at 85 Ma. (d) Depth to the EET at 67 Ma. (e) Depth to

the EET at 25 Ma. (f) Depth to the EET at 0 Ma. Strong variations in the thickness distribution of the EET are observed during the first 25 Ma after breakup when thermal cooling of the lithosphere has started. Since 100 Ma, the spatial pattern of the EET does not vary significantly, reflecting a rather slower cooling of the lithosphere plate, which approaches equilibrium.

4.4.3 Subsidence of the passive continental margin

The modelled overall subsidence of the passive continental margin is schematically illustrated in Figure 4.10. This figure exemplarily shows the amount of load induced, thermal as well as the sum of the total subsidence since the breakup of the South Atlantic Ocean (125 Ma) for three synthetic wells located beneath the major basins. The thermal subsidence curves show an exponential trend with rapid cooling during the first ~40 Ma after breakup. During the remaining ~85 Ma cooling rates slow down thus resulting in a flattening of the thermal subsidence curves. While the Walvis Basin and the Orange Basin experienced a similar amount of thermal subsidence (~2200 m) the Lüderitz Basin has a smaller amount of thermal subsidence of about 900 m.

A shift in sediment deposition is clearly visible in all subsidence curves. At 67 Ma, the area of the Orange Basin is characterised by a strong decrease in load induced subsidence (the area between the thermal subsidence curve and the total subsidence curve) which is in contrast to the high amount of load induced subsidence during the first 58 Ma after breakup. Nevertheless, the Orange Basin experienced the highest amount of load induced subsidence (~3200 m) compared to the amounts of load induced subsidence of the Walvis Basin and Lüderitz Basin. The latter two basins are characterised by a minor amount of load induced subsidence (Walvis Basin ~1800 m and Lüderitz Basin ~700 m). This trend scales linearly with the amount of sedimentation observed in the three basin areas.

The total subsidence calculated sums up to approximately ~5400 m in the Orange Basin, ~4000 m in the Walvis Basin and ~1600 m in the Lüderitz Basin.

Comparing those subsidence curves with the subsidence curves along the SW African margin using local isostatic compensation according to Dressel et al. (2015) shows differences in the thermal subsidence curves as well as in the total subsidence curves. These differences stems from differences in the two approaches. Indeed, the study by Dressel et al. (2015) did not consider either thermo-mechanical coupling or a spatio-temporal varying strength of the

lithosphere. Regarding the thermal subsidence curves, such coupling results in a larger amount of thermal subsidence due to dynamic interaction between thermal cooling and sediment deposition. By contrast, the total amount of subsidence is smaller for the 3D case than if based on a calculation assuming local isostatic compensation (i.e., constant EET=0). This aspect is related to the fact that local isostatic compensation, neglecting a finite rigidity of the lithospheric plate, corresponds to the end-member case of a weak lithosphere. Whereas the consideration of a finite in magnitude and laterally varying EET, by taking the effective strength of the lithosphere into account, results in a stronger configuration of the plate, thus resulting in less deflection.

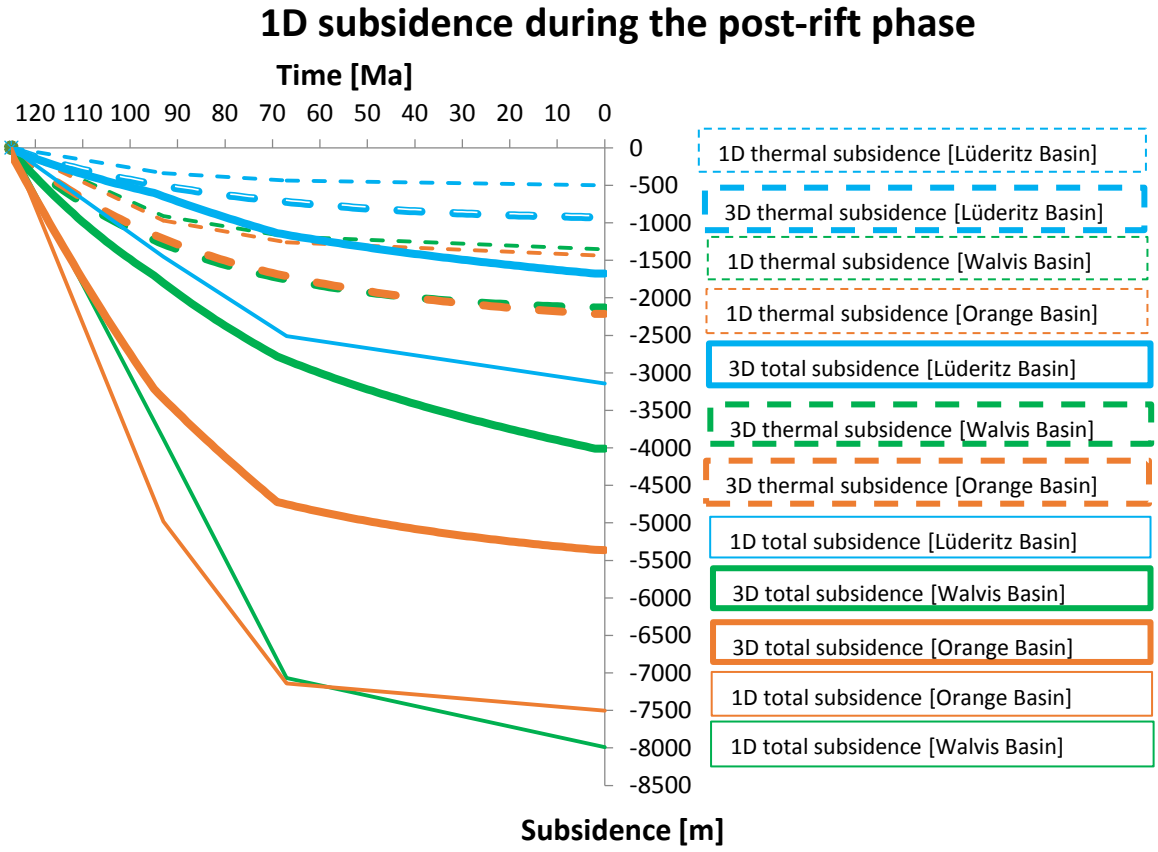

Figure 4.10: Comparison between subsidence curves of three synthetic boreholes within the Walvis Basin, Lüderitz Basin and Orange Basin calculated with the 3D forward modelling approach and a spatio-temporal EET and with local isostatic compensation (i.e., EET=0; Dressel et al., 2015). Dashed lines show the thermal subsidence curves with thick lines for the 3D case and thin lines for local isostatic compensation. Solid lines represent the total subsidence curve (i.e., load induced subsidence + thermal subsidence), again the thick lines show the 3D case whereas the thin lines represent the 1D case. The space in between the dashed and the solid curves indicate the amount of load induced subsidence. Again, the thick

lines show the subsidence curve for the 3D calculation and the thin lines mark the local isostasy calculation (see Figure 4.1 for location of the synthetic wells).

4.4.4 Paleobathymetric evolution

Using the information derived from the modelled thermal and mechanical (EET) evolution and linking it to the sedimentation history as constrained by the input 3D geological model allows restoring paleobathymetries for different time spans during the entire evolution of the continental margin.

Figure 4.11 illustrates paleobathymetric maps as calculated from the 3D forward numerical simulation at different times during the evolution of the margin in accordance to the resolution of the model used: 125 Ma (soon after the rifting ceased), 93 Ma and 67 Ma. The paleobathymetry obtained after instantaneous deposition of syn-rift sediments (125 Ma) shows already an elevation up to 900 meter above sea level (m.a.s.l.; i.e., positive paleotopography) in the norther domain and 500 m.a.s.l. in the south as well as in the central parts. Modelled positive paleotopographies at 93 Ma amount to 300 m.a.s.l. in the north, 50 m.a.s.l. in the central part, and 400 m.a.s.l. in the south. Finally, after the sediments of post-rift phase I and II have been deposited the positive paleotopographies at 67 Ma amount 900 m.a.s.l., both, in the north as well as in the south but only 200 m.a.sl. in the central part. The presence of these positive paleotopographies during the post-rift evolution calls for additional processes that likely affected the geodynamic history of the margin and that have been not considered in the present study. These are discussed in details in the paragraph that follows.

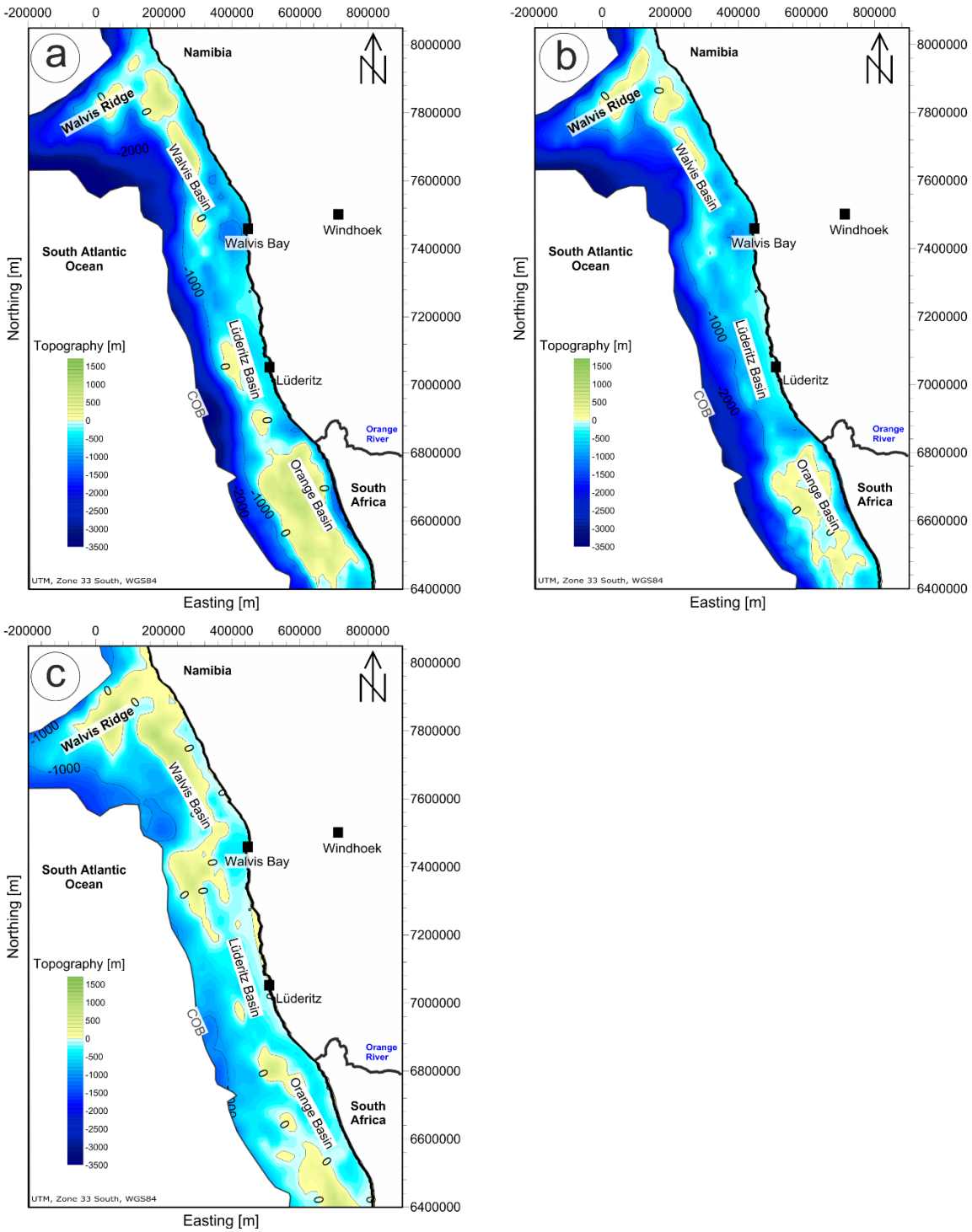

Figure 4.11: Modelled paleobathymetries for 67 Ma (a), 93 Ma (b), and 125 Ma (c). The maps indicate a positive paleotopography (elevation above sea level). The amount of this positive paleotopography varies through time.

4.5 Discussion

4.5.1 Implications for uplift

In an attempt to "validate" the modelling efforts, we compare observed present-day bathymetry of the SW African margin to the one predicted by the model. The model predicts a general deepening of the bathymetry towards the COB, which is in agreement with the general trend observed at present-day; however, local differences between modelling results and observations are found beneath the three major basins. In more details, modelled present-day bathymetry beneath the continental margin amounts to about 1000 meters below sea level (m.b.s.l.) in average and increases to about 2500 m.b.s.l. to 3000 m.b.s.l. at the COB. This is comparable to the present-day observed bathymetry at the COB with an amount of about 3000 m.b.s.l., whereas areas of main sedimentation are characterised by positive paleotopographies up to 1700 m.a.s.l. in the north, 450 m.a.s.l. in the south and about 850 m.a.s.l. in the central part (Figure 4.12). Within these domains, modelling results are therefore in conflict with the preserved configuration and thickness distribution of the sedimentary cover, which indicates ongoing subsidence throughout the post-rift evolution of the margin.

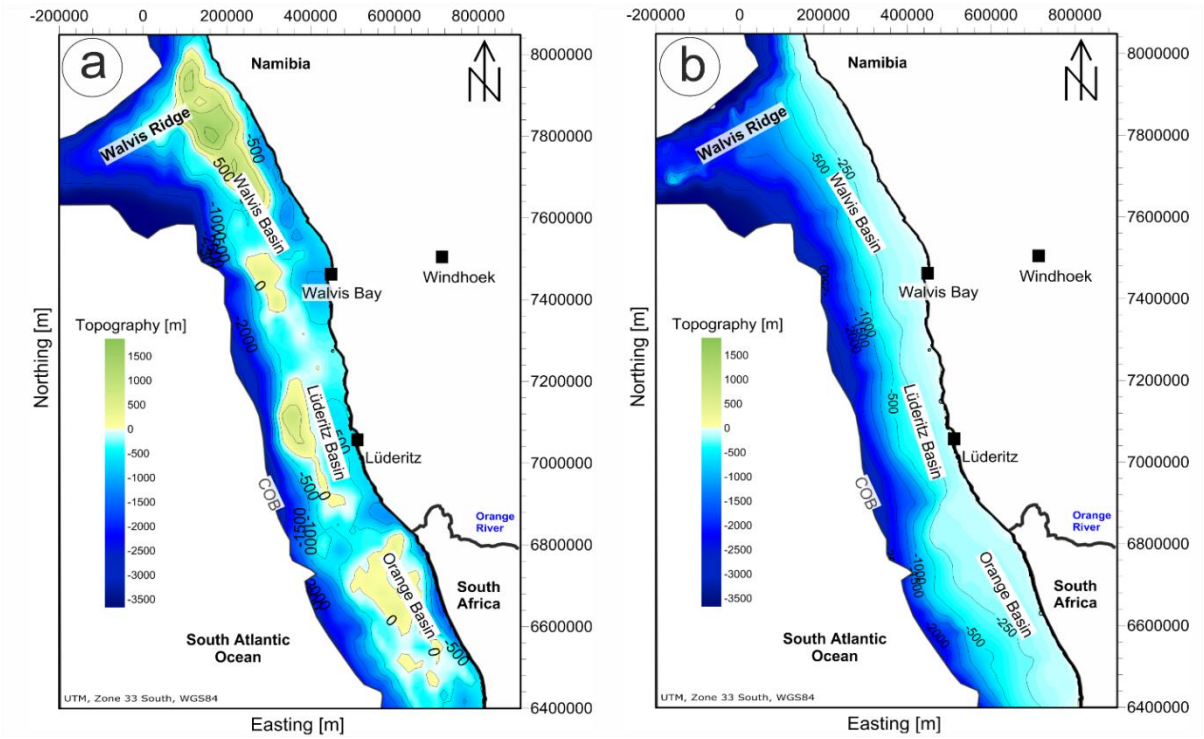

Figure 4.12: The maps show the reconstructed bathymetries for present-day (a) and the real present-day bathymetry (after IOC, IHO and BODC, 2003; b). Figure (a) shows elevations above sea level which are not observed at the real present-day (b).

On the one hand, dissimilarities observed between model results and observations can be explained, at least partly, by the occurrence of phases of margin uplift throughout the post-rift evolution of the margin. Indications for uplift events have been discussed by Paton et al. (2008) and Kuhlmann et al. (2011) using mapped erosional unconformities in the sedimentary succession. Furthermore, regarding the temporal occurrence of uplift events in southern Africa, Séranne and Anka (2005) discuss the Sennoninan-phase of uplift starting in the Turonian. This event temporally correlates with the obtained positive paleobathymetries of post-rift phase II (93 Ma until 67 Ma; Figure 4.11). In addition, our results are in accordance to previously published results based on apatite fission-track analysis by Kounov et al. (2013) which pointed to regional uplift during the time interval from 100-65 Ma. This temporal correlation between our modelling results and observations derived from seismic data and additional thermochronology strongly suggest the obtained positive paleotopographies to represent uplift events occurring during the post-rift evolution of the margin. According to our results, we would obtain ~450 m of uplift for the northern and southern area for the duration of post-rift phase II. Comparing this amount with the suggested denudation rate of 25 m/Ma as presented by Kounov et al. (2013) for the Late Cretaceous yields the same range of uplift. Additionally, magnitudes of this uplift event are in agreement with Kuhlmann et al. (2011), who determined 930 m of erosion, though these results concern the specific area of the Orange Basin, and are therefore difficult to extrapolate margin wide.

The amount of deduced relative uplift for the final post-rift phase (post-rift phase III: 67 Ma until present) is 800 m in the Walvis Basin and 650 m in the Lüderitz Basin, whereas the area of the Orange Basin is now subsiding. Our results agree with previous conclusions by Stollhofen et al. (2014), suggesting Pliocene-Pleistocene uplift based on a sedimentological study of a fan delta in Namibia. A study by Burke (1996) proposed that the southern African continent has been uplifted since 30 Ma, a conclusion, which finds a confirmation in our findings, at least for the northern part of our research area. Furthermore, Colli et al. (2014) also suggested major uplift events during the Oligocene-Miocene, which are again confirmed by our findings for post-rift phase III. The latter two studies proposed mantle processes as responsible for the observed uplift. Similarly, investigations on dynamic topography (e.g., Lithgow-Bertelloni and Silver, 1998 or Flament et al., 2013) indicated significant vertical motions by mantle flow. According to Braun et al. (2014), denudation onshore Africa was rather caused by a tilting of the African continent in response to a super plume.

Therefore, it is likely that the observed positive topographies along the margin might be explained by episodic tectonic uplift movements and sediment erosion. This aspect is consistent with several studies (e.g., Patridge and Maud, 1978; Burke, 1996; Moucha and Forte, 2011), which pointed to episodically uplift since Mesozoic times in areas near the coastal margins.

On the other hand, focusing only on the post-rift phase I (125-93 Ma), by subtracting the resulting paleotopographies at the top of the syn-rift phase (125 Ma) and at the top post-rift phase I (93 Ma) yields an amount of relative subsidence during this stage. The amount of relative subsidence ranges between 600 m in the Walvis Basin, 450 m in the Lüderitz Basin, and 100 m in the Orange Basin. Computed subsidence is nevertheless too small to compensate for syn-rift sediments, which have been accumulated, thus resulting in a positive paleotopography at the end of post-rift phase I. Given the above discussion, the observed positive paleotopographies can be related to a structural inheritance (weakening of the lithosphere) derived from the rifting that our study could not resolve. If this had been the case, a weaker lithosphere during rifting would have responded to the coeval deposition of the thick sequence of syn-rift sediments by higher wavelength of deflection, thus providing a thermo-mechanical intrinsic solution to the missing accommodation space soon after the rifting event ceased. This would also be in agreement with a previously study by Hirsch et al. (2010), which supported continuous subsidence during the youngest post-rift time interval for the Orange Basin. However, to test and quantify this hypothesis would require a more detailed investigation of the rifting dynamics of the margin, a subject that goes beyond the scope of the present study.

4.5.2 Implications for additional subsidence components

As mentioned in the previous chapter, the calculated positive paleobathymetry at 125 Ma, soon after the rifting event, already point to positive paleotopographies. As there are no observational evidence indicating uplift during the syn-rift phase and the duration of the syn-rift phase is unknown, it is likely that calculated positive paleotopographies result from limitations of the pure shear and uniform, instantaneous stretching model approximation adopted to model the rifting event. Our results clearly point to the fact that calculated syn-rift

subsidence from uniform stretching of the lithosphere could not create enough accommodation space to store the total amount of syn-rift sediments.

To provide a quantitative basis to our discussion, we carried out a sensitivity analysis in which we investigate first-order differences in the syn-rift configuration and their effects on the margin geometry. In a first attempt, we consider variation in the initial configuration of the crust and lithospheric mantle, by considering 40 km thickness for the former (instead of the 35 km assumed earlier) and 130 km for the latter (instead of 125 km). According to the new configuration, the remaining missing subsidence still attains of up to ~500 m (Figure 4.13).

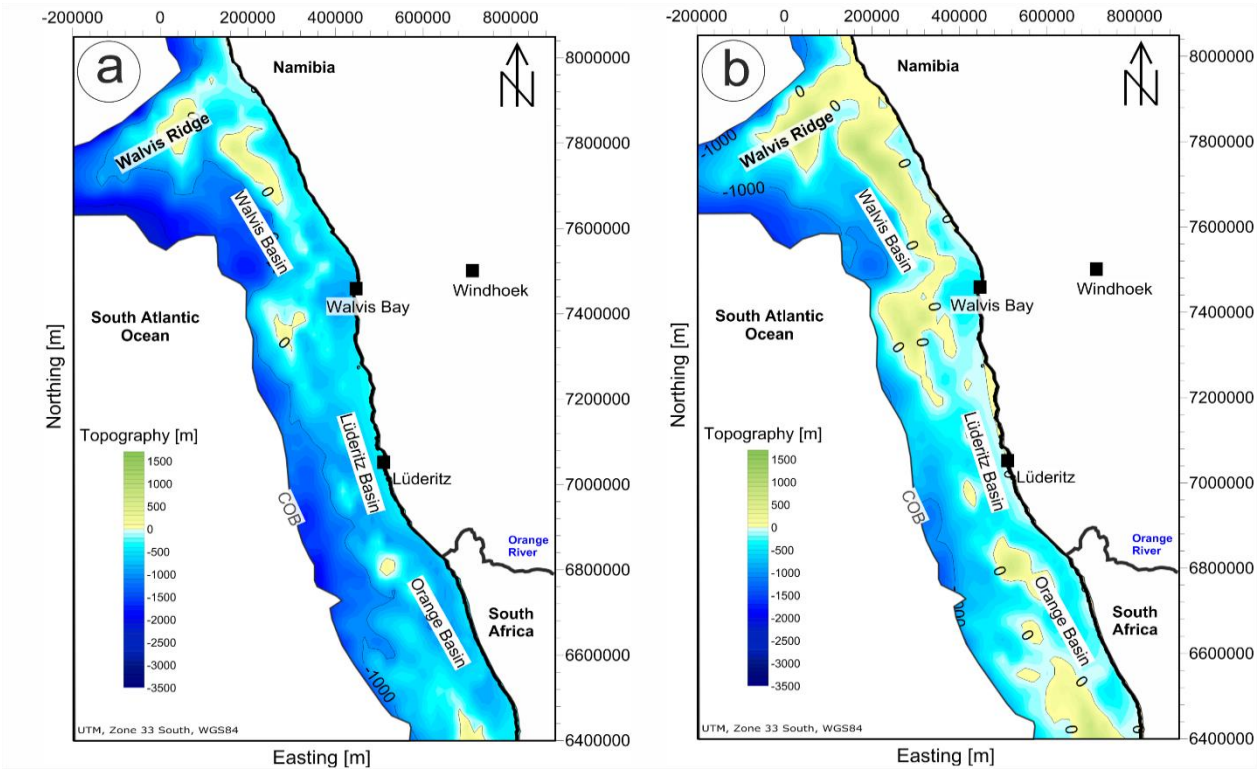

Figure 4.13: Comparison between the paleobathymetry at top of the syn-rift unit calculated with an initial configuration of 40 km crustal thickness and 130 km lithospheric thickness (a) with those paleobathymetry calculated with the initial configuration of 35 km for the crustal thickness and 125 km of lithospheric thickness (b).

For the reason that this configuration does also not yield enough accommodation space and the fact that 35 km crustal and 125 km lithospheric thickness represent areas at the African margin which are not affected by stretching we consider these values more appropriate. In

addition, the reconstructed depth along the COB using this configuration coincides with the present-day depth at the COB. Consequently, our obtained missing subsidence rather points to intrinsic limitations in the physics behind uniform lithospheric stretching, such as decoupling of the lithosphere, rather than on the initial lithospheric configuration as a source of error. Similar conclusions were derived from a previous study by Hirsch et al. (2010) centred on the Orange Basin. According to their subsidence analysis, the observed tectonic history and maturation of organic matter could not be reproduced by assuming uniform stretching of the lithosphere. Comparing these aspects to other conjugate margins leads to further insights on the rifting processes. The study by Espurt et al. (2012) analysing the Australian and Antarctic conjugate margins showed how complex the rifting procedure may occur. These authors propose a rather symmetric geometry, due to pure shear, of the rift system at the crustal as well as lithospheric scale during the initial stretching, followed by simple shear deformation shortly before breakup. The latter is justified by Espurt et al. (2012) showing that the ductile lower crust acting as a zone separating the brittle upper crust and the lithospheric mantle. Given this discussion, the SW African passive margin could also underwent such a rifting history in which the later decoupling causes the ductile flow of the crust with additional subsidence as a result.

As discussed by Burov and Diament (1995) and Burov and Poliakov (2001), the mechanical properties of the oceanic lithosphere can be approximated by a single layer while the continental lithosphere may be composed of mechanically decoupled layers. Mechanical decoupling at crustal and mantle levels may cause horizontal ductile flow in the lower crust that would, in turn, affect the subsidence history. The net result of these dynamics is additional subsidence mainly beneath areas of lower crustal flow. This could partly explain the observed positive paleotopographies, thus indicating that lower crustal flow might have played a prominent role during at least the first stage of the post-rift evolution of the SW African margin.

Similar conclusions were derived from a study by Huismans and Beaumont (2011). In their study, they were able to reproduce a margin setting as typically observed in the south Atlantic by means of a model in which the upper and lower lithosphere are decoupled during extension due to asthenospheric inflow. Based on their result, they concluded that depth-dependent rather than uniform lithospheric stretching would occur in these settings. A rheologically stratified lithosphere would increase the amount of subsidence, especially during early stages after the rifting and could therefore provide the “missing accommodation space” for the syn-

rift sediments. Additionally, the model by Huismans and Beaumont (2011) was also used to explain the dynamics of underplating due to mantle flow within a mechanically decoupled lithosphere. This last aspect brings some interesting similarities to the crustal configuration as constrained for the SW African margin, which is characterised by areas of high-density and high-shear wave velocity at different locations (Maystrenko et al., 2013). According to the architecture of the margin, as shown in Figure 4.2, high-density bodies and high-shear wave velocity bodies underlay the continental crust. To derive the modelling with focus on the post-rift phase we assume these bodies as part of the crystalline crust which is in agreement with Thybo and Artemieva (2013) who proposed that many passive margins experienced underplating during the late stages of rifting and breakup. However, the heterogeneous crustal configuration according to Maystrenko et al. (2013) and the discussion of underplating by Huismans and Beaumont (2011) point to underplating as coeval to the rifting rather than postpone to the post-rift phase.

Based on the discussion above, in a second step of our sensitivity analysis, we investigate the effects of underplating occurring after the main phase of rifting on the margin evolution. Therefore, to calculate the initial subsidence without these lower crustal bodies, we impose the lower crustal bodies as part of the mantle but not of the crystalline crust. Figure 4.14 shows the top of the syn-rift unit after calculating the syn-rift subsidence and depositing the syn-rift sediments. Similar to the scenario with lower crustal bodies as part of the continental crust, we still obtain positive paleotopographies, though they are smaller in magnitude (~700 m). Accordingly, and based on the results derived from our study, we can conclude that it is likely that the positive paleotopographies result from processes during the syn-rift (possible decoupling of the lithosphere).

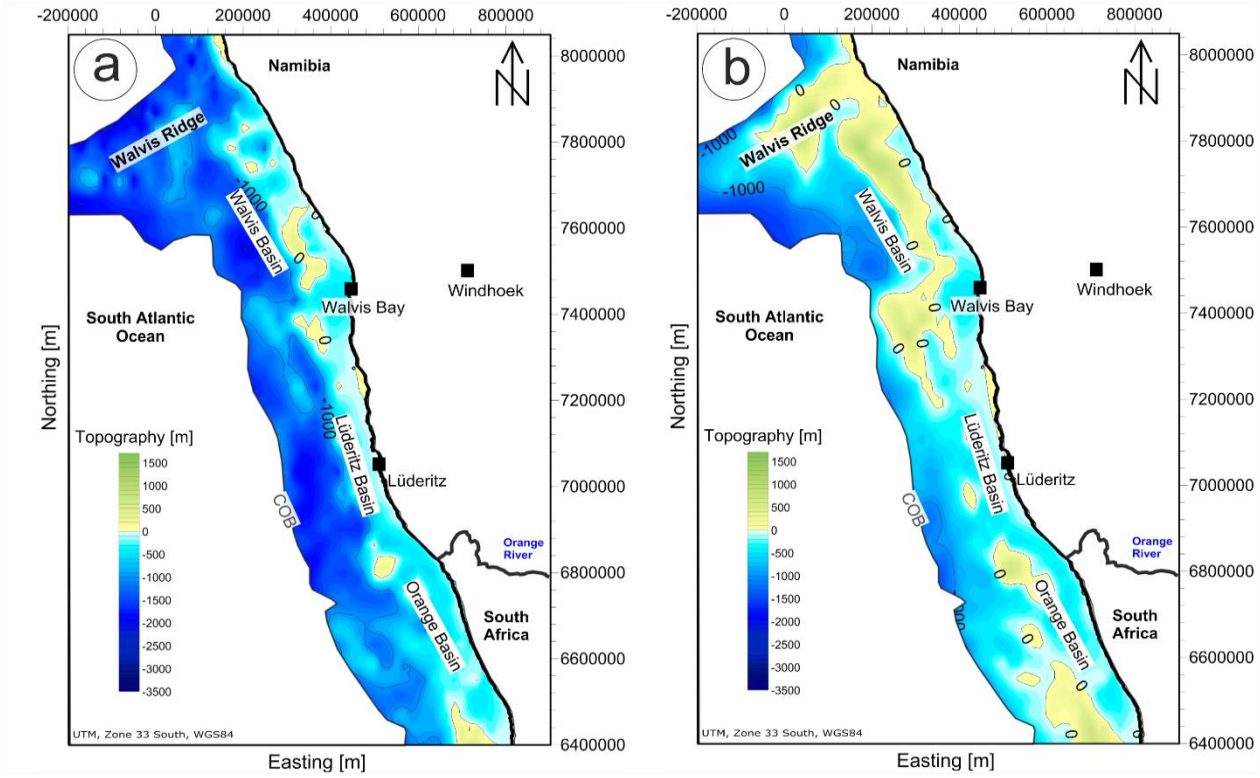

Figure 4.14: Comparison between the paleobathymetry at the top of the syn-rift unit calculated assuming lower crustal bodies as part of the mantle (emplacement post-breakup; a) and as part of the crystalline crust (emplacement pre-breakup; b).

4.5.3 Limitations

This work challenges conclusions derived from previous studies that proposed a relative uniform EET distribution close to an average value of 25 km (Stewart et al., 2000). Our results call for a highly variable flexural state of the lithosphere being characterised by values of EET, which are generally lower than the 25 km average of Stewart et al. (2000) during most of the post-rift stage. Despite current assumptions in parameterising the flexural state of the lithosphere by an isotherm, our results of ~20 km at the unstretched SW African coast are in close agreement with estimates based on gravity anomalies providing evidence for EET values lower than 25 km (McKenzie and Fairhead, 1997). Nevertheless, differences between modelling results and observations for the post-rift phases can be discussed in terms of some basic physical assumptions in our modelling approach that affect our results. As stated above, for the present study, we parameterise the EET by means of a specific isotherm (T=450°). The latter representing a common value adopted in several flexural studies, e.g., Watts (1978) and Rouby et al. (2013). However, while this value could be considered as a proxy for the flexural

rigidity of oceanic lithosphere, it might lead to an overestimation of the effective flexural state for the continental counterpart. As an example, Burov and Diament (1995) suggested an isotherm closer to 600°C to best represent the EET both for old oceanic and continental lithosphere. In an attempt to perform a sensitivity analysis, we show in Figure 4.15 the differences of the reconstructed present-day bathymetry, by assuming 600°C and 450°C, respectively, as the lower boundary for the EET. Inspecting Figure 4.15, it becomes clear that the former yields to higher amounts of positive paleotopography along the continental margin (up to 400 m). Observed differences should be related to a decrease in the amount of load induced subsidence for a 600°C isotherm, which leads to a stiffer lithosphere than for the 450°C isotherm case, characterised by a reduced amplitude of flexure and by an increase in the wavelength of deformation. On the base of these results, we conclude that the missing subsidence in the modelling cannot be solely explained by this assumption. Furthermore, approximating the EET by means of a constant, though varying in time isotherm, implicitly assumes an overall thermal control on the mechanical properties of the lithosphere, which represents a rather crude approximation for continental lithosphere (Burov and Diament, 1995). A continental lithosphere, which is cooling after a thermal event, will result in a plate elastic thickness that will increase in magnitude as the thermal anomaly is relaxed, in a similar way as for the oceanic case. Although this behavior can be modulated by mechanical softening related to viscous relaxation, it fails to account for possible stress redistribution within the plate, which might lead to overestimate the EET of the plate. This in turn might lead to an overly stiffer lithosphere, therefore less prone to subside under active sedimentation. A more detailed investigation based on a fully rheological parameterisation of the EET is subject of ongoing work.

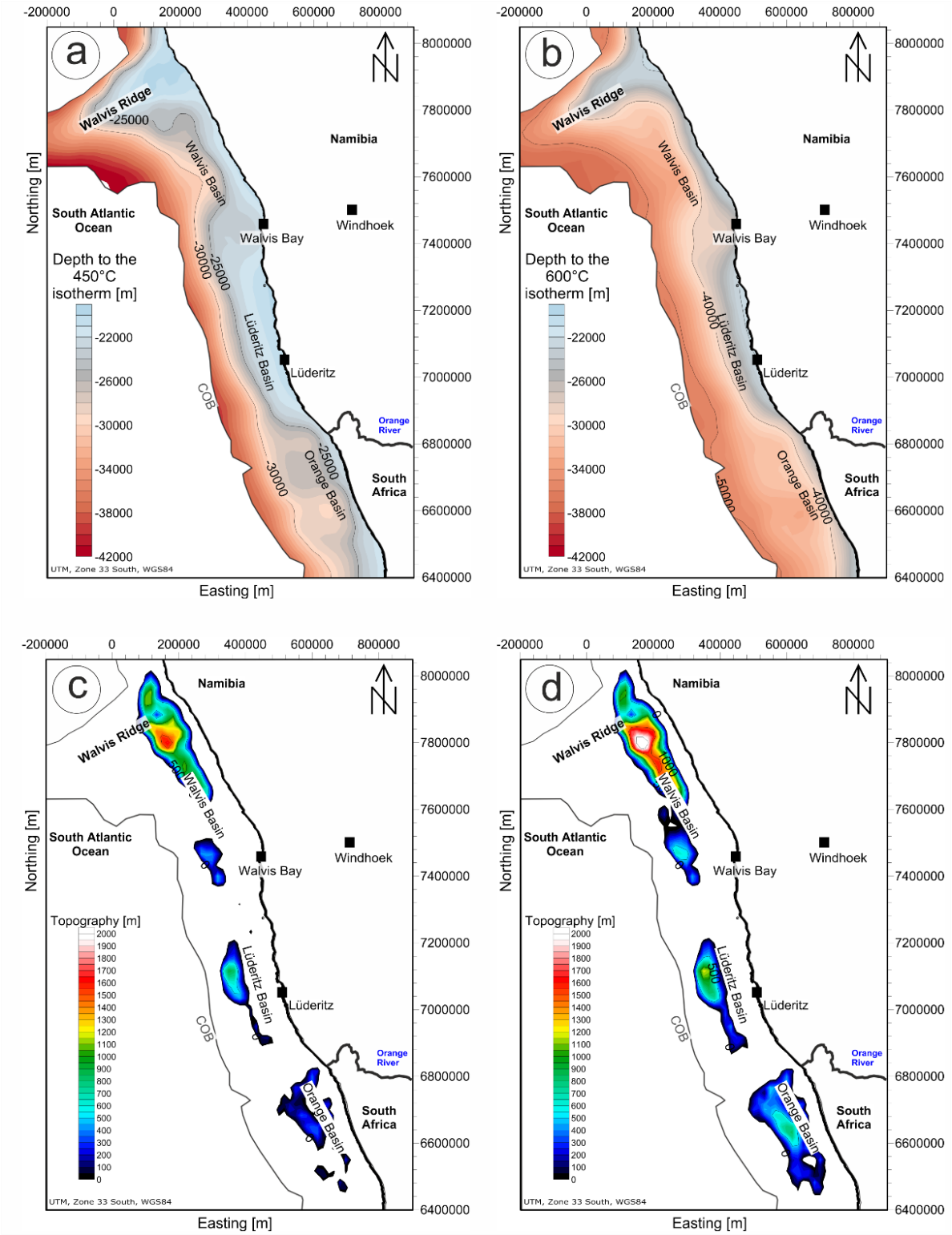

Figure 4.15: Map (a) and (b) exemplarily show the depth to EET (at 0 Ma) assuming its base at the 450°C isotherm and 600°C isotherm, respectively. Map (c) shows the restored paleotopography at 0 Ma using an EET=450°C while map (d) illustrates the resulting paleotopography at 0 Ma modeled with an EET=600°C. According to the different EETs, the paleotopographies vary in magnitude.

An additional assumption, which could have affected the conclusions derived from our analysis, can be related to the value of a potential mantle temperature adopted in the modelling for which a consensus among the geodynamic community is still lacking. While McKenzie et al. (2005) proposed a value close to 1315°C, more recently Grose (2012) suggested a potential mantle temperature of 1400°C which was increased by Stein and Stein (1992) up to 1450°C. In addition, Burov and Watts (2006) used 1330°C while Parson and Sclater (1977) used a slightly higher value of 1350°C. In our study, we imposed a fixed value of 1350°C, which represent an average of potential temperatures mentioned above. However, to further quantify the effects of varying this parameter, a sensitivity study has also been performed in which its value was gradually decreased down to 1300°C. The results of this analysis showed that changing the mantle potential temperature from 1350°C to 1300°C would cause a maximum difference of the positive paleotopographies of less than 20 m. Therefore, we can conclude that this not well constrained parameter would likely play only a secondary role in affecting the geodynamic evolution of the SW African margin.

4.5.4 Potentials for geo-resources

The final part of the discussion focuses on implications derived from the modelling results on the potential for geo-resource formation and evolution. Through time, organic matter, deposited in the sedimentary basin, matures according to increasing temperature and pressure and may migrate into potential reservoirs for hydrocarbons. As the oil window is reached at a temperature of ~130°C (Bjørlykke, 2010), this isotherm is an appropriate proxy for oil generation. Therefore, these temperatures are of primary interest within the major sedimentary basins. Our thermo-mechanical 3D forward modelling allows reconstructing the evolution of the oil window for oil-bearing sequences through time.

After Hartwig et al. (2012), the late Aptian and Albian black shales and organic rich dolomitic mudstones show a good source rock potential offshore southwestern Africa. The resolution of the input model does not resolve this unit in details, but it can be approximated by post-rift phase I unit which contains the oil-bearing sequence. Our post-rift phase I encompasses the sediments deposited from 125 Ma to 93 Ma. Consequently, the top of post-rift phase I is the base Turonian, which is about 7 Ma younger than the late Aptian and Albian black shales.

The forward modelling allows predicting the migration of the 130°C isotherm in depth and through time with respect to the oil-bearing unit. According to our model resolution, we infer the depth to the 130°C isotherm for three time steps during the post-rift phase.

Post-rift unit I reaches 130°C in the central western part of the Orange Basin in a depth of about 2950 m.b.s.l. at 93 Ma. At 67 Ma, after the second post-rift phase has been deposited, the location of the oil window remains under the same area though it increases spatially and reaches shallower depth levels. Correspondingly, the depth to the oil window is about 2900 m.b.s.l. beneath a larger area of the central part of the Orange Basin. Finally, post-rift phase I unit is buried to the 130°C isotherm to a depth of about 4000 m.b.s.l. in the Orange Basin at the modeled present-day. The Lüderitz Basin is now characterised by about 3400 m.b.s.l. to the depth of the 130°C isotherm. Shallowest depths of about 2000 m.b.s.l. to the oil window are obtained in the northern part of the Walvis Basin.

In comparison to the steady-state thermal model by Maystrenko et al. (2013), our modelled 130°C isotherm for today is located at shallower depths in the north, and at similar depths beneath the central part and greater depths in the south.

4.6 Conclusions

We have presented a margin-wide analysis of the post-rift evolution of the SW African margin by means of 3D thermo-mechanical forward numerical modelling techniques. Our approach permits to consider both, thermal cooling of the lithosphere and mechanical effects of sedimentation and their dynamic coupling on the resulting subsidence pattern. Furthermore, our modelling approach integrates available information about the configuration and geometry of the sedimentary units as well as information about the deeper crustal and lithospheric mantle domains as constrained at present. With respect to the thermo-mechanical coupling, we presented temporal and spatial variations in the EET (i.e., flexural rigidity) of the lithosphere throughout the post-rift evolution of the margin. This aspect is explained as a response of the plate to temporal cooling and active sedimentation dynamics.

In addition to the new insights on the EET, we restore paleobathymetries. These paleobathymetries point to elevations above sea level. Discussing the positive paleotopographies with respect to the method used lead to suggest lower crustal flow during the syn-rift phase. Accordingly, future work should focus on the processes during the syn-rift phase rather than processes of the post-rift phase.

Acknowledgements

This project was funded by the German Research Foundation (DFG, grant no. SCHE 674/5-3) within the priority program South Atlantic Margin Processes and Links with onshore Evolution (SAMPLE; SPP 1375). We thank Yuriy P. Maystrenko for providing the thickness maps used in this study. Furthermore, we thank F. Roure and an anonymous reviewer for their constructive comments which helped to improve the manuscript.

5 Final discussion

5.1 Evolution of passive continental margins of the southern South Atlantic Ocean

The primary objective of this work is to understand the history of vertical movements of the South Atlantic conjugate passive continental margins. Therefore, this study addresses the question *"What is the (post-rift) subsidence evolution of the South Atlantic margins inferred from information about the present-day structural configuration?"*. A subsidence analysis has been performed using a 1D backward and a 3D forward modelling approach based on 3D models of the present-day configuration of the SW African margin and the margin offshore Argentina to answer this main question. Accordingly, different subsidence components have been calculated to quantify the effect of load induced subsidence and thermal subsidence. Subsequently, paleobathymetries have been restored to evaluate the magnitude of past vertical movements.

As a result, it can be stated that the SW African margin and the SE South American margin are predominantly characterised by subsidence (up to ~5500 m on both margins). However, the modelling results for the SW African margin indicate local areas of positive paleotopographies (i.e., elevations above sea level) of up to ~1400 m, whereas no positive paleotopographies offshore SE South America have been obtained. These local positive paleotopographies are related to the fact that the restoration method used in this study does not consider additional forces affecting the margin in terms of uplift and only the preserved stratigraphic record entered into the calculation. The restoration results thus indicate a "missing amount of subsidence" at the SW African margin. According to the study by Kuhlmann et al. (2010, 2011), several erosional events affected the margin during the post-rift phase. For this reason, the present-day sedimentary record only preserves a minimum amount of sediments and consequently, the obtained positive paleotopographies represent a minimum estimate of seafloor uplift and the "missing subsidence" may have been even larger.

If these positive paleotopographies are interpreted to be the result of unconsidered seafloor uplift along the SW African margin (Chapter 2), this interpretation would be in agreement with investigations by Kuhlmann et al. (2011) and Hirsch et al. (2010). Kuhlmann et al. (2011) discussed uplift related erosion within the Orange Basin during the Late Cretaceous. The amount of erosion was quantified to ~930 m. Additionally, the work by Hirsch et al. (2010) had evidence for uplift of ~340 m in the Orange Basin for the same time period as

Kuhlmann et al. (2011) which is in the same range as the uplift detected in the present study (~250 m).

Further to the north, Strozyk et al. (2015) analysed the subsidence evolution north of the Walvis Ridge and estimated a total amount of uplift of about 1500 m to 2000 m. These numbers are comparable with the results of this study regarding the area south of the Walvis Ridge (500 m difference). Consequently, there appears to be a northward increasing amount of uplift.

Comparing the results of the approaches applied in this study, the 1D and the 3D methods result in almost the same distribution and magnitude of positive paleotopographies. However, given the methodological differences between the multi 1D backward modelling and the 3D forward modelling, both models need to be interpreted differently:

The 1D backward modelling approach goes back in time and starts at the present-day. For this reason, the total amount of cumulative subsidence of the past is stored within the configuration of the present-day, i.e., at the beginning of the modelling. Subsequent 1D backward modelling takes only the load induced subsidence and thermal subsidence into account. Additional processes and tectonic forces that may have affected the margin in terms of subsidence or uplift are not considered. Following this approach the obtained local paleotopographies, intermitting the paleobathymetries along the SW African margin, are interpreted as unconsidered phases of uplift during the post-rift phase (Chapter 2) whereas continuous subsidence without intermitting phases of uplift is obtained along the Argentine margin (Chapter 3).

By contrast, the 3D forward modelling performed in this study starts pre-breakup and therefore considers the initial syn-rift subsidence. In addition, this approach considers thermo-mechanical coupling of the subsidence processes (i.e., thermal subsidence and load induced subsidence) during the post-rift phase. In this case as well, a possible additional subsidence/uplift component is not taken into account during neither the syn-rift phase nor the post-rift phase. The forward modelling results show positive paleotopographies after calculating the syn-rift subsidence, as well as during the individual steps of the post-rift phase. These results could also point to an unconsidered process creating additional subsidence during the syn-rift phase and potentially during the post-rift phase (Chapter 4).

Although these differences in interpretation are present, both modelling approaches provide new insights into processes responsible for the characteristic margin evolution, if they are discussed with respect to geological processes happening in the South Atlantic. Such

geological processes inducing uplift or missing subsidence might be mechanisms related to variations in the stress regime, buoyancy forces or flexural effects. Flexural effects are taken into account when a spatially varying load according to the sediments deposited along the margin is considered. Additionally, the 3D forward modelling approach used in this study takes differences in the strength of the lithosphere into account, but neither compressional forces due to spreading of the South Atlantic Ocean, nor buoyancy forces within the deeper mantle are considered. Accordingly, the two most probable possibilities causing seafloor uplift (1, 2) as well as probable causes for the additional subsidence (3) are briefly discussed in the following paragraphs:

(1) Ridge-push hypothesis:

The South Atlantic Ocean is characterised by a spreading history with varying spreading rates through time. According to Colli et al. (2014) and their comparison of plate motion models, the fastest spreading (~6 cm per year) occurred at about 125 Ma ago, decreased to about 3 cm per year during the Late Cretaceous and increased again to about 6 cm per year during middle Eocene. At the present-day, spreading is still active with a spreading rate of about 4 cm per year (Müller et al., 2008). Ridge-push may thus have caused uplift along the continental margins of the South Atlantic (Japsen et al., 2012). However, according to the backward and forward modelling approaches used, ridge-push was obviously not sufficient to cause the positive paleotopographies on both sides of the South Atlantic for the following reasons: Firstly, if ridge-push had affected both passive continental margins during the post-rift phase, it would have resulted in a rather symmetrical post-rift evolution (in terms of vertical movements) and seafloor uplift would have a similar impact and extent offshore SE South America and SW Africa. The results of this study show an asymmetrical margin evolution of vertical movements suggesting that ridge-push alone is an insufficient explanation for seafloor uplift (Chapter 2 and Chapter 3). Secondly, positive paleotopographies are also partially obtained for the syn-rift phase (Chapter 4) when ridge-push was not yet a relevant factor.

(2) Deep mantle mechanism hypothesis:

As a second mechanism causing upward vertical movements, probable mantle processes during the post-rift phase as well as during the syn-rift phase need to be considered in

this discussion. Mantle mechanisms are a plausible explanation since several studies showed anomalies in the mantle beneath Africa, such as Ritsema et al. (1999) or Colli et al. (2013) who detected a slow seismic velocity area in the upper mantle below the SW African margin, but not below the Argentine margin, using tomographic models. Additionally, Heit et al. (2015) presented evidence for a mantle plume-crust interaction by analysing Vp/Vs ratios in Namibia, using receiver function analysis and Ryberg et al. (2015) showed that there is a relation between hot spot trails in Namibia related to large low-velocity regions at the core-mantle boundary.

In contrast to the geophysical studies mentioned above, in a geological study, Jelsma et al. (2009) reported that the emplacement of kimberlites in South Africa is in agreement with the timing of the occurrence of seafloor uplift inferred from the margin reconstruction within the present study. Since kimberlites originate from the mantle, they can be interpreted as traces of deep mantle processes.

Relating the modelling results of this study to those of the investigations mentioned above rather supports the presence of a deep mantle mechanism affecting the SW African margin. However, such mechanism are not considered in the approaches used. The reconstructions of this study therefore only help to quantify a minimum effect of processes that may have affected the margin evolution.

(3) Additional subsidence hypothesis:

Following the results of Chapter 4, an additional (unconsidered and therefore missing) subsidence component has affected the SW African margin. In the forward model, the paleobathymetry at the end of the syn-rift phase already hints at positive paleotopographies of up to ~900 m. Additionally, positive paleotopographies are intermittently present within the restored paleobathymetries of the post-rift phase. There is thus not sufficient space to accommodate even the preserved sedimentary succession. In this context, the often discussed decoupling of the lower and upper crust (Davis and Kusznir, 2004; Huismans and Beaumont, 2011) and possible lower crustal flow could provide a mechanism to create additional subsidence and therefore sufficient accommodation space for storing the syn-rift sediments.

Finally, linking the aspects from the discussion above, suggests that processes in the deep mantle combined with lower crustal flow could explain the evolution of the SW African

margin. By contrast, such a mantle mechanism does most probably not affect the SE South American margin.

5.2 Limitations and outlook

Knowledge of lithological composition and related physical rock properties is essential for reliable subsidence analysis. If the lithology is only poorly constrained, it is difficult to define values for the physical rock properties, which then lead to uncertainties in the modelling. In this work, the largest uncertainties are related to the configuration of the deep syn-rift unit for which the information from wells is limited or not publicly available and seismic resolution is not sufficient for a proper characterisation of rock properties.

In the models, the syn-rift unit is considered as a single unit deposited during the rifting phase and not assumed to be part of the crystalline crust. Nevertheless, the syn-rift unit partially consists of volcanic rocks and not entirely of siliciclastic sediments (Broad et al., 2006). Because of this heterogeneity, it is important to emphasise the characterisation of the syn-rift unit along each of the margins in future studies. Of course, more detailed results can be achieved in modelling the margin reconstruction if physical rock properties (e.g., density or compaction factor) are clearly defined by e.g., information from wells.

Together with the uncertainties related to physical rock properties, the available thickness maps of the syn-rift unit of the SW African margin can also lead to uncertainties in reconstructing paleobathymetries for the top of the syn-rift unit. This becomes evident in the literature where the gravity derived isopach map for the syn-rift unit along the SW African continental margin by Maystrenko et al. (2013) displayed a strongly varying syn-rift thickness between their starting model (1 km within the Walvis Basin and 7 km within the Orange Basin) and final model (12 km within the Walvis Basin and 8 km within the Orange Basin). Although the differences between the starting model and the final model are minor (1 km) in the Orange Basin, they are rather significant in the Walvis Basin (11 km). These discrepancies in syn-rift thicknesses would potentially yield a different margin reconstruction than the one derived in this study. Due to the fact that the syn-rift unit is deposited in the available accommodation space (calculated according to McKenzie's (1978) equation of initial syn-rift subsidence), another syn-rift thickness results in another magnitude of positive paleotopographies. Accordingly, a thinner syn-rift unit yields smaller magnitudes of positive

paleotopographies and vice versa. In this sense, detailed constraints regarding the thickness of the syn-rift unit, especially in the Walvis Basin area, are required to reduce the uncertainties in future margin reconstructions.

The datasets of Autin et al. (2013, 2015) give information about the structural configuration of the Colorado Basin that was originally located next to the Orange Basin on Gondwana. Systematically comparing the syn-rift thicknesses along the SW African margin with the ones of the SE South American margin could provide further insights regarding the uncertainties of the syn-rift thickness. However, investigations on how far the syn-rift phases of both margins are similar have not yet been completed. Autin et al. (2013) proposed a two staged rifting phase for the Colorado Basin, whereas no evidence for a two staged rifting is present within the Orange Basin (Hirsch et al., 2007; Kuhlmann et al., 2010).

To further improve the knowledge of the varying syn-rift thicknesses and to understand the subsidence evolution along both South Atlantic passive margins, future studies comparing the sedimentary basins offshore SE South America further to the north of the Colorado Basin with the Lüderitz Basin and the Walvis Basin on the SW African side to assess differences in the syn-rift thickness might prove useful. The same applies to the post-rift units as this study (Chapter 3) shows a larger load induced subsidence during the Cenozoic in the Colorado Basin than in the Orange Basin. Accordingly, a study focusing on comparing the structural configuration between the Lüderitz Basin (SW Africa) and the Salado Basin (SE South America) as well as between the Walvis Basin (SW Africa) and the Pelotas Basin (SE South America) might certainly help to identify structural uncertainties regarding the syn-rift units as well as post-rift units. It is however clear that comparing post-rift thicknesses may reveal differences rather than similarities, since the sediment has been supplied from different continents after the breakup of Gondwana. Nevertheless, further studies focusing on the post-rift evolution of the above mentioned conjugate settings and restoring paleobathymetries should be also carried out to investigate the subsidence evolution of the entire Southern Segment of the South Atlantic.

In addition to limited constraints on the structure and composition of the syn-rift unit, the assumption of a relatively simple approach for calculating the initial syn-rift subsidence might be associated with even more uncertainties. This study refers to the approach by McKenzie (1978). Accordingly, the calculation of the syn-rift subsidence is valid for an instantaneous syn-rift phase, ignores radiogenic heat production and assumes a fixed temperature at the base

of the lithosphere. McKenzie (1978) demonstrated that this calculation is only valid in 1D and for stretching events of less than 20 Ma. This is in contradiction to the results of Royden and Keen (1980), whose subsidence analysis along the continental margin of eastern Canada indicated an overestimation of the initial syn-rift subsidence in the McKenzie (1978) model. Unfortunately, there is no exact estimation of the duration of the syn-rift phase in the South Atlantic as the timing of the breakup is poorly constrained. The results presented in Chapter 4 of this study rather point to an underestimation than an overestimation of the subsidence during the syn-rift phase. Hence, a better understanding of the duration of the syn-rift phase in the South Atlantic as well as more sophisticated numerical solutions for calculating the amount of initial subsidence would greatly improve the understanding of the evolution of the South Atlantic margins. Such models have been presented by Huismans and Beaumont (2011) in a generic way. Future research should therefore seek to combine physical principles with the observed structural configuration.

Apart from uncertainties related to the theoretical calculation of the initial subsidence, the effect of voluminous volcanism prior to and during the early rifting phase may have played an important role for the subsidence history on both margins of the South Atlantic Ocean in terms of lithospheric cooling. According to Peate (1997), the Paraná-Etendeka large igneous province onshore Africa and South America is associated with the opening of the South Atlantic Ocean during the Early Cretaceous. Offshore, the Rio Grande Rise and the Walvis Ridge are interpreted to relate to this volcanic system as well (O'Conner and Duncan, 1990). The emplacement of this large igneous province may therefore have affected the margins thermally, since additional heat emitted from these volcanic systems that might have delayed the cooling history of the margins. Consequently, the amount of subsidence would differ in areas with a volcanic overprint.

An assumption that is made in the present study is that volcanic lower crustal bodies (underplating material) are emplaced pre-breakup. This is in agreement with other studies, such as Scheck-Wenderoth et al. (2007) or Thybo and Artemieva (2013) who proposed that underplating occurs pre-breakup or during the syn-rift phase but not during the post-rift phase. Nevertheless, future studies should also address the timing of emplacement of lower crustal bodies in order to further validate or discount the effect of volcanism and related effects on the subsidence evolution.

This study presents plausible results for the post-rift evolution of the South Atlantic margins using the uniform stretching model (Chapter 2 and Chapter 3). It also points to possible lower crustal flow (Chapter 4) during the syn-rift phase. The latter process may claim depth dependent stretching and therefore another understanding of the evolution of the South Atlantic passive margins. According to Hopper and Buck (1996), lower crustal flow occurs if weak lower crustal rheologies are present. To verify if lower crustal flow occurred along the margins, knowledge about the rheology of the lithosphere is essential. Goetze and Evans (1979) introduced yield strength envelopes to describe the rheological stratification. This description is rather valid for oceanic lithosphere but different for continental lithosphere due to its higher variability in composition and structure compared to oceanic lithosphere (e.g., Burov and Diament, 1995; Jackson, 2002). Since passive margins consist of continental lithosphere but still behave similar to oceanic lithosphere, in terms of lithosphere cooling, it is more difficult to describe their rheology (Burov, 2011). Furthermore, rheology descriptions integrating observations are restricted to the present-day (Tesauro et al., 2009) and studies explaining the rheology of the past remain generic in nature. It is clear that the stratification of the layered lithosphere probably changes during margin history due to a varying thermal field in response to lithosphere cooling. This study provides a first step in solving this problem (with the results of Chapter 4), combining present-day observations of margin configuration with thermo-mechanical process simulation.

The advantage of this study is the use of present-day observations on the configuration of the entire lithosphere and not only on the crystalline crust or the sediments. Accordingly, the results yield insights on paleobathymetries and lead to suggestions regarding processes behind margin evolution. To validate these suggestions, the research field needs to be expanded to also take into account the asthenosphere and corresponding lithosphere-asthenosphere interaction. As a consequence, the coupling between lithosphere and asthenosphere would improve the understanding of causative processes behind margin evolution. Similar work has been done by Burov and Gerya (2014), who investigated the topographic evolution affected by a mantle plume, and by Huismans and Beaumont (2011), who presented end-members of passive margins as the result of different modes of extension and the specific behavior of the lithosphere and the asthenosphere. Although these studies accomplish the coupling between lithosphere and asthenosphere, they do not consider present-day observations. Consequently,

combining detailed present-day observations with larger scale geodynamic aspects would be a strategy to finally understand the processes behind margin evolution.

6 Conclusions

The aim of this thesis was to achieve a better understanding of the subsidence evolution of the margins of the South Atlantic Ocean. 3D structural- and thermal models representing the present-day lithosphere-scale configuration of several sedimentary basins along the South Atlantic margins were used accordingly. These models archive information about the margin evolution and provide an excellent starting point for the margin reconstruction. Different modelling approaches (1D backward modelling and 3D forward modelling) have been applied that allowed the restoration of paleobathymetries. The paleobathymetries were then used to assess the margin evolution and to quantify past vertical movements as well as to discuss causative processes responsible for the characteristic subsidence evolution of the margins.

According to the results of the approaches used the following conclusions can be drawn:

(1) Using information on the present-day configuration in combination with analytical modelling solutions and modelling simulations considering first-order physical principles, the post-rift paleobathymetric evolution of the conjugate passive continental margins of the South Atlantic Ocean has been reconstructed and correspondingly, the subsidence evolution has been inferred.

(2) The two margins within the Southern Segment of the South Atlantic Ocean are characterised by different post-rift subsidence histories. The restored paleobathymetries indicated that continuous subsidence dominated the Argentine margin, whereas the subsidence history of the margin offshore SW Africa was interrupted by phases of seafloor uplift. Quantifying the minimum estimate of seafloor uplift during the entire post-rift phase yields up to 1200 m of uplift for the SW African margin.

(3) As present-day observations of the structural configuration were used, individual subsidence components were calculated. Accordingly, the amount of thermal

subsidence is in the same order of magnitude along the conjugate margins, but the amount of load induced subsidence was larger in the Colorado Basin than in the Orange Basin, especially for Cenozoic times. The possible causes are that larger sediment supply dominated the Argentine margin during Cenozoic times, compared to the African margin. A second cause is that because of erosion, not all the sediments were preserved offshore Africa. The latter may also be related to the obtained phases of vertical upward movements.

(4) A first reconstruction of the syn-rift phase on the SW African margin indicated a more complex evolution of this period than previously assumed. The corresponding results pointed to mechanical decoupling of the lower and upper crustal domains resulting in lower crustal flow. This might act as an additional process that creates more accommodation space already during the syn-rift phase.

(5) 3D forward modelling showed that sediments have a significant effect on the temperature distribution of the lithosphere. According to the location of the sediments, the temperature varied in time and space and delayed the mantle cooling throughout the entire post-rift phase. As a result of the thermal variations, the rigidity of the lithosphere also varied significantly along the entire margin, which in turn affected the deformation of the margin in response to sedimentary loading.

(6) The results of the 3D forward modelling considering present-day information about the configuration of the margin were also useful for economic interests. Due to the fact that the thermal structure was investigated through time, this study provided useful information in terms of hydrocarbon exploration as it is now possible to reconstruct the spatio-temporal evolution of the oil and gas windows.

(7) Comparing the results of the subsidence evolution derived from the different approaches used, indicated that ridge-push is insufficient as a causative process for uplift since the impact of ridge-push should have affected both margins to a similar extent. This leads to the proposition of a local mantle mechanism beneath SW Africa, affecting the subsidence evolution by an additional uplift component.

7 References

Airy, G.B. (1855) On the computation of the effect of the Attraction of Mountain-masses, as disdurbing the apparent astronomical latitude of station in geodetic surveys. Philos. Trans. R. Soc. London 145, 101-104.

Allken, V., Huismans, R.S., Thieulot C. (2012) Factors controlling the mode of rift interaction in brittle-ductile coupled systems: A 3D numerical study. Geochem. Geophys. Geosyst. 13 (5), Q05010. doi:10.1029/2012GC004077

Al-Hajri, Y., White, N., Fishwick, S. (2009) Scales of transient convective support beneath Africa. Geology 37, 883-886. doi:10.1130/G25703A.1

Anka, Z., Loegering M.J., di Primio, R., Marchal, D., Rodríguez, J.F., Vallejo, E. (2014) Distribution and origin of natural gas leakage in the Colorado Basin, offshore Argentina Margin, South America: seismic interpration and 3D basin modelling. Geologica Acta 12 (4), 269-285. doi:10.1344/GeologicaActa2014.12.4.1

Athy, L.F. (1930) Density, Porosity, and Compaction of Sedimentary Basins. Am. Assoc. Pet. Geol. Bull. 14, 1-24.

Austin J.A., Uchupi, E. (1982) Continental oceanic crustal transition off southwest Africa. Am. Ass. Petroleum Geologist Bull., 66, 1328-1347.

Autin, J., Scheck-Wenderoth, M., Loegering, M.J, Anka, Z., Vallejo, E., Rodriguez, J.F., Dominguez, F., Marchal, D., Reichert, C., di Primio, R., Götze, H.-J. (2013) Colorado Basin 3D structure and evolution, Argentine passive margin. Tectonophyiscs 604, 264-279. doi:10.1016/j.tecto.2013.05.019

Autin, J., Scheck-Wenderoth, M., Götze, H.-J., Reichert, C., Marchal, D. (2015) Deep structure of the Argentine margin inferred from 3D gravity and temperature modelling, Colorado Basin. Tectonophysics. doi10.1016/j.tecto.2015.11.023

Bauer, K., Neben, S., Schreckenberger, B., Emmermann, R., Hinz, K., Fechner, N., Gohl, K., Schulze, A., Trumbull, R.B., Weber, K. (2000) Deep structure of the Namibia continental margin as derived from integrated geophysical studies. J. Geophys. Res. 105, 25,829-25,853.

Bauer, K., Trumbull, R.B., Vietor, T. (2003) Geophysical images and a crustal model of intrusive structures beneath the Messum ring complex, Namibia. Earth Planet. Sci. Lett. 216, 65-80. doi:10.1016/S0012-821X(03)00486-2

Bjørlykke, K. (2010) Petroleum Geoscience. From sedimentary Environments to Rock Physics. Springer, Heidelberg, 508 p.

Blaich, O.A., Faleide, J.I., Tsikalas, F., Franke, D., León, E. (2009) Crustal-scale architecture and segmentation of the Argentine margin and its conjugate off South Africa. Geophys. J. Int. 178 (1):85-105. doi:10.111/j.1365-246X.2009.04171.x

Blaich, O.A., Faleide, J.I., Tsikalas, F. (2011) Crustal breakup and continent-ocean transition at South Atlantic conjugate margins. J. Geophys. Res. 115 (B01402), 1-38. doi:10.1029/2010JB007686

Bott, M.H.P. (1992) Passive margins and their subsidence. Journal of Geological Society, London, 149, 805-812.

Braun, J., Deschamps, F., Rouby, D., Dauteuil, O. (2013) Flexure of the lithosphere and the geodynamical evolution of non-cylindrical rifted passive margins: Results from a numerical model incorporating variable elastic thickness, surface processes and 3D thermal subsidence. Tectonophysics 604, 72-82. doi:10.1016/j.tecto.2012.09.033

Braun, J., Guillocheau, F., Robin, C., Baby, G., Jelsma, H. (2014) Rapid erosion of the Southern African Plateau as it climbs over a mantle superswell. J. Geophys. Res. Solid Earth 119, 6093-6112. doi:10.1002/2014JB010998

Boyd, D.L. (2010) Seismic Interpretation, Distribution, and Numerical Modelling of Natural Gas Leakage in Block 2 of the Orange Basin, Offshore South Africa. M.Sc. thesis, Universtiy of Cape Town.

Broad, D., Jungslager, E., McLachlan, I., Roux, J. (2006) Offshore mesozoic basins, in: Johnson, M.R., Anhausser, C.R., Thomas, R.J. (Eds.), Geology of South Africa. Geological Socienty of South Africa/Council for GeoScience, Pretoria, 553-571.

Brown, L.F., Benson, Jr., J.M., Brink, G.J., Doherty, S., Jollands, A., Jungslager, E.H.A., Keenan, J.H.G., Muntingh, A., Van, Wyk, N.J.S. (1995) Sequence stratigraphy in offshore South African divergent basins. An atlas on exploration for Cretaceous lowstand traps by Soeker (Pty) Ltd. AAPG, Studies in Geology 41.

Brune, S., Popov, A., Sobolev, S.V. (2013) Quantifying the thermo-mechanical impact of plume arrival on continental break-up. Tectoniphysics 604, 51-59. doi:10.1016/j.tecto.2013.02.009

Brune, S. (2014) Evolution of stress and fault patterns in oblique rift systems: 3-D numerical lithospheric-scale experiments from rift to breakup. Geochem. Geophys. Geosyst. 15, 3392-3415. doi:10.1002/2014GC005446

Brune, S., Heine, C., Pérez-Gussinyé, M., Sobolev, S. V. (2014) Rift migration explains continental margin asymmetry and crustal hyper-extension. Nat. Commun. 5, 4014. doi:10.1038/ncomms5014

Burke, K. (1996) The African plate. South African J. Geol. 99, 341-409.

Burov, E.B., Diament, M. (1995) The effective elastic thickness (Te) of continental lithosphere: What does it really mean? J. Geophys. Res. 100 (B3), 3905-3927

Burov, E.B., Poliakov, A. (2001) Erosion and rheology controls on synrift and postrift evolution: Verifying old and new ideas using a fully coupled numerical model. J. Geophys. Res. 106 (B8), 26,461-16,481.

Burov, E.B., Guillou-Frottier. L, (2005) The plume-continental lithosphere interaction using a tectonically realistic formulation for the lithosphere. Geophys. J. Int. 161, 469-490. doi:10.1111/j.1365-246X.2005.02588.x

Burov, E.B., Watts, A.B. (2006) The long-term strength of continental lithsophere: "jelly sandwich" or "crème brûlée". GSA Today, 16,1, 4-10. doi:10.1130/1052-5173(2006)016<4:TLTSOC>2.0CO;2

Burov, E.B., Guillou-Frottier, L., d'Acremont, E., Le Pourhiet, L., Cloetingh, S. (2007) Plume head-lithosphere interactions near intra-continental plate boundaries. Tectonophysics 343, 15-38. doi: 10.1016/j.tecto.2007.01.002

Burov, E.B., Cloetingh, S. (2010) Plume-like upper mantle instabilities drive subdaction initiation. Geophys. Res. Lett. 37, L03309, 1-6. doi:10.1029/2009GL041535

Burov, E.B. (2011) Rheology and strength of the lithosphere. Mar. Pet. Geol. 28, 1402-1443. doi:10.1016/j.marpetgeo.2011.05.008

Burov, E.B., Gerya, T. (2014) Asymmetric three-dimensional topography over mantle plumes. Nature 513, 85-89. doi:10.1038/nature13703

Cacace, M., Scheck-Wenderoth, M. (2014) Different subsidence components at passive margins. Geophys. Res. Abstracts 16. EGU2014-5281.

Cloetingh, S., Beekman, F., Ziegler, P. A., van Wees, J.-D., Sokoutis, D. (2008) Post-rift compressional reactivation potential of passive margins and extensional basins, in: Johnsen, H., Doré, A. G., Gatliff, R. W., Hildsworth, R., Lundin, E. R., Ritchie, J. D. (Eds.), The Nature and Origin of Compression in Passive Margins. Geol. Soc. London, Spec. Publ. 306, 27-70. doi:10.1144/SP306.2

Cobbold, P.R., Rossello, E.A., Roperch, P., Arrigada, C., Gomez, L.A., Lima, C. (2007) Distribution, timing, and causes of Andean deformation across South America. In: Ries, A.C., Butler, R.W.H., Graham, R.H. (Eds.), Deformation of the Continental Crust: The Legacy of Mike Coward. Geol. Soc. London, Spec. Publ., 272, 321-343.

Cohen, K.M., Finney, S.M., Gibbard, P.L., Fan, J.-X. (2013) The ICS International Chronostratigraphic Chart, Episodes 36 (3): 199-204.

Colli, L., Fichtner, A., Bunge, H.-P. (2013) Full waveform tomography of the upper mantle in the South Atlantic region: Imaging a westward fluxing shallow asthenosphere? Tectonophysics 604, 26-40. doi:10.1016/j.tecto.2013.06.015

Colli, L., Stotz, I., Bunge, H.-P., Smethurst, M., Clark, S., Iaffaldano, G., Tassara, A., Guillocheau, F., Bianchi, M.C. (2014) Rapid South Atlantic spreading changes and coeval vertical motion in surrounding continents: Evidence for temporal changes of pressure-driven upper mantle flow. Tectonics 32, 1304-1321. doi:10.1002/2014TC003612

Conrad, C.P., Steinberger, B., Torsvik, T.H. (2013) Stability of active mantle upwelling revealed by net characteristics of plate tectonics. Nature 498, 479-82. doi:10.1038/nature12203

Davies, M., Kusznier, N. (2004) Depth-dependent lithospheric stretching at rifted continental margins. in: Karner, G.D., Tayler, B., Driscoll, N.W., Kohlsted, D.L. (Eds.), Rheology and Deformation of the Lithosphere at Continental margins. Columbia Uni. Pr. 92-137

Demoulin, A., Zarate, M., Rabassa, J. (2005) Long-term landscape development: a persepctive from the southern Buenos Aires ranges of east central Argentina. Journal of South Am. Earth Sci. 19, 193-204. doi:10.1016/j.jsames.2004.12.001

Dingle, R.V., Hendey, Q.B. (1984) Late Mesozoic and Tertiary sediment supply to the eastern cape basin (SE Atlantic) and paleo-drainage systems in southwestern Africa. Mar. Geol. 56, 13-26.

Dominguez, F., Marchal, D., Sigismondi, M., Espejón, C., Vallejo, E. (2011) Caracterización de dominios estructuraled e influencia de estructuras preexistentes en hemigábenes de rift en el sector centro-norte de la Plataforma Continental Argentina. Actas XVIII Congreso Geológico Argentino.

Dressel, I., Scheck-Wenderoth, M., Cacace, M., Lewerenz, B., Götze, H.-J., Reichert, C. (2015) Reconstruction of the southwestern African continental margin by backward modeling. Mar. Pet. Geol. 67, 544-555. doi:10.1016/j.marpetgeo.2015.06.006

Dupré, S., Cloetingh, S., Bertotti, G. (2011) Structure of the Gabon Margin from integrated seismic reflection and gravity. Tectonophysics 506, 31-45. doi:10.1016/j.tecto.2011.04.009

Eldholm, O., Gladczenko, T.P., Skogseid, J., Planke, S. (2000) Atlantic volcanic margins: a comparative study, in: Nøttvedt A. et al. (Eds.) Dynamics of the Norwegian Margin. Geol. Soc. London, Spec. Publ. 167:411-428. doi:10.1144/GSL.SP.2000.167.01.16

Espurt, N., Callot, J.-P., Roure, F., Totterdell, J.M., Struckmeyer, H.I.M., Vially, R. (2012) Transition from symmetry to asymmetry during continental rifting. An example from the Bight Basin-Terre Adélie (Australien and Antarctic conjugate margins). Terra Nova 24:167-180. doi:10.1111/j.1365-3121.2011.01055.x

Faccena, C., Becker, T. (2010) Shaping mobile belts by small-scale convection. Nature 465, 602-605. doi:10.1038/nature09064

Fernàndez, M., Afonso, J. C., Ranalli, G. (2010) The deep lithospheric structure of the Namibian volcanic margin. Tectonophysics 481, 68-81. doi:10.1016/j.tecto.2009.02.036

Flament, N., Gurnis, M., Müller, R.D. (2013) A review of observations and model of dynamic topography. Lithosphere. doi:10.1130/L245.1

Forte, A., Quéré, S., Moucha, R., Simmons, N.A., Grand, S., Mitrovica, J.X., Rowley, D.B. (2010) Joint seismic-geodynamic-mineral physical modelling of African geodynamics: A

reconciliation of deep-mantle convection with surface geophysical constraints. Earth Planet. Sci. Lett. 295, 329-341. doi:10.1016/j.epsl.2010.03.017

Franke, D., Neben, S., Schreckenberger, B., Schulze, A., Stiller, M., Krawczyk, C.M. (2006) Crustal structure across the Colorado Basin, offshore Argentina. Geophys. J. Int. 165, 850-864. doi:10.1111/j.1365-246X2006.02907.x

Franke, D., Neben, S., Ladage, S., Schreckenberger, B., Reichert, C., Hinz, K. (2007) Margin segmentation and volcano-tectonic architecture along the volcanic margin off Argentine/Uruguay, South Atlantic. Mar. Geol. 244, 46-67. doi:10.1016/jmargeo.2007.06.009

Franke, D., Ladage, S., Schnabel, M., Schreckenberger, B., Reichert, C., Hinz, K. (2010) Birth of a volcanic margin off Argentina, South Atlantic. Geochem. Geophys. Geosyst. 11 (2), 1-20. doi:10.1029/2009GC002715

Gallagher, K., Brown, R. (1999) Denudation and uplift at passive margins: the record on the Atlantic Margin of southern Africa. Phil. Trans. R. Soc. Lond. A 357, 835-859.

Gladczenko, T.P., Skogseid, J., Eldholm, O. (1997) South Atlantic volcanic margins. Journal of the Geol. Soc. London 154, 465-470

Gladczenko, T.P., Skogseid, J., Eldholm, O. (1998) Namibia volcanic margin. Mar. Geophys. Res. 20, 313-341.

Goetze, C., Evans, B (1979) Stress and temperature in bending lithosphere as constrained by experimental rock mechanics. Geophys. J.R. astr. Soc. 58, 463-478.

Guillocheau, F., Rouby, D., Robin, C., Helm, C., Rolland, N., Le Carlier de Veslud, C., Braun, J. (2012) Quantification and causes of the terrigenous sediment budget at the scale of a continental margin. A new method applied to the Namibia-South Africa margin. Basin Res. 24, 3-30. doi:10/1111/j.1365-2117.2011.00511.x

Guillocheau, F., Dauteuil, O., Baby, G., Robin, C. (2013) Uplift of the South African Plateau: mantle-scale deformation, long wavelength relief growth and offshore sediment budget Geophys. Res. Abstracts 15, EGU2013-12743.

Gurnis, M., Mitrovica, J.X., Ritsema, J., van Heijst, H.-J. (2000) Constraining mantle density structure using geological evidence of surface uplift rates: The case of the African Superplume. Geochem. Geophys. Geosyst. 1, 1020. doi:10.1029/1999GC000035

Grose, C.J. (2012) Properties of oceanic lithosphere: Revised plate cooling model predictions. Earth Plat. Sci. Lett. 333-334, 250-264. doi:10.1016/j.epsl.2012.03.037

Haq, B.U., Hardenbol, J., Vail, P.R. (1987) Chronology of fluctuating sea levels since the triassic. Science 235, 1156-1167.

Hartwig, A., Anka, Z., di Primio, R. (2012) Evidence of a widespread paleo-pockmarked field in the Orange Basin: An indication of an early Eocene massive fluid escape event offshore South Africa. Mar. Geol. 332-334, 222-234. doi:10.1016/j.margeo.2012.07.012

Heit, B., Yuan, X., Weber, M., Geissler, W., Jokat, W., Lushetile, B., Hoffmann, K.-H. (2015) Crustal thickness and Vp/Vs ratio in NW Namibia from receiver functions: evidence for magmatic underplating due to mantle plume-crust interaction. Geophy. Res. Letter 42, 3330-3337. doi:10.1002/20125GL063704

Hinz, K., Neben, S., Schreckenberger, B., Roeser, H.A., Block, M., Goncalves de Souza, H. (1999) The Argentine continental margin north of 48°S: sedimentary successions, volcanic activity during breakup. Mar. Pet. Geol. 16, 1-25.

Hirsch, K.K., Scheck-Wenderoth, M., Paton, D.A., Bauer, K. (2007) Crustal structure beneath the Orange Basin, South Africa. South African J. Geol. 110, 249-260. doi:10.2113/gssajg.110.2-3.249

Hirsch, K.K., Bauer, K., Scheck-Wenderoth, M. (2009) Deep structure of the western South African passive margin - Results of a combined approach of seismic, gravity and isostatic investigations. Tectonophysics 470, 57-70. doi:10.1016/j.tecto.2008.04.028

Hirsch, K.K., Scheck-Wenderoth, M., van Wees, J.D., Kuhlmann, G., Paton, D.A. (2010) Tectonic subsidence history and thermal evolution of the Orange Basin. Mar. Pet. Geol. 27, 565-584. doi:10.1016/j.marpetgeo.2009.06.009

Holtar, E., Forsberg, A.W. (2000) Postrift development of the Walvis Basin, Namibia. Results from the exploration campagin in quadrant 1911, in: Mello, M.R., Katz, B.J. (Eds.), Petroleum systems of South Atlantic margins: AAPG Memoir 73, 429-446.

Hopper, J., Buck, W.R. (1996) Effects of lower crustal flow on continental extension and passive margin formation. J. Geophys. Res., 101, 20,175-29,194.

Huismans, R.S., Beaumont, C. (2011) Depth-dependent extension, two-stage breakup and cratonic underplating at rifted margins. Nature 473, 74-78. doi:10.1038/nature09988

Huismans, R.S., Beaumont, C. (2014) Rifted continental margins: The case for depth-dependent extension. Earth Planet. Sci. Lett. 407, 148-162. doi:10.1016/j.epsl.2014.09.032

IOC, IHO, and BODC (2013) Centenary Edition of the GEBCO Digital Atlas, published on CD-ROM on behalf of the Intergovernmental Oceanographic Commission and the International Hydrographic Organization as part of the General Bathymetric Chart of the Ocean; British Oceanographic Data Centre, Liverpool.

Jackson, J. (2002) Strength of the continental lithosphere: Time to abandon the jelly sandwich? GSA Today, 12, 9, 4-10. doi:101130/1052-5173(2002)012<0004:SOTCLT>2.0.CO;2

Jackson, M.P.A,, Hudec, M.R., Hegarty, K.A. (2005) The great West African Tertiary coastal uplift: Fact or fiction? A perspective from the Angolan divergent margin. Tectonics 24, TC6014. doi:1029/2005TC001836

Japsen, P., Chalmers, J.A., Green, P.F., Bonow, J.M. (2012) Elevated, passive continental margins: Not rift shoulders, but expressions of episodic, post-rift burial and exhumation. Glob. Planet. Change 90-91, 73-86. doi:10.1016/j.gloplacha.2011.05.004

Jelsma, H., Barnett, W., Richards, S., Lister, G. (2009) Tectonic setting of kimberlites. Lithos 112S, 155-165. doi:10.1016/j.lithos.2009.06.030

Jungslager, E.H.A. (1999) Petroleum habitats of the Atlantic margin of South Africa, in: Cameron, N.R., Bate, R.H., Clure, V.S. (Eds.), The oil and gas habitats of the South Atlantic. Geol. Soc. London, Spec. Publ. 153, 153-168. doi:10.1144/GSL.SP.1999.153.01.10

Karner, G.D., Driscoll, N.W. (1999) Tectonic and stratigraphic development of the West African and eastern Brazilien Margins: insights from quantitative basin modelling. In: Cameron, N.R., Bate, R.H., Clure, V.S. (Eds.) The Oil and Gas Habitats of the South Atlatnic. Geol. Soc. London, Spec. Publ. 153, 11-40.

Karner, G.D., Gambôa, L.A.P. (2007) Timing and origin of the South Atlantic pre-salt sag basins and their capping evaporites, in: Schreiber, B.C., Lugli, S., Babel, M. (Eds.) Evaporites Through Space and Time. Geol. Soc. London, Spec. Publ. 285:15-35. doi:10.1144/SP285.2

Katz, B.J., Mello, M.R. (2000) Petroleum Systems of South Atlantic marginal basins - an overview. in M.R. Mello and B.J. Katz (Eds), Petroleum systems of South Atlantic margins: AAPG Memoir 73, 1-13.

Kipata, M.L., Delvaux, D., Sebagenzi, M.N., Cailteux, J., Sintubin, M. (2013) Brittle tectonic and stress field evolution in the Pan-African Lufilian arc and its foreland (Katanga, DRC): from orogenic compression to extensional collapse, transpressional inversion and transition to rifting. Geol. Belgica 16, 1-17.

Kooi, H., Cloetingh, S. (1989) Some consequences of compressional tectonics for extensional models of basin subsidence. Geol. Rundsch. 78, 183-195.

Koopmann, H., Franke, D., Schreckenberger, B., Schulz, H., Hartwig, A., Stollhofen, H., di Primio, R. (2013) Segmentation and volcano-tectonic characteristics along the SW African continental margin, South Atlantic, as derived from multichannel seismic and potential field data. Mar. Pet. Geol. 50, 22-39. doi:10.1016/j.marpetgeo.2013.10.016

Koopmann, H., Brune, S., Franke, D., Breuer, S. (2014) Linking rift propagation barriers to excess magmatism at volcanic rifted margins. Geology 42 (12), 1071-1074. doi:10.1130/G36085

Kounov, A., Viola, G., de Wit, M., Andreoli, M.A.G. (2009) Denudation along the Atlantic passive margin: new insights from apatite fission-track analysis on the western coast of South Africa, in: Lisker, F., Ventura, B., Glasmacher, U.A. (Eds.), Thermochronological Methods: From Paleotemperature Constraints to Landscape Evolution Models. Geol. Soc. London, Spec. Publ. 324, 287-306. doi:10.1144/SP324.19

Kounov, A., Viola, G., Dunkl, I., Frimmel, H.E. (2013) Southern African perspectives on the long-term morpho-tectonic evolution of cratonic interiors. Tectonophysics 601, 177-191. doi:10.1016/j.tecto.2013.05.009

Kuhlmann, G., Adams, S., Campher, C., van der Spuy, D., di Primio, R., Horsfield, B. (2010) Passive margin evolution and its controls on natural gas leakage in the southern Orange Basin, blocks 3/4, offshore South Africa. Mar. Pet. Geol. 27, 973-992. doi:10.1016/j.marpetgeo.2010.01.010

Kuhlmann, G., Adams, S., Anka, Z., Campher, C., di Primio, R., Horsfield, B. (2011) 3D Petroleum Systems Modelling Within a Passive Margin Setting, Orange Basin, Blocks 3/4, Offshore South Africa - Implications for Gas Generation, Migration and Leakage. South African J. Geol. 114, 387–414. doi:10.2113/gssajg.114.3-4.387

Lavier, L.L., Manatschal, G. (2006) A mechanism to thin the continental lithosphere at magma-poor margins. Nature 440:324-328. doi:10.1038/nature04608

Le Pourhiet, L., Huet, B., May, D.A., Labrousse, L., Jolivet L. (2012) Kinematic interpretation of the 3D shapes of metamorphic core complexes. Geochem. Geophys. Geosyst. 13 (9), Q09002. doi:10.1019/2012GC004271

Liao, J., Gerya, T. (2015) From continental rifting to seafloor spreading: Insight from 3D thermo-mechanical modeling. Gondwana Res. 28 (4), 1329-1343. doi:10.1016(j.gr.2014.11.004

Light, M.P.R., Maslanyj, M.P., Greenwood, R.J., Banks, N.L. (1993) Seismic sequence stratigraphy and tectonics offshore Namibia, in: Williams, G.D., Dobb, A. (Eds.), Tectonics and Seismic Sequence Stratigraphy. Geol. Soc. London, Spec. Publ. 71, 163-191. doi:10.1144/GSL.SP.1993.071.01.08

Lithgow-Bertelloni, C., Silver, P. (1998) Dynamic topography, plate driving forces and the African superswell. Nature 395, 345-348.

Loegering, M., Anka, Z., Autin, J., di Primio, R., Marchal, D., Rodriguez, J.F., Franke, D., Vallejo, E. (2013) Tectonic evolution of the Colorado Basin, offshore Argentina, inferred from seismo-stratigraphy and depositional rates analysis. Tectonphysics 604, 245-263. doi:10.1016/j.tecto.2013.02.008

Marcano, G., Anka, Z., di Primio, R. (2013) Major controlling factors on hydrocarbon generation and leakage in South Atlantic conjugate margins: A comparative study of Colorado, Orange, Campos, and Lower Congo basins. Tectonophysics 604, 172-190. doi:10.1016/j.tecto.2013.02.004

Maystrenko, Y.P., Scheck-Wenderoth, M., Hartwig, A., Anka, Z., Watts, A.B., Hirsch, K.K., Fishwick, S. (2013) Structural features of the Southwest African continental margin according to results of lithosphere-scale 3D gravity and thermal modelling. Tectonophysics 604, 104-121. doi:10.1016/j.tecto.2013.04.014

McKenzie, D. (1978) Some remarks on the development of sedimentary basins. Earth Planet. Sci. Lett. 40, 25-32.

McKenzie, D., Fairhead, D. (1997) Estimates of the effective elastic thickness of continental lithosphere from Bouger and free air gravity anomalies. J. Geophys. Res. 102 (B12), 27,523-27,552.

McKenzie, D., Jackson, J., Priestley, K. (2005) Thermal structure of oceanic and continental lithosphere. Earth Planet. Sci. Lett. 233, 337-349. doi:10.1016/j.epsl.2005.05.005

McMillan, I. (2003) Foraminiferally defined biostratigraphic episodes and sedimentation pattern of the Cretaceous drift succession (Early Barremian to Late Maastrichtian) in seven basins on the South African and southern Namibian continental margin. S. Afr. J. Sci. 99, 537-576.

Millán, H., Den Bezemer, T., Vergés, J., Marzo, M., Muñoz, J.A., Roca, E., Cirés, J., Zoetemeijer, R., Cloetingh, S., Puigdefabregas, C. (1995) Paleo-elevation and effective elastic thickness evolution at mountain ranges: inferences from flexural modelling in the Eastern Pyrenees and Ebro Basin. Mar. Pet. Geol. 12 (8), 917-928.

Mjelde, R., Faleide, J.I., Breivik, A.J, Raum, T. (2009) Lower crustal composition and crustal lineaments on the Vøring Maring, NE Atlantic: A review. Tectonophysics 472, 183-193. doi:10.1016/j.tecto.2008.04.018

Mohriak, W., Nemčok, M., Enciso, G. (2008) South Atlantic divergent margin evolution: rift-border uplift and salt tectonics in the basins of SE Brazil, in: Pankhurst, R.J., Trouw, R.A.J., Brito Neves, B.B., De Wit, M.J. (Eds.) West Gondwana: Pre-Cenozoic Correlations Across the South Atlantic Region. Geol. Soc. London, Spec. Publ. 294, 365-398. doi:10.1144/SP294.19

Moucha, R., Forte, A.M. (2011) Changes in African topography driven by mantle convection. Nat. Geosci. 4, 707-712. doi:10.1038/ngeo1235

Moulin, M., Aslanian, D., Olivet, J.-L., Contrucci, I., Matias, L., Géli, L., Klingelhoefer, F., Nouzé, H., Réhault, J.-P., Unternehr, P. (2005) Geological constraints on the evolution of the Angolan margin based on reflection and refraction seismic data (ZaïAngo project). Geophys. J. Int. 162 (3), 793-810. doi:10.1111/j.1365-246X.2005.02668.x

Müller, R.D., Sdrolias, M., Gaina, C., Roest, W.R. (2008) Age, spreasing rates, and spreading asymmetry of the world's ocean crust. Geoch. Geophy. Geosys. 9 (4), 1-9. doi:10.1029/2007/GC001743

Nürnberg, D., Müller, R.D. (1991) The tectonic evolution of the South Atlantic from Late Jurassic to present. Tectonophysics 191, 27-53.

Nyblade, A., Robinson, S. (1994) The African superswell. Geophys. Res. Lett. 21, 765-768.

O'Conner, J.M., Duncan, R.A. (1990) Evolution of the Walvis Ridge-Rio Grande Rise Hot Spot System: Implications for African and South American Plate Motions Over Plumes. J. Geophys. Res. 95 (B11), 17,475-17,502.

Parson, B., Sclater, J.G. (1977) An analysis of the variation of ocean floor bathymetry and heat flow with age. J. Geophys. Res. 82 (5), 803-827.

Paton, D.A, di Primio, R., Kuhlmann, G., van der Spuy, D., Horsfield, B. (2007) Insights into the Petroleum System Evolution of the southern Orange Basin, South Africa. South African J. Geol. 110, 261-274. doi:10.2113/gssajg.110.2-3.261

Paton, D.A., van der Spuy, D., di Primio, R., Horsfield, B. (2008) Tectonically induced adjustment of passive-margin accommodation space; influence on the hydrocarbon potential of the Orange Basin, South Africa. Am. Assoc. Pet. Geol. Bull. 92, 589-609. doi:10.1306/12280707023

Patridge, T.C., Maud, R.R. (1987) Geomorphic evolution of southern Africa since the Mesozoic. South African J. Geol. 90 (2), 179-208

Paul, J.D., Roberts, G.G., White, N. (2014) The African landscape through space and time. Tectonics 33 (6), 898-935. doi:10.1002/2013TC003479

Pawlowski, R. (2008) The use of gravity anomaly data for offshore continental margin demarcation. The Leading Edge 27, 722-727. doi: 10.1190/1.2944156

Peate, D.W. (1997) The Paraná-Etendeka Province. in: Mahoney, J.J., Coffin, M.F. (Eds.), Large Igneous Provinces; Continental, Oceanic, and Planetary Flood Volcanis. Geophysiccal Monograph Series, 100. AGU, Washington DC. 214-245.

Pedoja, K., Husson, L., Regard, V., Cobbold, P.R., Ostanciaux, E., Johnson, M.E., Kershaw, S., Saillard, M., Martinod, J., Furgerot, L., Weill, P., Delcaillau, B. (2011) Relative sea-level fall since the last interglacial stage: Are coasts uplifting worldwide? Earth-Science Rev. 108, 1-15. doi:10.1016/j.earscirev.2011.05.002

Péron-Pinvidic, G., Manatschal, G., Minshull, T.A., Sawyer, D.S. (2007) Tectonosedimentary evolution of the deep Iberia-Newfoundland margins: Evidence for a complex breakup history. Tectonics 26 (TC2011), 1-19. doi:10.1029/2006TC001970

Pratt, J.H. (1855) On the attraction of the Himalay Mountains, and if the elevated Regions beyond them, upon the Plumb-Line in India. Philos. Trans. R. Soc. London 145, 53-100.

Raab, M.J., Brown, R.W., Gallagher, K., Carter, A., Weber, K. (2002) Late Cretaceous reactivation of major crustal shear zones in northern Namibia: Constraints from apatite fission track analysis. Tectonophysics 349, 75-92.

Rabinowitz, P.D., Labrecque, J. (1979) The Mesozoic South Atlantic Ocean and evolution of its continental marings. Journal of Geophy. Res. 84 (B11), 5973-6002

Reston, T.J., Pérez-Gussinyé (2007) Lithospheric extension from rifting to continental breakup at magma-poor margins: rheology, serpentinisation and symmetry. Int. J. Earth Sci. 96, 1033-1046. doi:10.1007/s00531-006-0161-z

Reston, T.J. (2009) The structure, evolution and symmetry of the magma-poor rifted margins of the North and Central Atlantic: A synthesis. Tectonophysics 468, 6-27. doi:10.1016/j.tecto.2008.09.002

Ritsema, J., van Heijst, H.J., Woodhouse, J.H. (1999) Complex Shear Wave Velocity Structure Imaged Beneath Africa and Iceland. Science 286, 1925-1928. doi:10.1126/science.286.5446.1925

Roberts, G.G., White, N. (2010) Estimating uplift rate histories from river profiles using African examples. J. Geophys. Res. 115 (B02406), 1-24. doi:10.1029/2009JB006692

Rouby, D., Bonnet, S., Guillocheau, F., Gallagher, K., Robin, C., Biancotto, F., Dauteil, O., Braun, J. (2009) Sediment supply to the Orange sedimentary system over the last 150 My: An evaluation from sedimentation/denudation balance. Mar. Pet. Geol. 26, 782-794. doi:10.1016/j.marpetgeo.2008.08.004

Rouby, D., Braun, J., Robin, C., Dauteuil, O., Deschamps, F. (2013) Long-term stratigraphic evolution of Atlantic-type passive margins: A numerial approach of interactions between surface processes, flexural isostasy and 3D thermal subsidence. Tectonophysics 604, 83-103. doi:10.1016/j.tecto.2013.02.003

Rodyen, L., Keen, C.E. (1980) Rifting processes and thermal evolution of the continental margin of eastern canada determined from subsidence curves. Earth Planet. Sci. Lett. 51, 343-361.

Ryberg, T., Haberland, C., Haberlau, T., Weber, M., Bauer, K., Behrmann, J.H., Jokat, W. (2015) Crustal structure of northwest Namibia: Evidence for plume-rift-continent interaction. Geology 43 (8), 739-742. doi:10.1130/G36768.1

Sachse, V.F., Strozyk, F., Anka, Z., Rodriguez, J.F., di Primio, R. (2015) The tectono-stratigraphic evolution of the Austral Basin and adjacent areas against the background of Andean tectonics, southern Argentina, South America. Basin Res., 1-21. doi:10.1111/bre.12118

Salomon, E., Koehn, D., Passchier, C., Hackspacher, P.C., Glasmacher, U.A. (2014) Contrasting stress fields on correlating margins of the South Atlantic. Gondwana Res. 28 (3), 1152-1167. doi:10.1016/j.gr.2014.09.006

Scharf, T.E., Codilean, A.T., de Wit, M., Jansen, J.D., Kubik, P.W. (2013) Strong rocks sustain ancient postorogenic topography in southern Africa. Geology 41 (3), 331-334. doi:10.1130/G33806.1

Scheck, M., Bayer, U. (1999) Evolution of the Northeast German Basin - inferences from a 3D structural model and subsidence analysis. Tectonophysics 313, 145-169.

Scheck, M., Bayer, U., Lewerenz, B. (2003) Salt redistribution during extension and inversion inferred from 3D backstripping. Tectonophysics 373, 55-73. doi:10.1016/S0040-1951(03)00283-X

Scheck-Wenderoth, M., Raum, T., Faleide, J.I., Mjelde, R., Horsfield, B. (2007) The transition from the continent to the oean: a deeper view on the Norwegian margin. Journal of Geol. Soc. London 164, 855-868. doi:10.1144/0016-76492006-131

Scheck-Wenderoth, M., Cacace, M., Dressel, I. (2015) Multiple uplift phases inferred from the southwest African Atlantic margin. Geophys. Res. Abstracts 17. EGU2015-7230.

Schnabel, M., Franke, D., Engels, M., Hinz, K., Neben, S., Damm, V., Grassmann, S., Pelliza, H., Dos Santos, P.R. (2008) The structure of the lower crust at the Argentine continental margin, South Atlantic at 44°S. Tectonophysics 454, 14-22. doi:10.1016/j.tecto.2008.01.019

Schut, E.W., Uenzelmann-Neben, G. (2005) Cenozoic bottom current sedimentation in the Cape basin, South Atlantic. Geophys. J. Int. 161, 325–333. doi:10.1111/j.1365-246X.2005.02578.x

Sclater, J., Christie, P. (1980) Continental stretching: An explanation of the post-Mid-Cretaceous subsidence of the central North Sea Basin. J. Geophys. Res. 85, 3711-3739.

Séranne, M., Anka, Z. (2005) South Atlantic continental margins of Africa: a comparison of the tectonic vs climate interplay on the evolution of equatorial west Africa and SW Africa margins. J. African Earth Sci. 43, 283–300. doi:10.1016/j.jafrearsci.2005.07.010

Sibuet, J.C., Hay, W.W., Prunier, A., Montadert, L., Hinz, K., Fritsch, J. (1984) Early evolution of the South Atlantic Ocean: role of rifting episode. DSDP Volume LXXV, 483-508. doi:102973/dsdp.proc.75.1984

Stanley, J.R., Flowers, R.M., Bell, D.R. (2013) Kimberlite (U-Th)/He dating links surface erosion with lithospheric heating, thinning, and metasomatism in the southern African Plateau. Geology 41 (12), 1243-1246. doi:10.1130/G34797.1

Stein, C.A., Stein, S. (1992) A model for the global variation in oceanic depth and heat flow with lithospheric age. Nautre 359, 123-129

Stewart, J., Watts, A.B., Bagguley, J.G. (2000) Three-dimensional subsidence analysis and gravity modelling of the continental margin onshore Namibia. Geophys. J. Int. 141, 724-746.

Stollhofen, H., Stanistreet, I.G., von Hagke, C., Nguno, A. (2014) Pliocene–Pleistocene climate change, sea level and uplift history recorded by the Horingbaai fan-delta, NW Namibia. Sediment. Geol. 309, 15-32. doi:10.1016/j.sedgeo.2014.05.008

Strozyk, F., Back, S., Kukla, P.A. (2015) Regional Seismic-Based Comparison of Syn- and Postrift Sequences in Salt and Salt-Free Basins Offshore Brazil and Angola/Namibia, South Atlantic. GCSSEPM 2015.

Talwani, M., Abreu, V. (2000) Inferences Regarding Initiation of Oceanic Crust Formation from the U.S. East Coast Margin and conjugate South Atlantic Margins, in: Mohriak, W., Talwani, M. (Eds.), Atlantic Rifts and Continental Margins. American Geophysical Union, Washington D.C., 211-233. doi:.10.1029/GM115p0211

Tesauro, M., Kaban, M.K., Cloetingh, S.A.P.L. (2009) A new thermal and rheological model of the European lithosphere. Tectonophysics 476, 478-495. doi:19.1016/j.tecto.2009.07.022

Thorne, M.S., Garnero, E.J., Grand, S.P. (2004) Geographic correlation between hot spots and deep mantle lateral shear-wave velocity gradients. Phys. Earth Planet. Inter. 146, 47-63. doi:10.1016/j.pepi.2003.09.026

Thybo, H., Artemieva, I.M. (2013) Moho and magmatic underplating in continental lithosphere. Tectonophysics 609, 605-619. doi:10.1016/j.tecto.2013.05.032

Tinker, J., de Wit, M., Brown, R. (2008a) Mesozoic exhumation of the southern Cape, South Africa, quantified using apatite fission track thermochronology. Tectonophysics 455, 77-93. doi:10.1016/j.tecto.2007.10.009

Tinker, J., de Wit, M., Brown, R. (2008b) Linking source and sink: evaluating the balance between onshore erosion and offshore sediment accumulation since Gondwana break-up, South Africa. Tectonophysics 455, 94-103. doi:10.1016/j.tecto.2007.10.009

Torsvik, T.H., Rousse, S., Labails, C., Smethurst, M.A. (2009) A new scheme for the opening of the South Atlantic Ocean and the dissection of an Aptian salt basin. Geophys. J. Int. 177, 1315-1333. doi:10.1111/j.1365-246X.2009.04137.x

Torsvik, T.H., Steinberger, B., Gurnis, M., Gaina, C. (2010) Plate tectonics and net lithosphere rotation over the past 150 My. Earth Planet. Sci. Lett. 291, 106-112. doi:10.1016/j.epsl.2009.12.055

Trumbull, R.B., Reid, D.L., de Beer, C., van Acken, D., Romer, R.L. (2007) Magmatism and continental breakup at the west margin of southern Africa: A geochemical comparison of dolerite dikes from northwestenr Namibia and the Western Cape. South African J. Geol. 110, 477-502. doi:10.2113/gssajg.110.2-3.477

Uenzelmann-Neben, G., Schlüter, P., Weigelt, E. (2007) Cenozoic oceanic circulation within the South African gateway: indications from seismic stratigraphy. South African J. Geol. 110, 275-294. doi:10.2113/gssajg.110.2-3.275

van Wees, J.D., Cloetingh, S. (1996) 3D Flexure and intraplate compresison in the Norht Sea Basin. Tectonophyiscs 266, 343-359.

von Nicolai, C., Scheck-Wenderoth, M., Warsitzka, M., Schødt, N., Andersen, J. (2013) The deep structure of the South Atlantic Kwanza Basin - Insights from 3D structural and gravimetric modelling. Tectonophsics 694, 139-152. doi: 10.1016/j.tecto.2013.06.016

Waples, D.W., Waples, J.S. (2004) A review and evaluation of specific heat capacities of rocks, minerals, and subsurface fluids. Part1: Minerals and Nonporous Rocks. Natural Resources Research 14 (2), 97-122. doi.org/10.1023/B%3ANARR.0000032647.41046.e7

Watts, A.B., Ryan, W. (1976) Flexure of the lithosphere and continental margin basins. Tectonophysics 36, 25-44.

Watts, A.B. (1978) An Analysis of Isostasy in the World's Oceans 1. Hawaiian-Emperor Seamount Chain. J. Geophys. Res. 83 (B12), 5989-6004.

Watts, A.B. (1992) The effective elastic thickness of the lithosphere and the evolution of foreland basins. Basin Research 4, 169-178.

Watts, A.B. (2009) Isostasy and flexure of the lithosphere. Cambridge University Press, 480 p.

Watts, A.B., Burov, E.B. (2003) Lithospheric strength and its relationship to the elastic and seismogenic layer thickness. Earth Planet. Sci. Lett. 213, 113-131. doi:10.1016/S0012-821X(03)00289-9

Weigelt, E., Uenzelmann-Neben, G. (2007) Early Pliocene change of deposition style in the Cape Basin, southeastern Atlantic. Geol. Soc. Am. Bull. 119, 1004-1013. doi:10.1130/B26110.1

Will, T.M., Frimmel, H.E. (2013) The Influence of Inherited Structures on Dike Emplacement during Gondwana Breakup in Southwestern Africa. J. Geol. 121, 455-474. doi:10.1086/671398

White, R.S., McKenzie, D. (1989) Magmatism at Rift Zones: The Generation of Volcanic Continental Margins and Flood Basalts. J. of Geophy. Res. 94 (B6), 7685-7729.

White, R.S., Smith, L.K., Roberts, A.W., Christie, P.A.F., Kusznier, N.J. and the rest of the iSIMM Team (2008) Lower-crustal intrusuion on the North Atlantic continental margin. Nature 452:460-464. doi:10.1038/nature06687

8 Acknowledgements

I would like to thank my supervisor Prof. Dr. M. Scheck-Wenderoth for her patience and support during this project. Leni, I appreciate your feedback, the amount of time you invested in this project and for trusting me. Whenever it was necessary you provided me advice for several aspects related to this project. I also want to thank Prof. P. A. Kukla, Ph.D. for his supervision and for discussions during several SAMPLE workshops.

I want to thank the German Research Foundation (DFG) for funding within the priority program SAMPLE SPP 1375 "South Atlantic Margin Processes and Links with onshore Evolution" and the Helmholtz-Centre Potsdam – German Research Centre for Geosciences (GFZ) for the opportunity to do this work in such a pleasant place with such a wide and interdisciplinary working environment.

I am also very grateful to all colleagues within the SAMPLE SPP. I really liked the fruitful discussions during the annual workshops and the group meetings. Especially, I would like to thank Prof. Dr. H.-J. Götze for his support and constructive discussions on the evolution of the South Atlantic. Additionally, I would like to thank Prof. Dr. H.-P. Bunge for several discussions on geodynamics and vertical movements related to the asthenosphere. I am grateful to both of you (Hajo and Peter) for inviting me and giving me the chance to present my work at their universities. I would also like to thank the SAMPLE-colleague Dr. F. Strozyk for intensive discussions on the uplift history of the Central and Southern Segment of the South Atlantic Ocean.

Furthermore, I would like to thank the present and former members of section 6.1 – Basinmodelling of the GFZ for their support and the time spent together. In particular, I want to thank Judith and Mauro for their inputs and advices. I am also very grateful to Lew for helping with GMS. I would like to thank Katharina for her assistance in checking the use of English. Thanks also to Peter and Antoine making the days (and nights) as funny as possible.

Of course, I want to thank all the people that are not particularly linked to this work. Thanks to my "geoscientific-friends" for discussions and support during the last three years. Thanks also to the "non-geoscientific-friends" for various support and encouragement (e.g., during the time spending on the bike). As you are so many, I cannot name you but I would like to thank all of you!

Finally, I want to express my deepest gratitude to my family and Esther for all their care, support, friendly ear and motivation in manifold ways.

9 Appendix

List of publications and conference contributions related to this thesis

Journals:

Dressel, I., Scheck-Wenderoth, M. (submitted): Subsidence history of the Colorado basin, offshore Argentina and the differences in evolution of the South Atlantic conjugate margins.

Dressel, I., Cacace, M., Scheck-Wenderoth, M. (accepted): Coupled thermo-mechanical 3D subsidence analysis along the SW African passive continental margin. Arabian Journal of Geosciences. doi:10.1007/s12517-016-2407-9

Dressel, I., Scheck-Wenderoth, M., Cacace, M., Lewerenz, B., Götze, H.-J., Reichert, C. (2015): Reconstruction of the southwestern African continental shelf by backward modelling. Marine and Petroleum Geology 67, 544-555. doi:10.1016/j.marpetgeo.205.06.006

Talks:

Dressel. I., Scheck-Wendeorth M, Cacace, M. (2016): Comparison between the post-rift subsidence evolution of the Colorado Basin, SE South America, and the Orange Basin, SW Africa. Oral presentation, DGG Münster, 14. March – 17. March 2016.

Dressel, I., Scheck-Wenderoth, M., Cacace, M., Götze, H.-J., Franke, D., Bunge, H.-P. (2015): 3D subsidence analysis in offshore sedimentary basins along the southwestern African continental shelf, DGG Hannover, 23. March – 26. March 2015.

Dressel, I., Scheck-Wenderoth, M., Cacace, M., Götze, H.-J., Franke, D., Bunge, H.-P. (2014): Paleotopographies offshore SW Africa: The possibility to localize and quantify vertical movements, Oral presentation, GeoFrankfurt, 21. September – 24. September 2014.

Scheck-Wenderoth, M., Götze, H.-J., Reichert, C., Maystrenko, Y., Autin, J., **Dressel, I.**, Sonibare, W.., Sippel, J. (2013): Recent progress on lithosphere-scale models in the South Atlantic. SAMPLE Workshop, Heidelberg, 11. June – 14. June 2013.

Invited talks:

Dressel, I., Scheck-Wenderoth, M., Cacace, M., Götze, H.-J., Franke, D., Bunge, H.-P. (2015): Subsidence evolution at the conjugate continental margins of the South Atlantic. Invited talk at the geodynamic group meeting of the LMU München, 01. December 2015.

Dressel, I., Scheck-Wenderoth, M., Cacace, M., Götze, H.-J., Franke, D., Bunge, H.-P. (2015): Subsidence evolution at the conjugate Argentine and SW African passive continental margins. Invited talk to the geophysical colloquium of the CAU Kiel, 18. November 2015.

Poster:

Dressel, I., Scheck-Wenderoth, M., Cacace, M. Götze, H.-J., Franke, D., Bunge, H.-P. (2015): Subsidence evolution of the South Atlantic passive margins. GeoBerlin, Berlin, 04. October – 07. October 2015.

Klinge, L., **Dressel. I**, Götze, H.-J., Scheck-Wenderoth, M, Sippel, J. (2015): Gravitational potential energy and stress in the South Atlantic – a contribution to a "dynamic" interpretation of gravity fields. SAMPLE Workshop Monschau, 2015.

Dressel, I., Scheck-Wenderoth, M., Götze, H.-J., Reichert, C. (2014): Evolution of the SW African passive continental margin during the post-rift phase. European Geoscience Union, Vienna, 27. April – 02. May 2014.

Scheck-Wenderoth, M., **Dressel, I.**, Maystrenko, Y., Autin, J., Götze, H.-J., Reichert C. (2013): Subsidence analysis of the South Atlantic passive margins. American Geophysical Union, 09. December – 13. December 2013.

Scheck-Wenderoth, M., Maystrenko, Y., Autin, J., Lewerenz, B., Sippel, J., Götze, H.-J., Reichert, C., **Dressel, I.** (2013): Subsidence analysis of the South Atlantic passive margins. European Geosciences Union, Vienna, 07. April – 12. April 2013.

Abstract

Even though the present-day structure of the South Atlantic passive continental margins has been thoroughly investigated, uncertainties remain, particularly regarding the subsidence evolution during the post-rift phase and its causative processes. This thesis therefore focuses on the subsidence history of the passive continental margins within the Southern Segment of the South Atlantic Ocean. The subsidence history is inferred from restored paleobathymetries along the passive margins using their present-day structural configuration as well as their thermal field.

In a first part of this thesis a 1D backward modelling approach is used to reconstruct the paleobathymetries offshore SW Africa. Therefore, individual subsidence components are separated according to the load induced by the sediments and the thermal cooling of the lithosphere. Starting from the present-day configuration, sedimentary units are successively "backstripped" to quantify the amount of load induced subsidence. The amount of thermal subsidence is calculated assuming uniform stretching of the lithosphere. Considering both subsidence components allows reconstructing paleobathymetries of the SW African margin in order to infer its subsidence history. The results obtained show a general subsidence of the margin with intermittent phases of seafloor uplift, as indicated by elevations above sea level in some parts of the research area. Summing up, the amount of elevations above sea level (i.e., seafloor uplift) during the post-rift phase yields about 1200 m. Although this quantification cannot fully identify the causative processes behind the vertical movements, their timing and magnitude give evidence for a mantle mechanism causing seafloor uplift rather than ridge-push related to spreading of the South Atlantic Ocean.

Improving the understanding of the subsidence evolution of the South Atlantic passive margins requires also a subsidence analysis along the conjugate margin offshore SE South America. Hence the Colorado Basin along the Argentine margin is investigated. To accomplish this, the present-day structural configuration of the Colorado Basin is used and the same subsidence analysis used to analyse the SW African margin is applied. The results of the backward modelling approach show continuous subsidence of the Colorado Basin since the breakup of Gondwana. Therefore, they are in contrast with the subsidence history of the sedimentary basin on the conjugate margin, where the general subsidence pattern was interrupted by multiple phases of seafloor uplift. In terms of causative processes responsible

for the subsidence history, a tectonic force alone, such as ridge-push due to seafloor spreading, is unlikely to cause the seafloor uplift along the SW African margin, since the effects of ridge-push should have the same impact on both margins. This further supports the hypothesis of a mantle mechanism rather than ridge-push as cause for the seafloor uplift along the SW African margin.

Finally, to assess how far the obtained seafloor uplift is influenced by the assumptions of the 1D backward modelling and in order to also take the initial syn-rift subsidence into account, 3D forward modelling is performed for the same research area along the SW African margin as in the first part of this work. The 3D forward modelling approach used in this study has the particular advantage of coupling the thermal and mechanical subsidence components. Hence, the interaction between thermal relaxation of the lithosphere and the flexural isostatic response due to sedimentary loading, as well as the interplay of both is considered. The results also indicate elevations above sea level with a similar magnitude, as shown in the backward modelling approach and only minor temporal variations. Following the interpretation of the forward modelling results, it appears that the elevations above sea level are strongly related to the syn-rift phase. Taking the limitations of the approach used to reconstruct the syn-rift phase into account leads to the conclusion that the elevation above sea level might be the result of missing subsidence during the syn-rift phase. This missing subsidence component might be related to unconsidered lower crustal flow while calculating the syn-rift subsidence.

According to the previously described approaches, a successful analysis of the subsidence history of the South Atlantic passive continental margins based on present-day observations is possible. After summarizing the results of the three parts of this work and integrating them into a comprehensive discussion of the possible causative processes behind the evolution of the South Atlantic passive continental margins, it is evident that a mantle mechanism affected the SW African margin causing phases of uplift.

Zusammenfassung

Ziel der vorliegenden Arbeit ist die Erforschung der Subsidenzgeschichte des südlichen Segmentes des Südatlantiks. Die Subsidenzgeschichte wird aus Paleobathymetrien abgeleitet, die basierend auf Informationen der heutigen strukturellen Konfiguration und des thermischen Feldes der Kontinentalränder rekonstruiert werden. Diese Herangehensweise liefert genauere als die bislang vorliegenden Erkenntnisse bezüglich der post-rift Subsidenz. Darüber hinaus lassen die Ergebnisse der vorliegenden Arbeit Rückschlüsse auf die Mechanismen zu, welche die Subsidenzgeschichte beeinflusst haben.

Im ersten Teil dieser Arbeit wird eine 1D Rückwärtsmodellierung durchgeführt, um Paleobathymetrien des Kontinentalrandes vor SW Afrika zu rekonstruieren. Für diese Rekonstruktion werden einzelne Subsidenzkomponenten entsprechend der sedimentären Last und der thermischen Abkühlung der Lithosphäre separiert. Der Betrag der last-induzierten Subsidenz wird berechnet, indem durch „backstripping“ einzelne Sedimentpakete, beginnend mit dem heutigen Zeitpunkt, schrittweise entfernt werden. Im Gegensatz dazu wird der Betrag der thermischen Subsidenz unter der Annahme uniformer Lithosphärendehnung berechnet. Unter Berücksichtigung beider Subsidenzkomponenten ist es schlussendlich möglich, Paleobathymetrien zu rekonstruieren und daraus die Subsidenzgeschichte abzuleiten. Die Ergebnisse zeigen, dass der SW Afrikanische Kontinentalrand durch die Zeit abgesunken ist, jedoch einzelne Phasen vertikaler Aufwärtsbewegungen (d.h. Meeresboden-Hebung) auftraten. Letztere lassen sich durch Erhebungen oberhalb des Meeresspiegels identifizieren und belaufen sich auf einen Gesamtbetrag von 1200 m für die Gesamtdauer der post-rift Phase. Ihr zeitliches Auftreten und ihre Magnitude geben Hinweise darauf, dass ein Mantel-Mechanismus für die Hebung verantwortlich ist.

Um die Subsidenzentwicklung der passiven Kontinentalränder des Südatlantiks genauer zu verstehen, ist zusätzlich eine Erforschung des konjugierten Kontinentalrandes vor SE Südamerika notwendig. Aus diesem Grund wird im zweiten Teil der Arbeit das Colorado Becken vor der Küste Argentiniens auf seine Subsidenzentwicklung hin untersucht. Für diese Untersuchung wird der heutige Zustand der strukturellen Konfiguration des Colorado Beckens verwendet und dabei dieselbe Methode genutzt, wie sie im ersten Teil der Arbeit für das Untersuchungsgebiet vor SW Afrika verwendet wurde. Im Gegensatz zu dem

Sedimentbecken am konjugierten Kontinentalrand SW Afrikas mit seinen Phasen der Meeresboden-Hebung ist im Colorado Becken seit dem Aufbrechen Gondwanas ausschließlich kontinuierliche Subsidenz zu erkennen. In Bezug auf die charakteristische Subsidenzentwicklung beider Kontinentalränder ist es den Ergebnissen nach eher unwahrscheinlich, dass einzig „Ridge-Push“ (durch Spreizung des Südatlantiks) eine treibende Kraft für etwaige Hebung ist, da diese sich auf beide Seiten des Südatlantiks mit einer ähnlichen Stärke auswirken sollte. Diese Erkenntnis stützt die Hypothese eines Mantelmechanismus, welcher Einfluss auf die Subsidenzgeschichte des SW Afrikanischen Kontinentalrandes genommen hat.

Im dritten Teil der Arbeit wird eine 3D Vorwärtsmodellierung entlang des SW Afrikanischen Kontinentalrandes durchgeführt und mit den vorherigen Ergebnissen der 1D Rückwärtsmodellierung verglichen. Die 3D Vorwärtsmodellierung hat den Vorteil, dass neben der Subsidenz während post-rift Phase auch die der syn-rift Phase berücksichtigt wird. Zusätzlich werden thermische und mechanische Prozesse während der post-rift Phase gekoppelt, sodass die Wechselbeziehung zwischen thermischem Abkühlen der Lithosphäre und flexurell-isostatischer Kompensation durch Sedimentauflast berücksichtigt wird. Die Ergebnisse zeigen, ähnlich wie die der 1D Rückwärtsmodellierung, Erhebungen oberhalb des Meeresspiegels gleicher Magnitude, jedoch mit leicht unterschiedlichem zeitlichem Auftreten. Allerdings lassen die Ergebnisse der Vorwärtsmodellierung eine starke Abhängigkeit zur syn-rift Phase erkennen. Unter Berücksichtigung methodischer Einschränkungen bei der Rekonstruktion der syn-rift Phase zeigt sich, dass die Erhebungen oberhalb des Meeresspiegels auf fehlende Subsidenz während der syn-rift Phase zurückzuführen sind. Diese könnte mit möglichem Fließen der Unterkruste während der syn-rift Phase zusammenhängen, welches bei der Vorwärtsmodellierung nicht berücksichtigt wird.

Die beschriebenen Untersuchungen zeigen, dass eine Analyse der Subsidenzgeschichte unter Verwendung von Informationen über die heutige Konfiguration der Kontinentalränder möglich ist. Aus den Ergebnissen lässt sich folgern, dass die Subsidenzgeschichte des SW Afrikanischen Kontinentalrands sehr wahrscheinlich durch einen Mantelmechanismus beeinflusst wurde, welcher für die Meeresbodenhebung verantwortlich ist.